Developing novel 2,6-pyridinedicarboxamide-1,2,3 triazole ligands for luminescent lanthanide materials

A thesis presented in partial fulfilment of the requirements for the degree

of

Master of Science

in

Chemistry

School of Natural and Computational Sciences

Massey University, Albany

New Zealand

By

Nethmie Jayasooriya

2020

Developing novel 2,6-pyridinedicarboxamide-1,2,3 triazole ligands for luminescent lanthanide materials

By

Nethmie Jayasooriya

Student ID : [redacted]

SUPERVISOR: Dr. Jonathan A. Kitchen

School of Natural and Computational Sciences

Massey University, Albany

New Zealand

ABSTRACT

Lanthanide complexes possess unique photophysical properties leading to a vast number of applications in a wide range of areas. Emission of lanthanides, however, show much lower absorption coefficients with slow emissive rates and longer lifetimes. Therefore, lanthanides are usually excited through organic ligands. Research reveals that ligands rich in oxygen and nitrogen atoms are more favourable for developing metallosupramolecular lanthanide systems. Recent studies have shown that PDC (2,6-pyridyldicarboxamide) based ligand systems are excellent candidates because of their predictable coordination number and structural advantage towards complexing with Lanthanides. In addition to that PDC-based ligands are easy to functionalize with various substituents to enhance coordination and sensitize emission of lanthanides. Therefore, this project is focused on developing new 1,2,3-triazole containing PDC-derived ligands for the subsequent preparation of luminescent complexes with europium and terbium. Six ligand systems; (four of them were symmetrical systems [**L1**-**L4**] while [**L5**, **L6**] were asymmetrical ligand systems) have been successfully synthesized using the CuAAC reaction. All ligands were characterized by UV-Vis, FTIR, ^{1}H NMR and ^{13}C NMR spectroscopy. Europium and terbium complexes were synthesized using **L1**, **L2**, **L4** and **L5** ligands and photophysical studies were carried out in acetonitrile solution. The presence of characteristic europium and terbium emission bands demonstrate the successful coordination of lanthanides to the ligands. Complexation and self-assembly studies of **L5** ligands with Eu^{3+} using UV-Vis and fluorescence spectroscopic titrations show that the expected 3:1 ligand: lanthanide ratio is observed and the bulky triazole substituents do not affect complex formation. This is important as it will allow us to move on to more complex and larger ligands that incorporate amino acids/peptides. This will allow for more favourable/stronger self-assembly and potentially self-assembly in water – giving access to biological (imaging) and sensing applications.

ACKNOWLEDGEMENT

I would like to express my deepest gratitude and sincere thanks to Dr Jonathon A. Kitchen, (senior lecturer, Massey University, Albany) for providing me with valuable guidance and support as my supervisor throughout the study despite his overwhelming schedule. Without his advice and supervision, this study would hardly have been succeeded.

I am also grateful for my colleague Alex O'Neil for supporting and giving thoughtful feedback and suggestions in relation to the research.

I take this opportunity to express my gratitude to Professor John Harrison, laboratory technicians Jade Pope and Erin Moffet and all the faculty members of the Department of Chemistry, Massey University for helping me in completion of this study.

I would also like to thank Dr Jack Chen, Auckland University of Technology for making it possible to carry out experiments in their department.

Last but not least, special thanks go to my parents and my sister for the encouragement and immense support given and to my supportive husband for all the help given throughout the time period.

TABLE OF CONTENTS

LIST OF TABLES

LIST OF FIGURES

LIST OF SYMBOLS

Ag - Silver

Au - Gold

C- Celcius

C- Celsius

Ce - Cerium

Dy - Dysprosium

Er - Erbium

Eu - Europium

Gd - Gadolinium

Ho - Holmium

La - Lanthanum

Ln- Lanthanide

Lu - Lutetium

M- Molar concentration

Me - Methyl

mmol- millimoles

ms- milliseconds

nm- nano meter

Pr - Praseodymium

Si - Silicon

Sm - samarium

Tb - Terbium

Tm - Thulium

Xe - Xenon

Yb – Ytterbium

ε- Molar absorption coefficient

λ- Wavelength

τ- Lifetime

LIST OF ABBREVIATIONS

atm- The standard atmosphere

$CDCl_3$- Deuterated Chloroform

CuACC- Copper-catalysed azide–alkyne cycloaddition

DMF - Dimethylformamide

DMSO- Dimethyl sulfoxide

EDTA- Ethylenediaminetetraacetic acid

ET – Energy Transition

Et_3N- Triethyl amine

FT-IR – Fourier Transform Infrared

HPLC – High Performance Liquid Chromatography

LCD – Liquid Crystal Display

LC-MS – Liquid Chromatography – mass Spectrometry

LED – Light Emitting Diode

LRMS- low resolution mass spectrometry

NIR – Near Infrared

NMR – Nuclear Magnetic Resonance

ppm- parts per million

UV/ Vis – Ultraviolet–visible

CHAPTER 1: INTRODUCTION

1.1 LANTHANIDE CHEMISTRY

During the last few decades, lanthanide luminescence has been a significant area of research interest in the field of coordination chemistry owing mainly to its ability to be used in bio-probe applications. Although coordination chemistry was highly biased towards transitional metal complexes in the past, in recent years, interest towards lanthanide luminescent complexes has been rapidly growing in the field of coordination chemistry. It also plays a significant role in the field of material chemistry due to their unique photophysical and magnetic properties. In fact, lanthanide luminescent complexes have been developed to a point where they are used in a vast range of applications as diverse as luminescent sensors, light-emitting devices, immunoassays, telecommunications, lasers, barcoding and security marking. **Figure 1** shows some applications of lanthanide photonics used at present.[1]

Figure 1: Some applications of lanthanide photonics. Image adapted from [40]

1.1.1 Basics of Lanthanide Properties

Lanthanides were first discovered in 1787 in Scandinavia as an unusual black colour mineral referred to as gadolinite which was thereafter separated into its lanthanide elements. The whole series of elements possess very similar physical and chemical properties hence the discovery of the entire lanthanide series took almost a century. In 1869, Mendeleev was not able to position all lanthanides in the periodic table due to the lack of an acceptable atomic theory and a set of elements for comparison. It was not until Moseley and Bohr collectively revealed a new series of elements from lanthanum to lutetium and later discovered the fourth quantum shell which allowed the lanthanide series to be positioned on the modern periodic table. Although lanthanides were initially termed as "rare metals" due to the limited abundance of their mineral component, this term is not quite accurate as their crustal relative abundance (Ce = 66 ppm, La = 35 ppm) is comparatively much higher than other metals like Ag and Au (Ag=0.07 ppm Au= 0.004 ppm).[2–4]

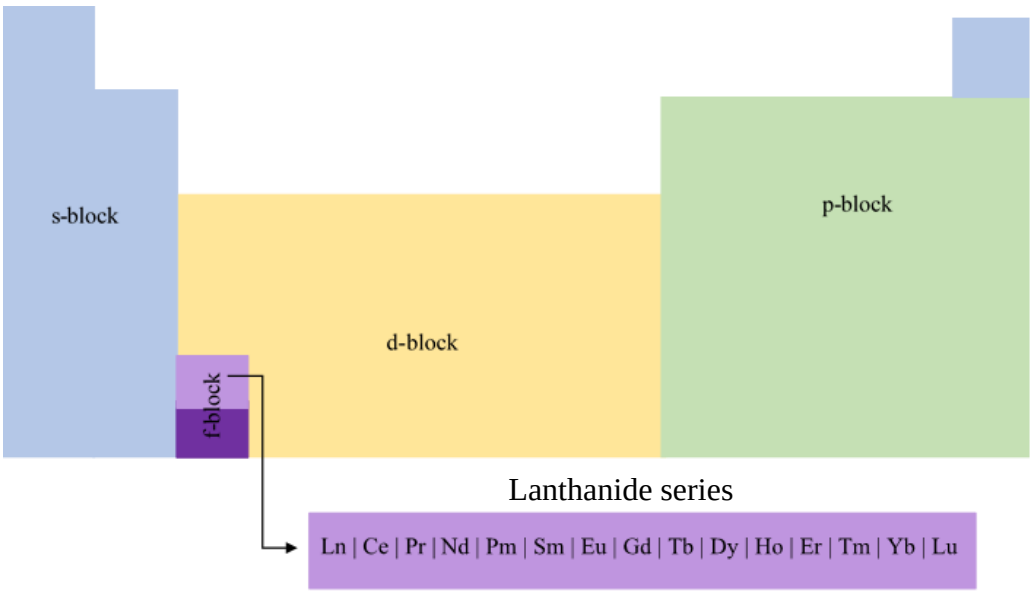

Figure 2: Location of the lanthanides in the periodic table

The lanthanide series; otherwise referred to as 4f elements include 15 elements with atomic numbers 57 to 71. **Figure 2** shows the location of the lanthanide series in the periodic table.

Lanthanides are generally found in their most stable +3 oxidized state with an electronic configuration of [Xe] $4f^n$ (where n=0-14).[5] They demonstrate several properties that are unique to those of d-block elements. Unlike in d-block elements, crystal field effects do not govern the geometry of lanthanide-ligand complexes while their geometries depend on ligand steric factors. Lanthanides possess coordination numbers varying from 6-12 although numbers 8 and 9 are common.[6–8]

The 4f orbitals of lanthanides are gradually filled following the Hund's rule. Extrinsic perturbations to the 4f electrons are shielded by the filled $5s^2$ and $5p^6$ subshells of lanthanides thus inducing extraordinary chemical, optical and magnetic characteristics, including the 4f subshells not engaging in ligand bonding.[7]

The 4f electrons are poor at shielding the $5s^2$ and $5p^6$ subshells so "lanthanide contraction" is observed where the radii of lanthanides gradually decreases as the atomic number increases. [9] This phenomenon arises as the 4f electrons do not effectively shield the $5s^2$ and $5p^6$ from the increasing nuclear charge.

The lanthanides appear as soft silvery metals and are highly reactive with dilute acids. When exposed to air, an oxide layer is formed tarnishing the surface. Melting and boiling points of lanthanides are comparatively high. Their physical properties are much the same along the period even though the melting points of samarium, ytterbium and europium are lower compared to the elements within the same series.[2]

1.2 PHOTOPHYSICAL PROPERTIES OF LANTHANIDES

Luminescence is the phenomenon where a substance gives out light by means of either a chemical, electrical, biochemical or thermal process. Various types of luminescence can be identified depending on the source of excitation; for example, electromagnetic excitation

causes “photoluminescence” and, excitation due to an electric field causes “electroluminescence”, whereas emission due to a chemical reaction is defined as “chemiluminescence”. Fluorescence is a process where a spin allowed transition happens from a singlet state to a singlet state. Likewise, in phosphorescence, a spin-forbidden transition happens from a triplet state to a singlet state which is usually a slow process due to a change in electron spin.

Figure 3: Visible emission of aqueous solutions of ligand complexes with europium, terbium, dysprosium and samarium. Image adapted from [44]

Some of the lanthanide ions display luminescent properties upon ultraviolet irradiation (**Figure 3**) and their colours solely depend on the lanthanide itself. For example, Eu^{3+}, Tb^{3+} and Sm^{3+} emit in the visible region while Nd^{3+} and Yb^{3+} are prominent in emission in the near-infrared region. Trivalent ions Pr^{3+}, Sm^{3+}, Dy^{3+}, Ho^{3+}, and Tm^{3+} also exhibit emissions in the near-infrared region whereas emission of Gd^{3+} occurs in the ultraviolet region. [7,8,10]

“Photoluminescence” is one of the most significant characteristics of lanthanides and is due to the forbidden 4f electron transitions caused by electric and magnetic dipoles. The filled $5s^2$ and $5p^6$ orbitals mask the partially filled 4f electrons from the outside making it responsible for the long-lived excited states of 0.5-3 milliseconds and narrow line-like emissions with discrete energy levels. What makes lanthanides prominent is that the lifetimes of lanthanides last for

milliseconds while even heavy transition metals such as Rh, Pt and Ir hardly display lifetime not exceeding 1/10th of a nanosecond. [7,8,10–12]

The two main factors which affect the intensity of luminescence are the quantum yield and the portion of light absorption. Lanthanides are poor at absorbing light which results in very low absorption coefficients (less than 10 $LM^{-1}cm^{-1}$) and poor luminescence.[13] Therefore, in order to acquire an adequate population of the excited state to generate a powerful photoluminescent process, the "antenna effect" or "sensitization" come in to play.[7,11,14,15]

1.2.1 Sensitized Emission Process

The photo-sensitization process was first discovered by Weissmann in 1942 when he observed that the intensity of Eu^{3+} ion was escalated in the presence of some organic compounds. The chromophore absorbs light at a specific frequency and transfers that energy to the triplet excited state of the ligand through the intersystem crossing. During these processes, energy is lost by means of fluorescence/phosphorescence, energy transfer, or non-radiactive pathways.

The process by which the energy is migrated was first proposed by Crosby and Whan. **Figure 4** clearly explains the possible ways of energy migration within the lanthanide and organic ligand.[16] The lanthanide-centred ligand is excited to vibrational levels in its first excited singlet state upon (typically UV) irradiation (i.e. S0→S1). Then the ligand rapidly undergoes intramolecular vibrational relaxation to a lower vibrational level in S1due to the interaction with solvent molecules. IC would put the molecule back into the S0 manifold. Molecular "fluorescence" occurs when the excited singlet state is deactivated to the ground state ($S_1 \rightarrow S_0$) by radiative decay. The triplet state is then radiatively brought down to the ground state giving rise to "phosphorescence". This process ($S_0 \rightarrow T_1$) is a spin forbidden transition since $\Delta S \neq 0$. Therefore, the T_1 state is long-lasting. Alternatively, the energy can be then intramolecularly transferred from the T_1 to a lower-lying excited state of the lanthanide ion via nonradiative

energy transfer.[7,11,17,18] From here the lanthanide excited state depopulates and gives rise to the characteristic emission profile.

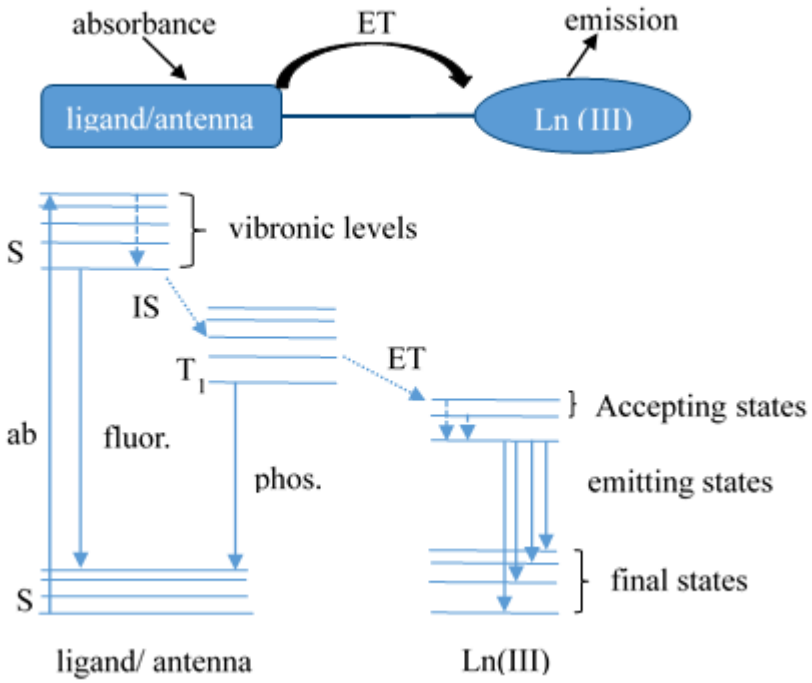

Figure 4: Schematic representation of mechanism for sensitized lanthanide luminescence

1.2.2 Sensitized Luminescence Requirements

In order to achieve a strong sensitization, the donor molecule (antenna group) and the accepter lanthanide ion should be located adjacent in close proximity, as shown in **Figure 5**. If the energy levels of the lanthanide excited states are located higher than that of the organic molecule, effective sensitisation cannot occur, and instead a back transfer followed by non-radiative emission dominates. Therefore, the lowest triplet state of the complex should always be just above the energy level of the lanthanide ion. The ideal energy gap between the S_1 and T_1 of the ligand molecule is $\Delta E \approx 5000\ cm^{-1}$ to cause an efficient T_1 population and intersystem crossing.[3] Luminescence due to indirect excitation of the antenna is temperature-sensitive since the triplet excited state depends on the temperature. Additionally, deactivation by vibrational

collisions and interaction with solvent molecules which lead to quenching should be minimized.[6,8,14,15]

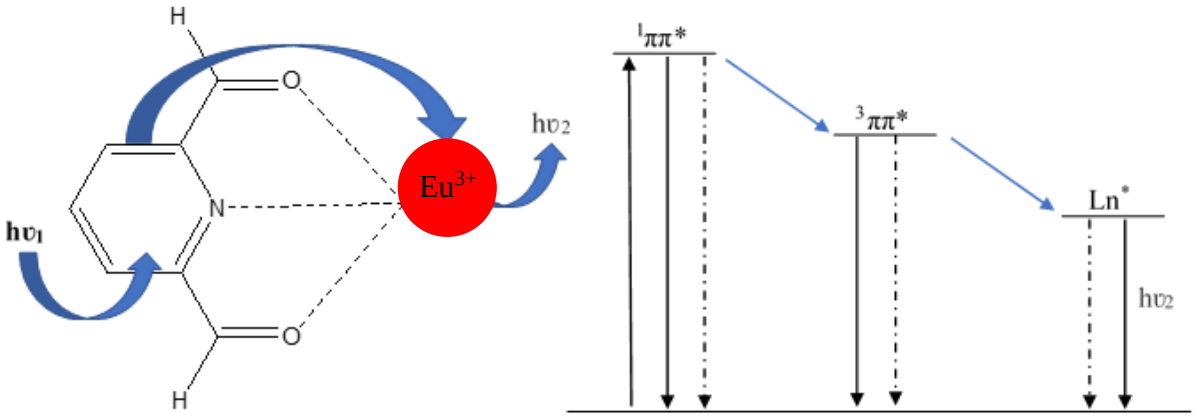

Figure 5: Schematic representation of intramolecular energy transfer / (antenna effect)

1.3 LIGANDS FOR LANTHANIDE CHEMISTRY

Research reveals that effective emission of lanthanide complexes depends on several factors namely, the structure of the ligand, and the coordination and photophysical properties of the chromophore. Excitation wavelengths can also be shifted to the NIR/visible region by modifying the ligand.[21] Metal ligand binding is an example of Lewis acid-base interaction. Lewis bases are divided into two types, namely hard bases and soft bases. Soft bases, which are polarizable, consist of relatively larger atoms such as phosphorous and sulphur, whereas, non-polarizable hard bases consist of donor atoms such as nitrogen, oxygen and fluorine. As a result, ligands rich in oxygen and nitrogen atoms are more favourable for lanthanide-based metallosupramolecular systems since lanthanide ions act as strong Lewis acids.[22] Therefore, when designing ligands for effective lanthanide photoluminescence, ligand substituents should be carefully selected without disturbing the coordination sphere. To achieve that, three strategies are followed when designing the ligand. The first approach is to design a non-chromophoric ligand that can be strongly bound to the metal at a stoichiometric ratio of 1:1. For example, diethylene tri-aminepentaacetic acid-derived systems (**Figure 6**) with carboxylic

acids, which are generally connected to a sensitizer through an amide bond. The next strategy is to include chromophoric units to increase the number of lanthanide centres in a complex while increasing the extinction coefficient. Another approach is to enhance the energy transfer rate by direct coordination of the lanthanide to the sensitizer. Pyridine and beta-diketones based ligands ensure an appropriate binding site coordinating with the ligand in close proximity to the lanthanide ion.[23]

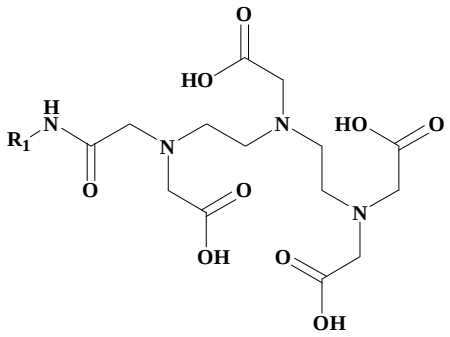

Figure 6: Diethylene tri-aminepentaacetic acid-derived core structure (R_1= substituent group)

The PDC unit (2,6-pyridyldicarboxamide), shown in **Figure 16**, is known to be a potent binding site for a lot of lanthanides demonstrating a metal to ligand stoichiometric ratio of 1:3 and reducing the effect of the ligand field around the lanthanide ion. Moreover, the absorption of the PDC unit appears below 300 nm in the short-wave UV range allowing no excitation at the PDC site due to a far lying sensitizer which absorbs in the long-wave UV range. Recent studies have shown that PDC based ligand systems are prominent because of their predictable coordination number and structural advantage towards complexing with lanthanides. In many cases, PDC-based ligands represent tri-capped trigonal prismatic geometry exhibiting coordination number 9 (**Figure 11**). [23,24]

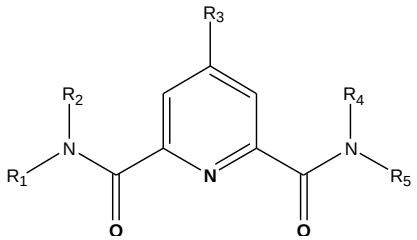

Figure 7: Simplest form of a PDC-based ligand (where R_1, R_2, R_3 and R_4 and R_5= Hydrogen)

Tanase and team were the first to synthesize the simplest form of PDC-based ligand shown in **Figure 7**, and its Eu^{3+} and Tb^{3+} complexes.[25] They observed that both complexes possessed the predicted coordination geometry which is a tri-capped trigonal prismatic geometry. In addition, they discovered the most important feature that this ligand is effective in sensitizing both Eu^{3+} and Tb^{3+} in solid-state. This discovery led to the development of more PDC-based lanthanide ligand systems. During the last decade, Gunnlaugsson and team were successful in synthesizing a series of chiral Ln^{3+} supramolecular structures. **Figure 8** (A) shows the ligand they developed with a chiral naphthalene antenna which is excellent to sensitize the Eu^{3+} ion. Moreover, they discovered that the formation of complexes occurred demonstrating a lanthanide: ligand ratio of 1:3 through self-assembly studies. Structural analysis of the ligand showed that π---π stacking between the naphthalene group and the pyridyl unit made a firmly packed "ball-like" structure. Developing the ligand illustrated in **Figure 8** (B), revealed a significant discovery that the naphthalene substituent could affect the ligand structure and its geometry. Crystallographic studies showed that unlike A, B does not contain π---π interactions and hence does not form a ball-like structure as predicted due to the subtle change of naphthalene substituent. This discovery revealed the importance of ligand selection in supramolecular chemistry, when designing a supramolecular architecture.[26]

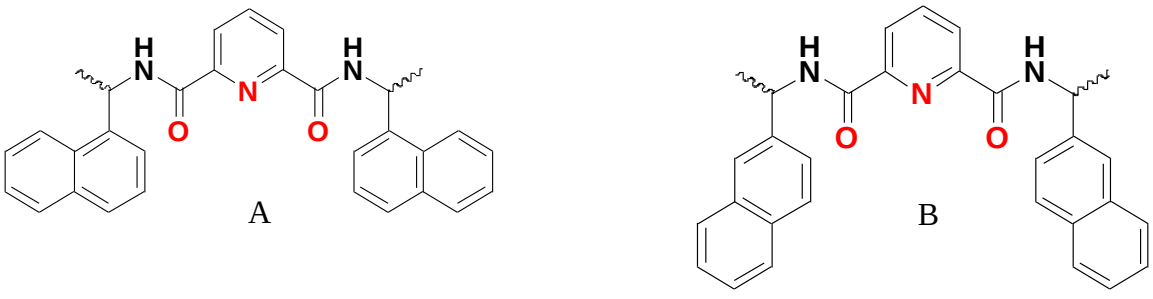

Figure 8: (A) First example of chiral PDC ligand with chiral naphthalene antenna groups, (B) PDC ligand with different naphthalene substituent groups

When forming multi-nuclear structures, the ligand design should include linkers with an appropriate length (**Figure 10**) in order to prevent the ligand folding around the lanthanide ion.[26] Research has recently been targeting the development of di-nuclear helical architectures which resemble biological self-assemblies such as the DNA helix.[27] Therefore, PDC-based lanthanide-ligand complexes have been utilized to synthesis triple-stranded helicases.

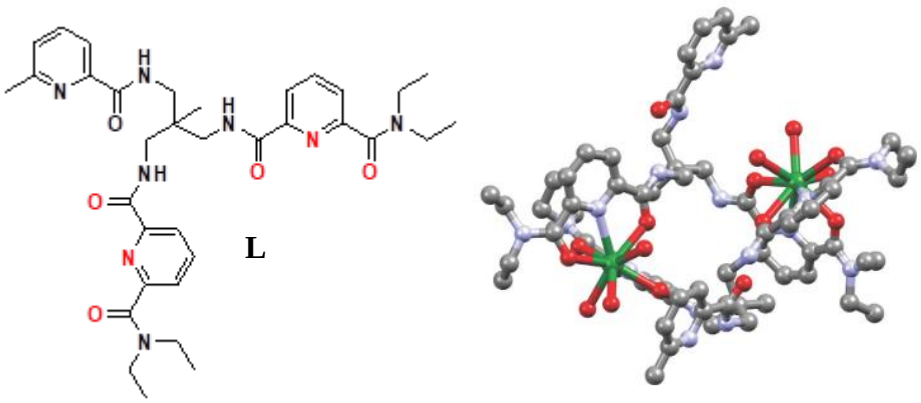

Figure 9: Ligand developed by Hamacek to form a dinuclear system (left). Molecular structure of the $[Eu_2(\mathbf{L}_8)_2(MeOH)_6]^{6+}$ complex (right). Image (right) adapted from [28]

Hamacek and team developed a dinuclear system with the bridged PDC-based ligand which is shown in **Figure 9**.[28] During their study, it was discovered that complex mixtures of dinuclear complexes were formed in solutions with different lanthanides such as lanthanum, neodymium, europium, terbium and lutetium. The single-crystal structure of the europium ligand complex was also identified thus revealing the molecular structure of the complex as shown in **Figure 9**.

A ligand which can coordinate at two different sites is known as a "ditopic" ligand. Gunnlaugsson and his team synthesised a chiral ditopic PDC-based ligand which can effectively shift the chirality from the ligand to helix.[29] To develop the chiral ditopic f-helicates, they used a similar architecture as **Figure 8** (A) as the naphthalene moieties give rise to highly ordered, stable chiral structures, but also are effective in lanthanide excitation.[26] **Figure 10** shows the chiral ditopic ligands synthesised by Gunnlaugsson and team to form dinuclear

triple-stranded helicates. Crystallographic data could not be obtained for the above-mentioned systems. However, NMR, luminescence, circular dichroism spectroscopies, circular polarized spectroscopies and UV/Vis studies were carried out.[30]

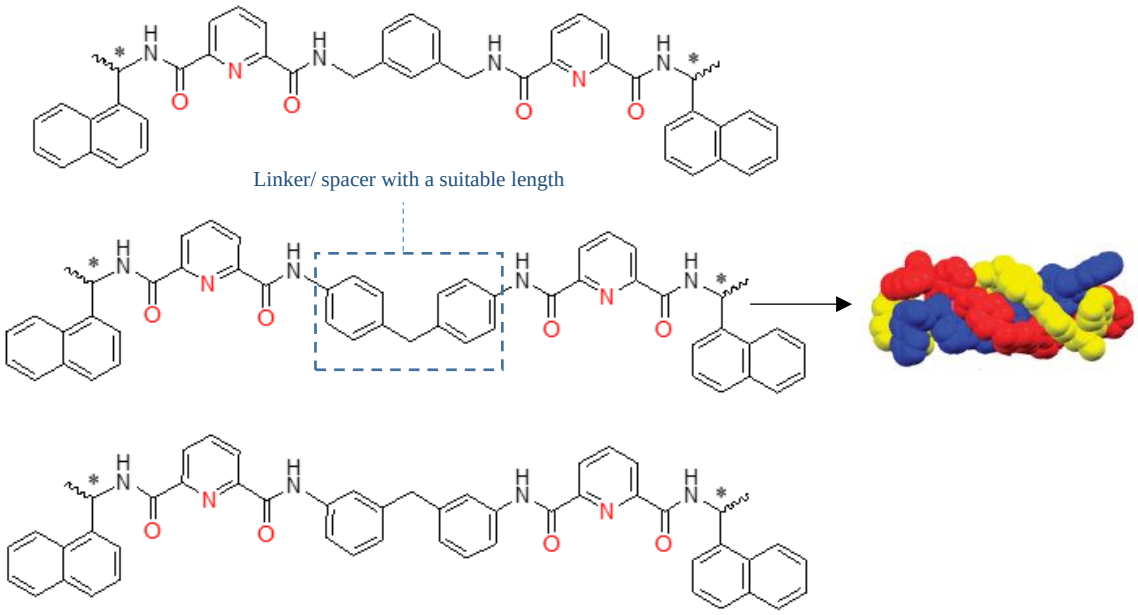

Figure 10: Chiral ditopic ligands synthesised by Gunnlaugsson and team to form dinuclear triple stranded helicates. When developing mutinuclear helicates, it is important to use an appropriate linker.

1.4 COORDINATION CHEMISTRY OF LANTHANIDES

The coordination number depends on several factors, such as the number of donor atoms, size of the coordination sphere and ligand, electron configuration, and the charge of the central metal ion. The discovery of higher coordination numbers of lanthanides arose in 1965 with the progress of X-ray diffraction techniques. Unlike transition metals, lanthanides do not have a specific coordination number and they show significant differences in their coordination. Therefore, the coordination number of lanthanides can only be derived from X-ray diffraction studies and cannot be predicted by the absorption spectrum or the colour. Lanthanides always

tend to possess high coordination numbers compared to transition metals as they are large and highly positively charged.[31]

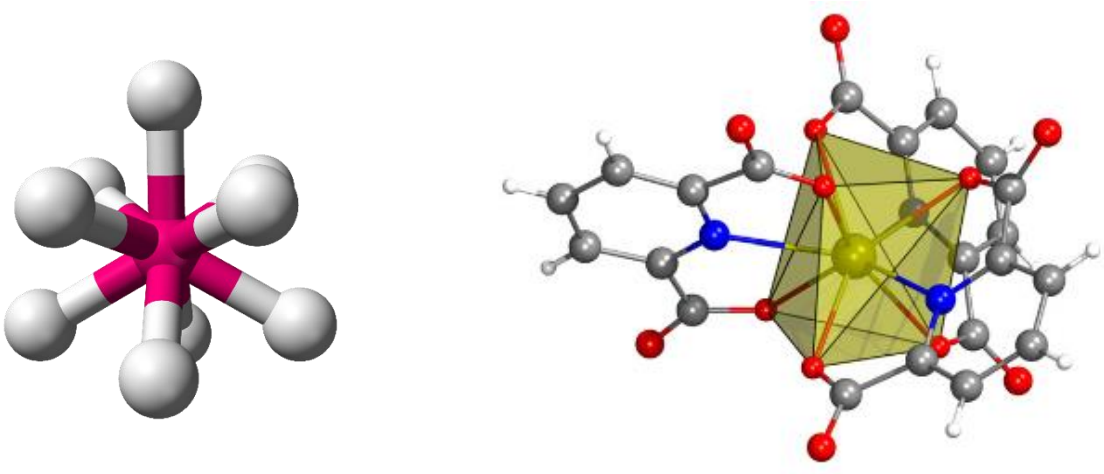

Figure 11: Representation of tri-capped trigonal prismatic molecular geometry exhibiting coordination number 9. Image adapted from [25]

Two concepts have been put forward when explaining coordination chemistry: the *first-order* and *second-order* steric effect. The *first-order* steric effects otherwise known as "inter-donor repulsions", can be observed in halide ions, oxide ions and non-congested small molecules such as water and thiocyanate. This concept refers to the overcrowding of the donor atoms of the ligand that interacts with the lanthanide ion directly.[32] In this case, the repulsion between donor atoms of the ligands free up space enabling other atoms to be directly bound to the lanthanide ion. The *second-order* steric effects are applicable in bulky ligands such as amides, alkoxides, $–N(SiMe_3)_2$, $–C(SiMe_3)_3$, and $–CH(SiMe_3)_2$. These bulky ligands are bound to donor atoms such as oxygen, nitrogen or carbon, although the number of ligands bound to the lanthanide ion is decided by the repulsion amongst the substituent groups of the ligand.[31]

1.5 COPPER(I) CATALYZED AZIDE ALKYNE COUPLING REACTION

'Click' chemistry was discovered by Nobel laureate Barry Sharpless in 2001 which led to a reawakening of the field of organic and polymer chemistry. The copper (I) catalyzed azide-

alkyne cycloaddition (CuAAC) is the most widely used reaction among 'click' reactions in a broad range of areas because of its efficiency, regioselectivity and compatibility with different functional groups.[33] This reaction succeeds over a broad range of temperature and pH (4-12). Compared to the uncatalyzed classic cycloaddition reactions, the rate acceleration of the CuAAC reaction is significantly high (10^7-10^8). **Figure 12** shows the catalytic mechanism for the CuAAC reaction to form 1,2,3-triazoles.[34]

The CuAAC reaction is a safe and straightforward process which utilizes mild conditions. One of the key features of the CuAAC reaction is the possibility of using a series of various solvent conditions. This synthesis scheme allows the easy synthesis of 1,2,3-triazole ligands from respective halides, sodium azide and alkynes. Therefore, the possibility to synthesis a series of 1,2,3- triazole-based ligands provides access to a wide range of lanthanide-based luminescent complexes.[35,36]

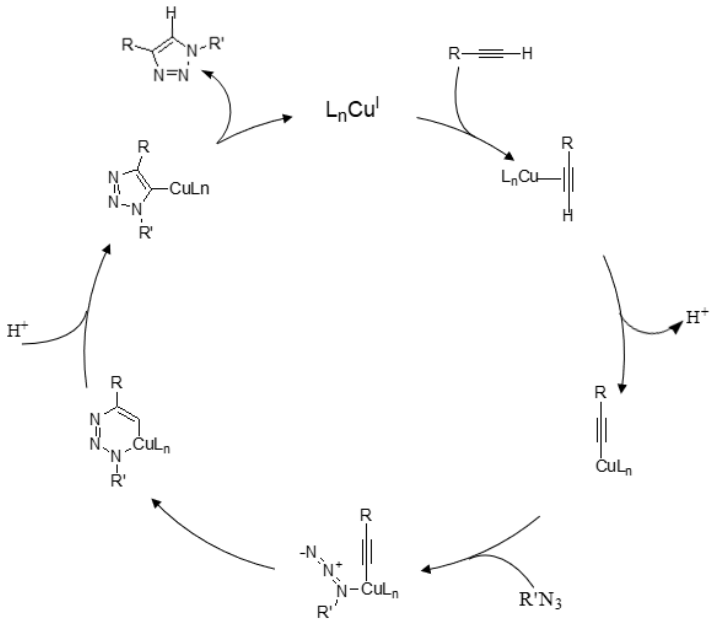

Figure 12: Catalytic mechanism for the copper catalysed alkyne/azide cycloaddition to form 1,2,3-triazoles

In this reaction, sodium ascorbate is used as the reducing agent. For a rapid reaction, the substrates and the Cu(I) catalyst should be well solubilized in the solvent mixture. The

solubility of substrates and the cyclic bond-formation are favoured by polar solvents. Thus, a mixture of dimethylformamide (DMF) and water is the ideal solvent for this reaction.[35]

1.6 APPLICATIONS OF LANTHANIDE SYSTEMS

When reviewing the applications of lanthanides over the years, one can discuss them in the context of material-directed applications and with respect to photonic applications. One of the earliest applications of lanthanides was to produce a series of an alloy known as the "mischmetal" composed of iron and mainly cerium and different amounts of lanthanum and neodymium. This series of alloys have been used to form a consistent layer of lanthanide oxysulfide which was able to resist deformation at elevated temperatures in steel production.[37,38] Lanthanides have also been used as catalysts in industrial processes like oil refining to accelerate the conversion of crude petroleum to gasoline.[39] However today with the breakthrough of photophysical properties of lanthanides, use of lanthanide luminescent substances has gradually emerged in a vast number of applications.

1.6.1 Lanthanides in Lighting

Lanthanides are broadly used in developing lighting devices since they are good triplet quenchers. **Figure 13** gives a rough idea about the improvement of lighting devices over the past few decades and their power efficiencies. Throughout the years, LEDs have replaced most of the traditional lighting devices. As of today, micro-LEDs are being produced which potentially generate 1mW light with an increased intensity of 300 Wcm^{-2}. Eu^{2+} and Eu^{3+} ions are doped into several inorganic phosphors such as aluminates, silicates, selenides and nitrides to improve efficiency, resolution, brightness and longer lifetimes than LCD and LED technologies. In near future, micro-LEDs will replace the conventional display screens in computers, phones, televisions and cinema.[40]

Figure 13: Improvement of lighting devices over the last few decades and their power efficiency. Image adapted from [40]

1.6.2 Lanthanides in Biological Applications

During the past decade, hundreds of articles have been published in the area of lanthanide luminescence in biological applications. The unique optical ability of lanthanides to convert long-wavelength excitation to short-wavelength emission is known as the "anti-stokes shift luminescence" (**Figure 14**). This allows greater penetration for a vast number of *in vivo* applications as it refers to NIR (near-infrared) emission.

Figure 14: The anti-stokes shift luminescence of lanthanides and its applications in biology. Image adapted from [42]

Optical analysis of live cells and biological imaging in deep tissues is limited due to a phenomenon called "autofluorescence" under UV or blue light illumination. This issue can be

addressed by replacing the devices by lanthanide probes due to their long lifetimes, photostability, and the slow emission rates.[31] The noise due to autofluorescence of tissues can be reduced as the anti-stoke luminescence signal can be easily identified.[42] Therefore, probes with Eu-chelated tags improve the noise to signal ratio by eliminating the background autofluorescence, and the luminescence is detected by time-resolved microscopy. Since the 1970s, the time-resolved ability of lanthanide-based probes has enabled the discovery of immunoassays, enzyme activity and protein staining methods. In immunoassays, the antibody is directly or indirectly labelled with a luminophore which will be later identified using an analytical device. This is carried out by incorporating lanthanide ions into the immunocomplex via a chelating agent. These methods open up the possibility of identifying diseases in early stages.[1,40,43,44]

1.6.3 Lanthanides in Security Devices

Applications of lanthanides extend to safety signage, security inks and recognition codes. These luminescent tags appear to be invisible unless triggered by UV or NIR illumination or applying pressure. The principle behind some of these applications is the downshifting luminescence of lanthanides. In other words, luminescent compounds absorb high energy in UV/visible range and emit lower-energy photons in the near-infrared range.

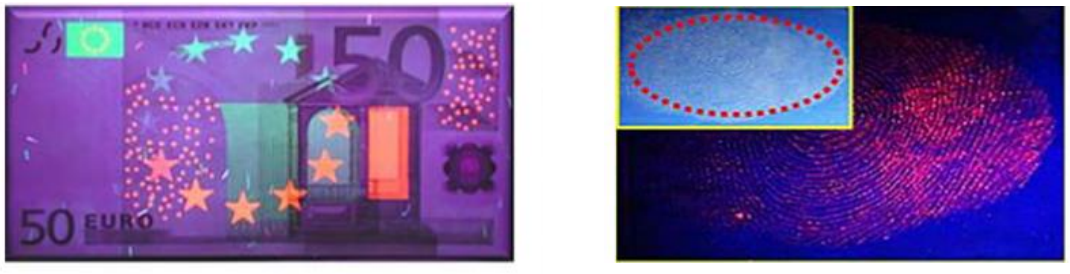

A B

Figure 15: (A) showing the reddish orange emission of Euro banknote upon UV-illumination. (B) displaying latent fingerprint revealed upon illumination. Image adapted from [1]

Some bank notes make use of a pigment doped with europium ions which emits a reddish orange luminescence upon UV irradiation (**Figure 15** A). Another example is utilizing nanoparticles doped with europium ions to reveal latent fingerprints (**Figure 15** B). Security codes are implanted into microparticles in mixtures of up to five lanthanide ions such as europium, samarium, terbium, caesium, and dysprosium. It generates more than a thousand combinations, maximizing the security with a 99.99% reliability.[1,40]

1.7 SUPRAMOLECULAR MATERIALS

Supramolecular chemistry is an interesting discipline which looks beyond the chemistry of an individual molecule and rather focuses on designing larger constructs. The term "supramolecular chemistry" was first introduced by Lehn in 1969 and he defined this area as "the chemistry of the intermolecular bonds".[45] The emergence of supramolecular materials began when chemists started to design chemical structures mimicking the biological processes which do not involve strong covalent bonds.[3] Today this field of chemistry has opened up a wide range of possibilities in material science (engineering polymers), drug designing and biological applications.

1.7.1 Engineering of supramolecular architectures

Formation of supramolecular structures is a spontaneous process which is referred to as "self-assembly".[46] Supramolecular materials are linked together by intermolecular forces. Many weak intermolecular interactions can occur within supramolecular architectures, but only a few of those interactions can be easily identified. Such weak interactions make predicting the exact supramolecular structure difficult, and means that supramolecular structures are not always stable in solution for long periods.[47]

The non-covalent intermolecular forces which lead to supramolecular assembly include isotropic and anisotropic forces. Medium-range isotropic forces contain van der Waals forces

and they are responsible for defining the shape and the size of the single molecule. Large-range anisotropic interactions occur due to electronegative atoms such as nitrogen, oxygen and chlorine. Examples of such interactions include hydrogen bonds, π-π stacking and cation–π interactions. Therefore, anisotropic forces are important to define the 3D orientation and the shape of the molecule. When designing supramolecular constructs, it is important to focus on the anisotropic interactions since the directional and functional effects depend on them.[6,45,48]

1.8 RESEARCH PROBLEM

During the last decade, researchers have focused on preparing Ln^{3+} assemblies with PDC-based ligands because of their predictable coordination to lanthanide ions. This combination offers easy addition of many substituents through "click" triazole formation providing an excellent Ln^{3+} binding site (PDC), and a good antenna for sensitized emission. The PDC unit has the potential to target many application areas by incorporating substituents. **Figure 16** shows a schematic representation of PDC ligand design which is focused on this research project.

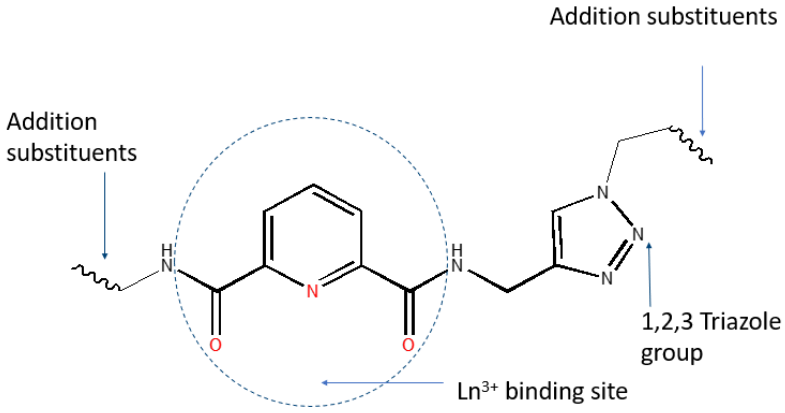

Figure 16: Schematic representation of PDC ligand design which is focused in this research project

Even so, very little research has been carried out to prepare PDC-based ligands containing the 1,2,3-triazole unit which allows easy addition of many substituents for an enhanced sensitization process. Therefore, the aims of this project were:

- to develop six novel PDC-based ligand systems containing 1,2,3 triazole unit (**Figure 16**).
- to fully characterize the six synthesised ligands by ^{1}H NMR, ^{13}C NMR, FTIR, and mass spectrometry.
- to synthesise lanthanide-ligand complexes with europium, terbium and lanthanum and characterize those by FTIR, and UV-Vis.
- to determine the photophysical properties of the synthesised Ln-ligand systems using UV-Vis, fluorescence and phosphorescence studies.

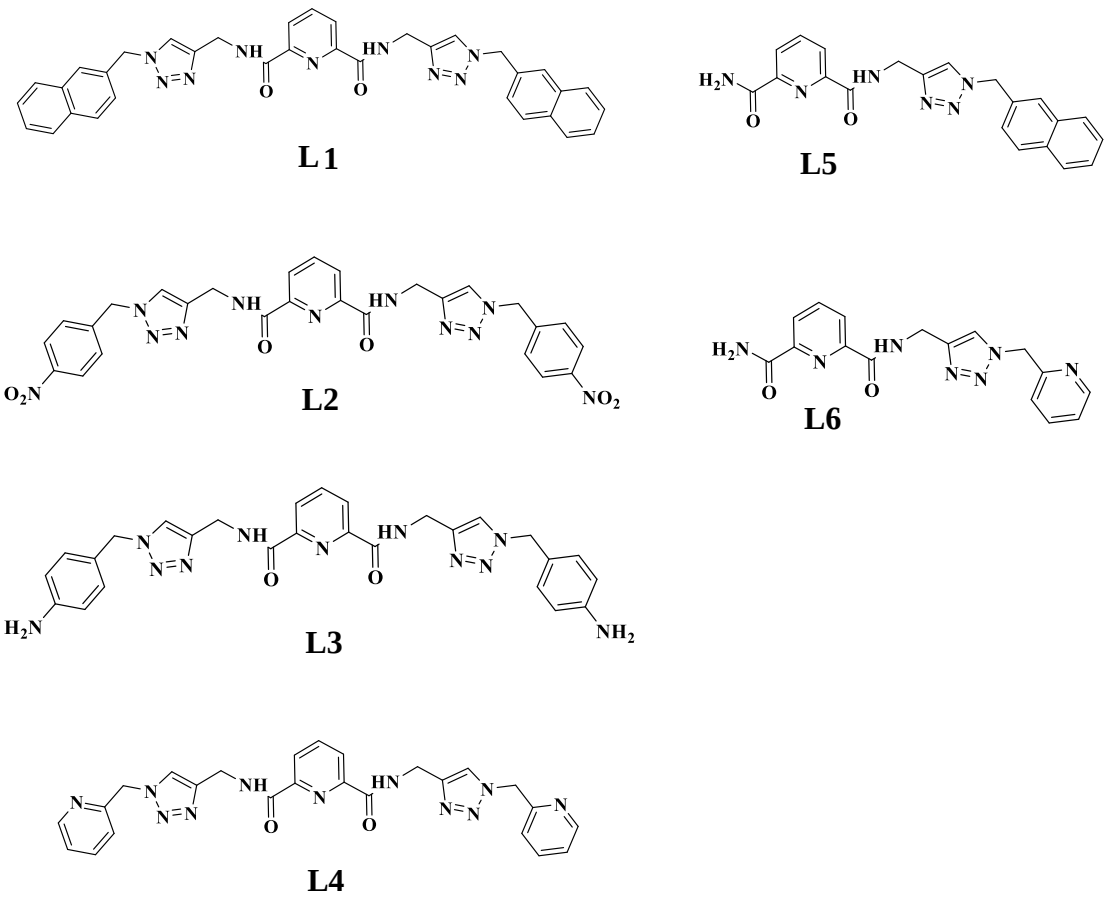

Figure 17: Synthesized ligands

CHAPTER 2: RESULTS AND DISCUSSION

2.1 PREPARATION OF LIGANDS AND COMPLEXES

In this research, two ligand systems were focused on. The two systems were based on the PDC scaffold: one symmetrical system with two substituent groups on either side of the PDC unit and one asymmetrical system with an NH_2 group on one side (**Figure 17**). The pyridine-2,6-dicarboxamide scaffold is significant as the donor atoms oxygen and nitrogen favour the coordination of lanthanide ions. When reacting the lanthanide salts with the ligand in solvents such as acetonitrile, it also avoids crystal hydration by suppressing the non-radiative relaxation process of Ln^{3+} excited state due to O-H coupling.[25]

The bis PDC-based ligands were synthesized using 2,6-pyridinedicarbonyl dichloride as the starting material. 2,6-pyridinedicarbonyl dichloride was reacted with propargyl amine and the resulting bis-alkyne was then subjected to "CuACC" reaction to generate 1,2,3-triazole rings. The mono PDC-based ligand systems were synthesized from 2,6 pyridinium dicarboxylic acid as the starting material followed by addition of benzyl bromide to obtain the mono-protected pyridine-2,6-dicarboxylicmonobenzyl ester. The ester product was then subjected to chlorination prior to converting it to the mono-alkyne. Then the alkyne was subjected to hydrolyzation to deprotect the attached benzyl group into its corresponding amide. The deprotected version subsequently was clicked with the relevant substituent. A detailed synthetic procedure for each ligand and their characterization data are given in the experimental section (Chapter 4).

Molecular weights and the structures of the synthesized bis-systems are given in **Table 1**.

All molecular weights were automatically calculated using Chemdraw software.

Table 1: Molecular weights of **L1**, **L2**, **L3**, **L4, L5 and L6**

Ligand	Molecular weight ($gmol^{-1}$)
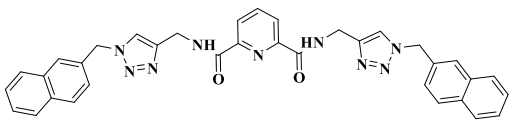	607.66
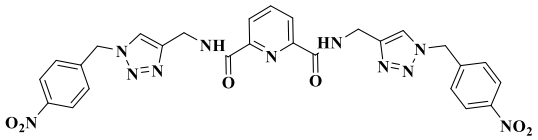	597.54
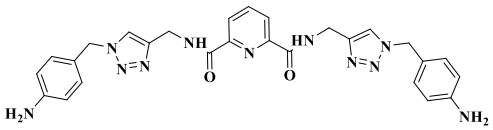	537.58
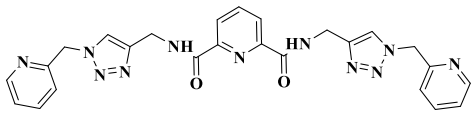	509.53
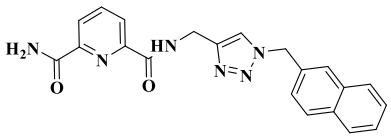	386.42
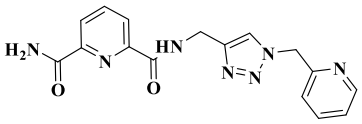	337.34

2.1.1 Bis 1,2,3 Triazole PDC-Ligand Systems (L1, L2, L3, L4)

1,2,3 triazole, pyridine dicarboxylic-derived ligands **L1**, **L2**, and **L4** were synthesized according to the copper(I)-catalysed alkyne-azide cycloaddition (CuACC) mechanism. **L1**, **L2**, and **L4** symmetrical ligand systems were synthesized using N^2,N^6-Di-2-propyn-1-yl-2,6-pyridinedicarboxamide as the starting material. This was reacted with the desired alkyl bromide in the presence of NaN_3 to generate the required azide for the click reaction. The cyclic formation and the solubility of substrates are favoured by polar solvents. Therefore, DMF:H_2O (4:1) was used as the solvent system for this reaction and the reaction was carried out at room temperature.[35] EDTA in ammonia solution (0.5 $moldm^{-3}$) was added to remove excess Cu^{2+} present in the reaction mixture. Three of the synthesized ligands precipitated upon addition of EDTA and the resulting white colour solid was filtered and washed with water to remove excess DMF from the previous click reaction.

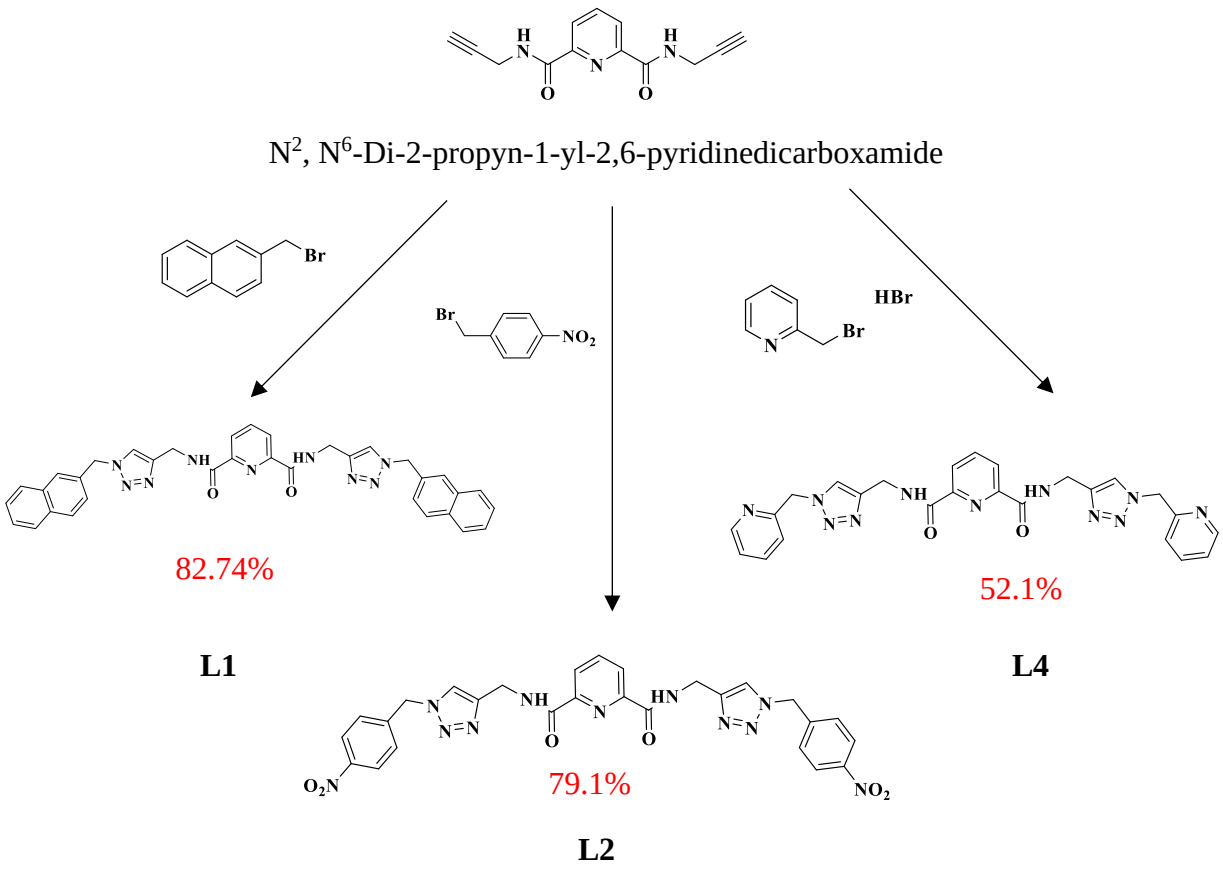

Figure 18: Reaction scheme of synthesis of **L1**, **L2** and **L4**

Synthesis of **L1**, **L2** and **L3** was quite straightforward and resulted in a high yield (82.74%, 79.1%, 52.1 % respectively). **Figure 18** shows the reaction scheme of the synthesized ligands **L1**, **L2** and **L4**.

The formation of ligands **L1**, **L2**, and **L4** were then confirmed by ^{1}H NMR, ^{13}C NMR and FT-IR data. (spectra are given in the appendices). The singlet peak (at ≈ 8.0 ppm) in the ^{1}H NMR spectrum of ligands **L1**, **L2**, **L3** and, **L4** refers to the proton of the 1,2,3-triazole unit. Therefore, the formation of the 1,2,3-triazole unit was confirmed by the ^{1}H NMR spectrum which is shown in **Figure 19**. Additionally, the disappearance of the characteristic alkyne signal at ≈ 2.2 ppm is further evidence of successful formation of the ligands.

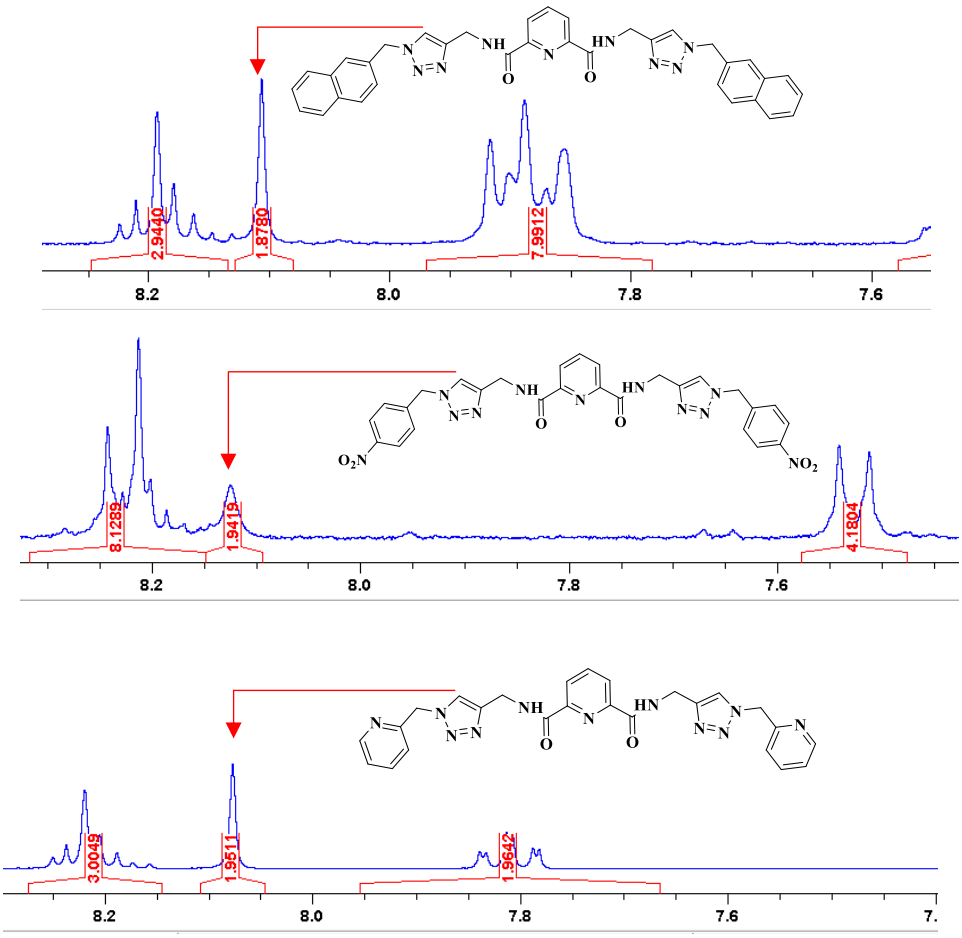

Figure 19: ^{1}HNMR spectra of **L1**, **L3** and, **L4** showing the triazole peak at ≈8.0 ppm

Figure 20 shows the stacked FT-IR spectra of N^2,N^6-Di-2-propyn-1-yl-2,6-pyridinedicarboxamide and **L1**. The disappearance of characteristic peaks due to C≡C and C-H stretches of the alkyne in **L1** spectra suggests that the click reaction was successful.

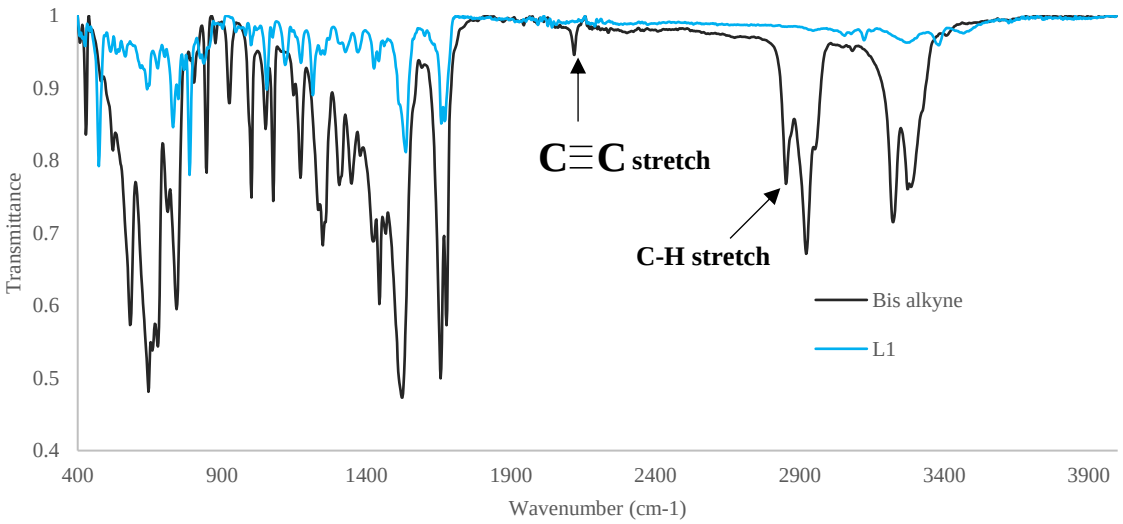

Figure 20: Stacked FT-IR spectra of N^2,N^6-Di-2-propyn-1-yl-2,6-pyridinedicarboxamide and **L1** showing the C≡C and C-H stretches of the alkyne

A sharp characteristic peak is observed for all ligands **L1**, **L2**, **L3** and **L4**, due to the C=O stretch at ≈ 1600 cm^{-1}. **Figure 21** shows the FT-IR spectrum of **L4**.

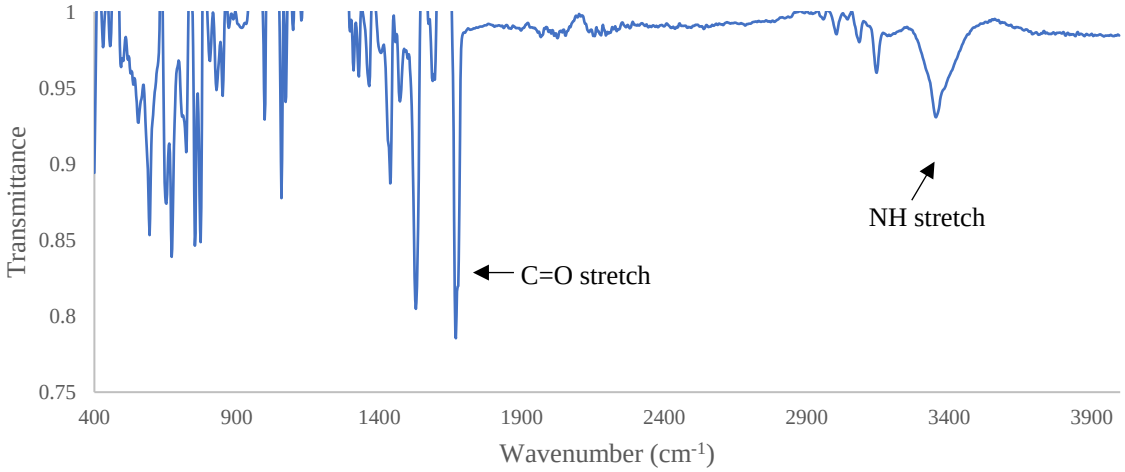

Figure 21: FT-IR spectrum of **L4** showing the C=O and NH stretch around 1600 and 3000 cm^{-1} respectively

When synthesizing **L3**, the NO_2 group on **L2** was reduced to NH_2 using hydrazine hydrate ($N_2H_4.H_2O$) as the reducing agent and Pd/C as the catalyst in ethanol. **Figure 22** shows the reaction scheme of the synthesis of **L3**. **L2** is completely immiscible in ethanol but the final **L3** product was obtained as a well dissolved-colourless solution after the reduction at 60 ^{0} C. Hot gravity filtration was carried out to remove the excess Pd/C present in the colourless solution. After evaporating the resulting solution *in vacuo*, a pale-yellow colour solid was obtained with a percentage yield of 90.0%.

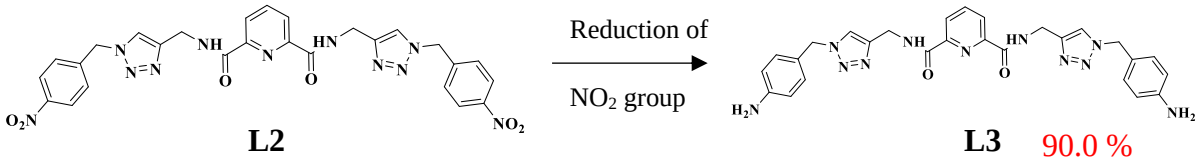

Figure 22: Reaction scheme for the synthesis of **L3**

Reduction of the NO_2 group of **L2** was confirmed by comparing the FT-IR spectrum of **L2** and **L3**. **Figure 23** shows the FT-IR spectra of **L2** and **L3**. The NO_2 stretch is clearly observed at 1338 cm^{-1} on the FT-IR spectrum of **L2**. The absence of a significant peak at ≈ 1300 cm^{-1} for **L3** indicates that the NO_2 group was successfully reduced to NH_2. Moreover, the two sharps bands at 3300 cm^{-1} and 3400 cm^{-1} show the presence of a primary amino group. For aromatic amines, C-N stretch is found around 1200 cm^{-1}. For **L3**, a band appears at 1268 cm^{-1} indicating the presence of NH_2 group of **L3**.

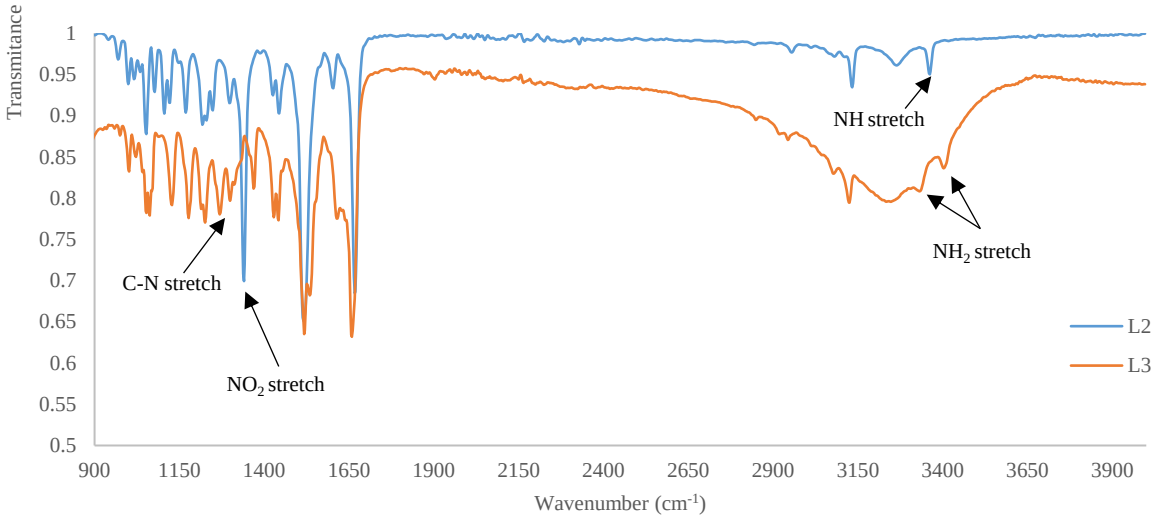

Figure 23: Stacked FT-IR spectra of **L2** and **L3** showing the NO_2 stretch of **L2** and NH_2 stretch of **L3**

2.1.2 Mono- 1,2,3 Triazole PDC-Ligand Systems

Synthesis of mono 1,2,3 triazole, pyridine dicarboxylic-derived ligands were carried out using 2,6 pyridine dicarboxylic acid as the starting material. Initially, the dicarboxylic acid was protected with a benzyl group prior to the chlorination of the carboxylic group with $SOCl_2$. The chlorinated compound was then converted into the corresponding alkyne using propargyl amine. The alkyne product was subjected to "click" reaction with 1.2 equivalents of nitro benzyl bromide in the presence of NaN_3, $CuSO_4.5H_2O$ and Na_2CO_3 as shown in **Figure 24**. De-protection of the benzyl group of the ligand into its corresponding amide was not successful due to the low aqueous solubility of the NO_2 compound in NH_4OH (aq) (23%) solution at 100^0 C. ^1H NMR spectrum of the product confirmed that the compound contained benzyl alcohol and therefore needed further purification. The proton NMR spectra showed that the product still contained traces of benzyl alcohol even after several water washes.

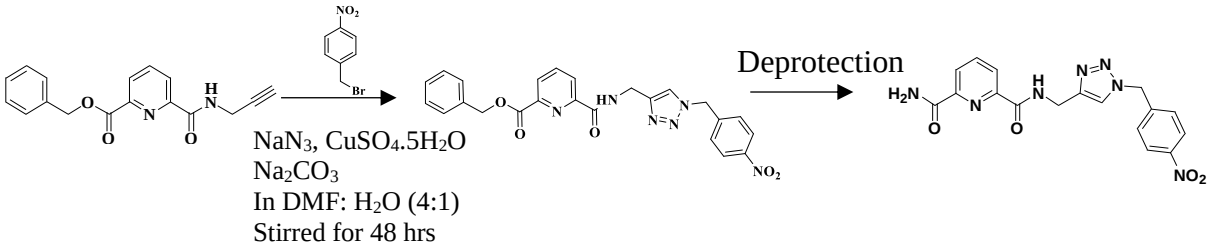

Figure 24: Reaction scheme of deprotection of the benzyl group after the "click".

Meanwhile, a different approach was needed to synthesize the mono ligand systems due to the difficulties faced in deprotection of the benzyl group after the click reaction. When the mono alkyne product was subjected to deprotection in NH_4OH prior to "CuACC click" reaction, it successfully produced the amide and the substituent group was added afterwards. To synthesise the mono alkyne product, as shown in **Figure 25**, pyridine-2,6-dicarboxylicmonobenzyl ester was first reacted with $SOCl_2$ followed by propargyl amine to produce the 6-Prop-2-ynylcarbamoyl-pyridine-2-carboxylic acid benzyl ester (protected-alkyne) compound. Then it was reacted in NH_4OH solution at 60° C for 12 hours. The resulting solution was separated with DCM. The DCM layer was then washed with water and the water layer was evaporated *in vacuo* to obtain the mono alkyne product.

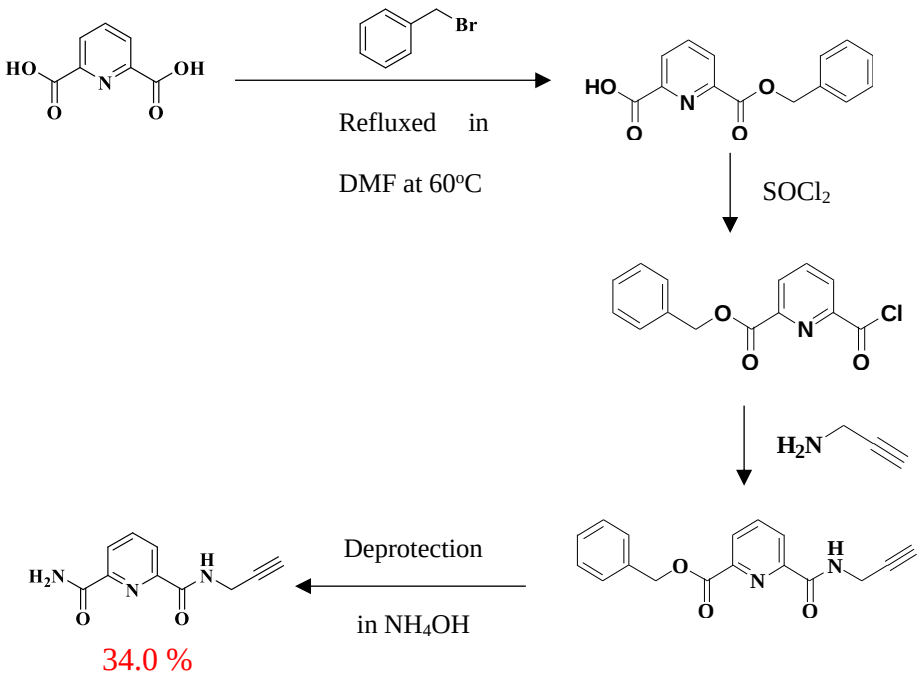

Figure 25: Reaction scheme showing the synthesis of mono alkyne product

Although the resulting alkyne product was clean, the percentage yield of the deprotected alkyne compound was low (34.0 %) because of the difficulty in separation of the aqueous layer. Therefore, large amounts of starting material (pyridine-2,6-dicarboxylicmonobenzyl ester) was required to produce a reasonable amount of the alkyne.

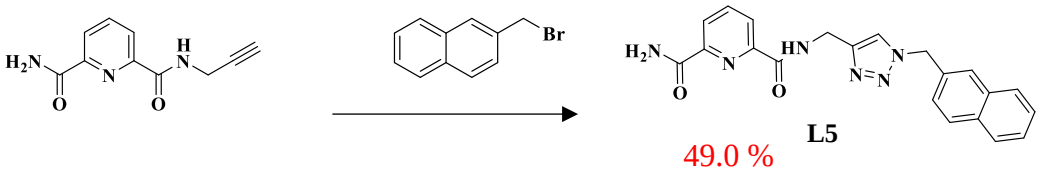

Figure 26: Reaction scheme for the synthesis of **L5**

Figure 26 shows the reaction scheme of **L5**. The deprotected alkyne was reacted with 1.2 equivalents of 2-(Bromomethyl)naphthalene to produce **L5**. Unlike in bis systems, the end product could not be obtained as a solid directly from the reaction. Therefore, further separation was needed to obtain **L5** as a clean product. **L5** was separated in DCM and evaporated in *vacuo* to obtain a pale-yellow colour solid at a percentage of 49.0%. Formation of the 1,2,3-triazole was again confirmed by the proton NMR of **L5** which is shown in **Figure 27** where a triazole signal was observed at 8.10 ppm. The multiplet at 8.15 ppm is due to the 3 protons of the pyridyl group while the multiplets at 7.86 ppm and 7.50 ppm refer to the naphthalene ring. Other resonances were consistent with the remainder of the compound (e.g. CH_2 signals at 6.0 and 5.73 ppm). The chemical structure was further confirmed by mass spectroscopy ((m/z) calculated for $(C_{21}H_{18}N_6O_2 + Na)^+$ 409.1 found at 409.2 and calculated for $(C_{25}H_{23}N_{11}O_2 + K)^+$ 425.5 found at 425.0)).

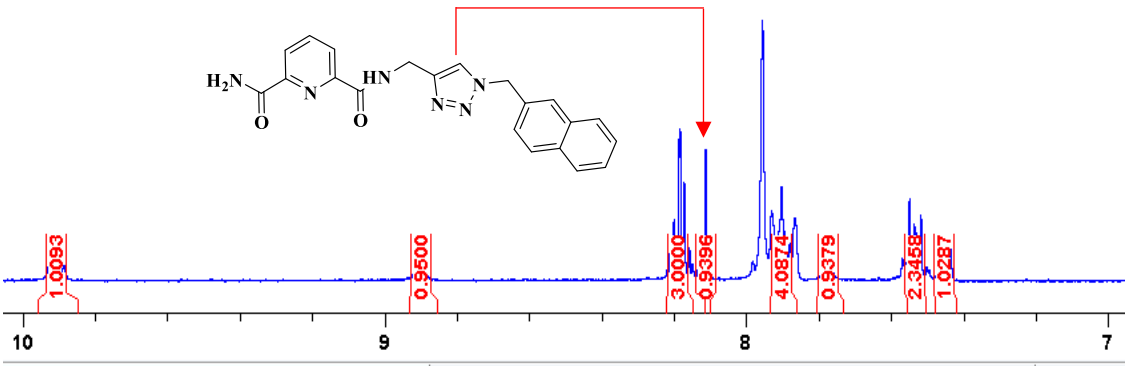

Figure 27: ^{1}HNMR spectra of **L5** showing the triazole peak at 8.1 ppm

Synthesis of **L6** was carried out by reacting the deprotected-alkyne with 1.2 equivalents of 2-(Bromomethyl)pyridine hydrobromide as shown in **Figure 28**. Separation of **L6** was not as straightforward as bis-systems. Once EDTA was added to remove excess Cu^{2+} present, the EDTA layer was vigorously stirred in DCM with a magnetic stirrer. The DCM layer was then separated and washed with distilled water. The water layer became a cloudy solution indicating that **L6** had a higher solubility in water due to the amino group. Instead of separation with DCM, the solution was kept under the fume hood to evaporate and the resulting solid was dissolved in DCM and extracted with water. The water layer was evaporated *in vacuo* and a pale-yellow colour solid was obtained at a percentage yield of 84.3%.

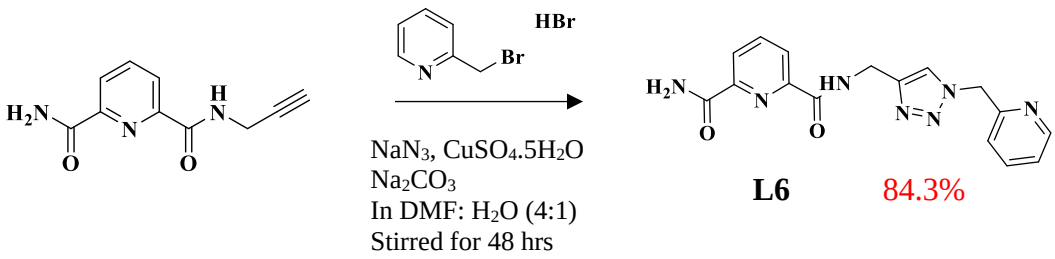

Figure 28: Reaction scheme for the synthesis of **L6**

Formation of the triazole was confirmed by ^{1}H NMR of **L6** given in **Figure 29**, where the triazole signal was observed at 8.00 ppm. The multiplet due to the protons of the pyridyl group appeared at 8.08 ppm. The peaks referring to protons due to the attached pyridyl ring appeared at 8.45 ppm and 7.21 ppm giving a multiplet and a doublet respectively. The chemical structure was further confirmed by mass spectrometry ((m/z) calculated for $(C_{16}H_{15}N_7O_2 + Na)^+$ 360.3 found at 360.0 and calculated for $(C_{16}H_{15}N_7O_2 + K)^+$ 376.4 found at 375.9).

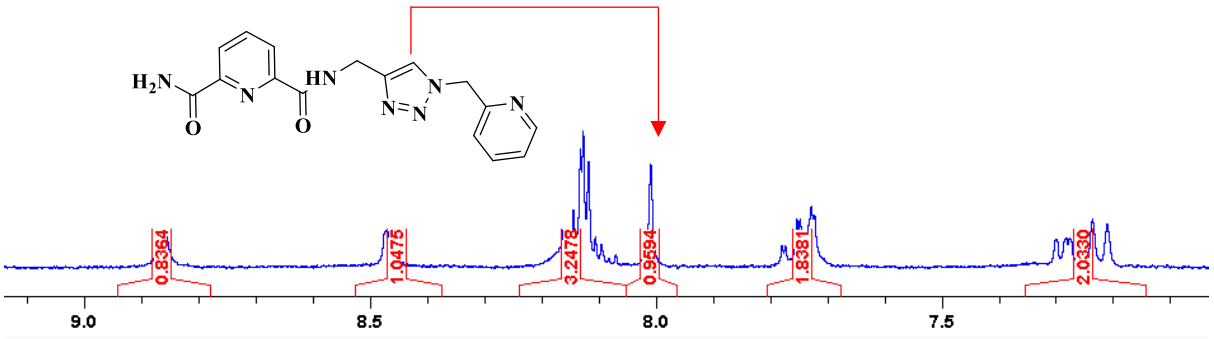

Figure 29: ^{1}HNMR spectra of **L6** showing the triazole peak at 8.0 ppm

Unlike the bis-systems, when synthesising the asymmetrical ligand systems, using the exact amount of $CuSO_4.5H_2O$ (0.2 eq) had a significant impact on the final product. It was observed that using more than 0.4 equivalents of $CuSO_4.5H_2O$ resulted in impure product as excess Cu^{2+} ions can be coordinated with the PDC unit.

2.1.3 Lanthanide Complexes

L1, **L2**, **L3**, **L4** and **L5** ligands were complexed with $Eu(CF_3SO_3)_3 \cdot 6H_2O$ (europium triflate), $Tb(CF_3SO_3)_3 \cdot 5H_2O$ (terbium triflate), and $La(CF_3SO_3)_3 \cdot 9H_2O$ (lanthanum triflate). Initially, the ligands were refluxed with the relevant lanthanide in a 3:1 ratio, for 48 hours in acetonitrile solvent at 50^0 C. Then the resulting solvent was subjected to vapour diffusion in diethyl ether solution. Even though the reaction solvent was luminescent under UV irradiation, none of the complexes obtained by refluxing were luminescent under UV irradiation. The FT-IR spectrum

of the lanthanide complexes showed that the coordination was unsuccessful as a peak shift was not observed. Therefore, a different approach was carried out to make the lanthanide complexes.

A preliminary study was carried out to observe lanthanide luminescence of the synthesized ligands (**L1** and **L4**) with europium under UV irradiation. The ligand and europium(III) trifluoromethanesulfonate were weighed (3:1) on to a laboratory mortar and the solids were ground using the pestle. The resulting solid mixture was observed under UV irradiation as shown in **Figure 30**. Although solid-state synthesis sounds promising for metal complexes, it has some drawbacks. Lanthanides tend to react with oxygen and form oxides and also due to the lack of contact between reactants, the complexation was carried out in solvent.

L4 ligand with europium produced bright red luminescence under UV irradiation while **L1** produced a blue luminescent solid. This study showed that the **L4** and **L1** compounds produce luminescent complexes with europium. The red luminescence observed for **L4** complex is due to the $^5D_0 \rightarrow {}^7F_2$ transition while **L1** ligand itself is luminescent (hence the blue emission observed).

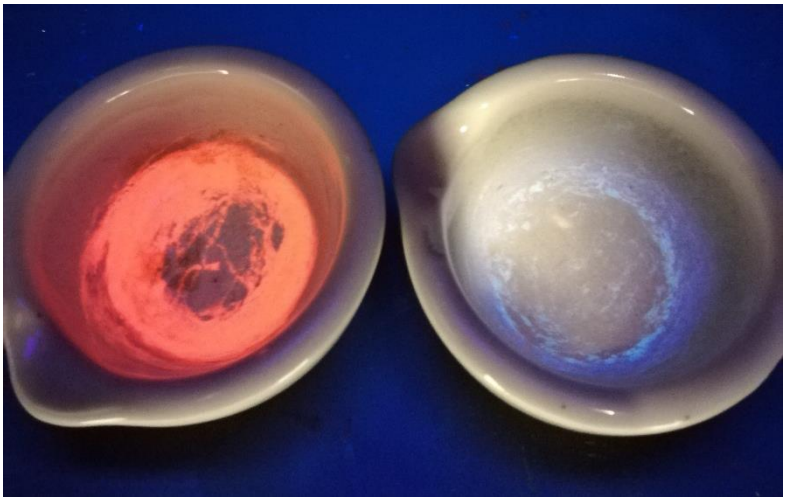

Figure 30: L4 and **L1** ligand complexes with europium under UV irradiation

Solutions of the lanthanide salts and the ligands were then reacted in a microwave reactor at a ratio of 3:1 ligand to metal ratio prior to vapour diffusion. A concentrated solution of the lanthanide-ligand mixture was prepared (40 mg of the ligand dissolved in 10 mL of solvent). For this method, the choice of solvent was quite important as the non-polar solvents are microwave transparent. Therefore, the complexation reactions had to be carried out in polar solvents such as methanol.

After reacting in the microwave, all lanthanide complexes were obtained using the vapour diffusion method with diethyl ether as the precipitant solvent (**Figure 31**). In the vapour diffusion method, a binary solvent system is used; one in which both the lanthanide and ligand are fully dissolved, and the second solvent has a lower boiling point than that of the first solvent (volatile solvent). Diethyl ether, which was the volatile solvent in this case, slowly diffused into the small glass vial causing oversaturation and nucleation of the complexes.[49] During the vapour diffusion process, it was vital to keep the containers on a steady surface to avoid mechanical disturbances such as vibrations or swirling.

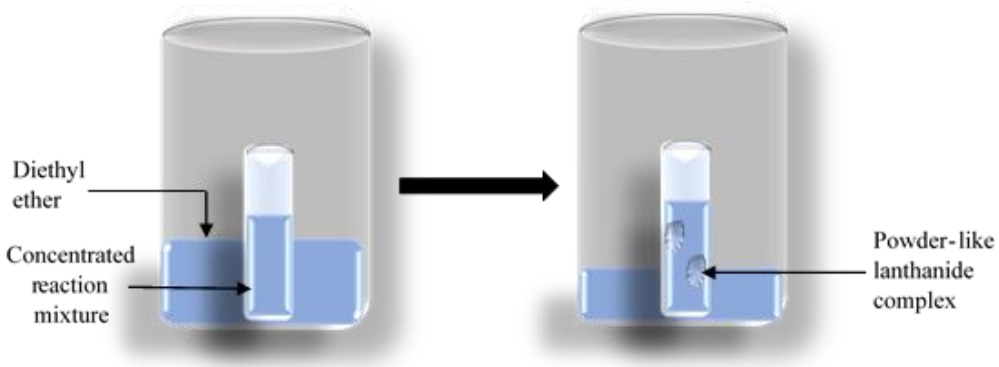

Figure 31: Schematic representation of vapour diffusion method used to obtain lanthanide complexes

Attempts were made to obtain single crystals of the lanthanide complexes using slow vapour diffusion method in three different solvents: hexane, petroleum ether and diethyl ether. However, lanthanide complexes were obtained as glass-like substances that formed on the

walls of the vials. These were scratched off and obtained as colourless solids. **Figure 32** shows the **L4** ligand complexed with europium, terbium and lanthanum salts after microwave irradiation.

Figure 32: Lanthanide complexes in solution under UV excitation; (left to right) **L4** complexed with europium, terbium and lanthanum respectively.

As shown in **Figure 32**, unlike the other two solutions, the lanthanum complex appears to be a colourless solution under UV irradiation. This is due to the filled electron configuration of lanthanum and therefore, it is not possible to observe any emission since direct excitation of 4f electrons is impossible. La^{3+} was chosen as a diamagnetic species so that the NMR of complexes could be obtained.[50]

Figure 33: L4 complexes with europium, terbium and lanthanum under UV excitation. (left to right)

Figure 33 shows the **L4** complexes obtained from vapour diffusion. When observed under UV irradiation, **L4** complexes of Eu^{3+} and Tb^{3+} showed bright luminescence in the solid state.

2.2 UV-VIS ANALYSIS OF LIGANDS AND LANTHANIDE COMPLEXES

UV-Vis spectra of all synthesized ligands and complexes were obtained at a concentration of 1 x 10^{-5} moldm^{-3} in different solvent systems depending on their solubility. For **L1**, maximum absorption was shown at a wavelength of 225 nm while other significant peaks of interest due to naphthalene ring appeared at 274 nm and 285 nm. The UV-Vis spectrum was obtained in acetonitrile. However, the ligand was initially dissolved in a mixture of DCM and methanol (3:7) due to low solubility issues and thereafter diluted in acetonitrile. The absorbance of Eu(**L1**)$_3$, Tb(**L1**)$_3$ and La(**L1**)$_3$ complexes at 274 cm^{-1} are aligned at the same wavelength range as of **L1**, showing 0.483, 0.373 and 0.370 absorbance values respectively which are nearly three times the value that of **L1** absorbance. Therefore, as shown in **Figure 34**, it demonstrates that three ligands of **L1** are chelated with one lanthanide ion at a 1:3 metal to ligand ratio.

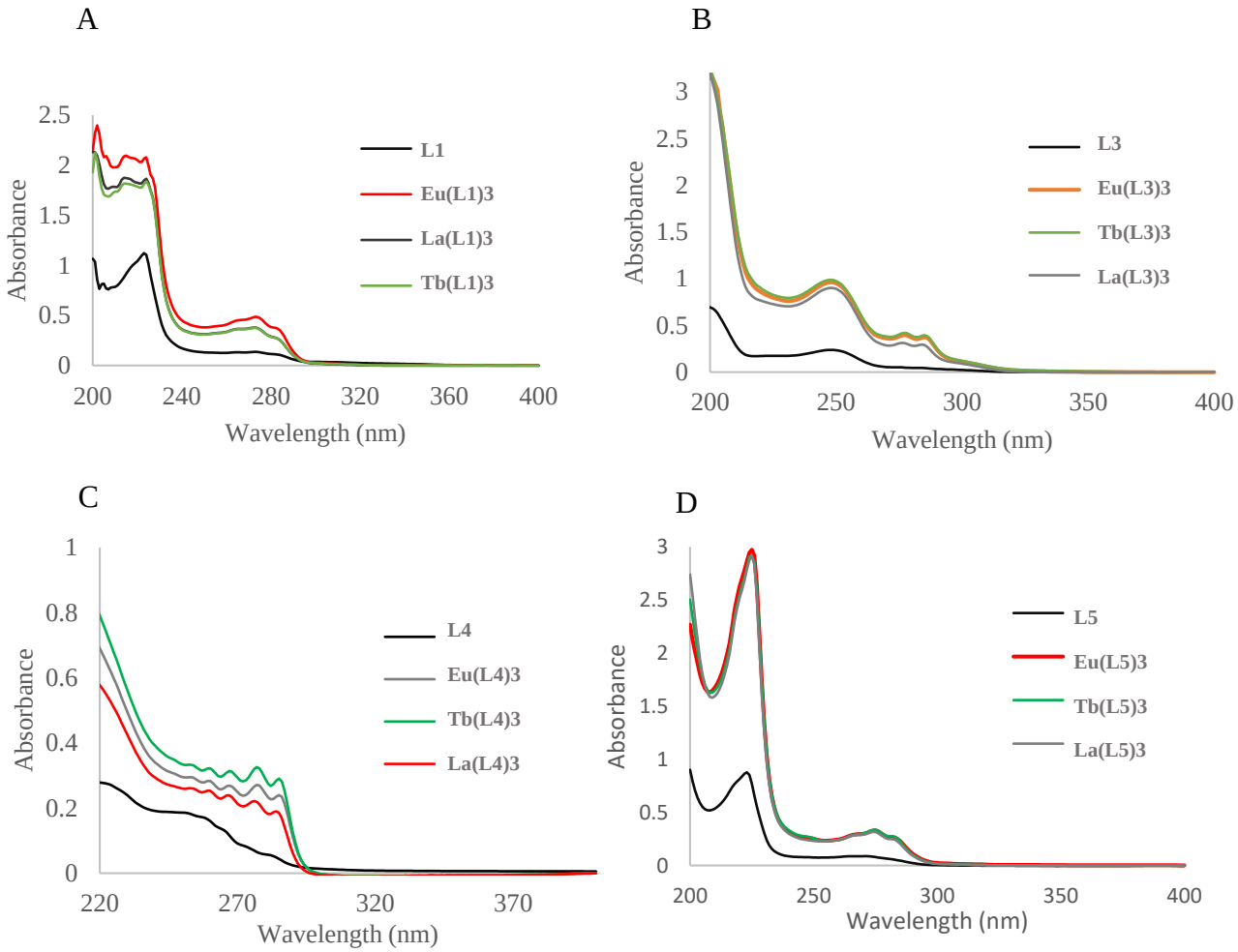

Figure 34: Absorbance spectra of complexes of ligands **L1** (A), **L3** (B), **L4** (C) and **L5** (D) with Eu^{3+}, Tb^{3+} and La^{3+}.

Other ligand complexes also showed a similar trend like **L1** complexes in absorbance demonstrating a 1:3 binding ratio of the ligand to metal as shown in **Figure 34**.

2.3 STRUCTURAL ANALYSIS OF LIGANDS AND COMPLEXES

Fourier transform infrared (FT-IR) spectrum is a widely used tool in structural analysis of complexes since it provides significant information about functional groups and shift on coordination to a metal.

In FT-IR spectra of all synthesized ligands, a characteristic sharp peak is observed in the range of ≈1600 cm^{-1} which corresponds to the C=O stretching of the PDC unit. The NH stretch is in the range 3200-3400 cm^{-1}. The formation of ligand complexes can be proved by the downfield shift of the C=O peak by 30-40 cm^{-1} to lower energy.[51] Furthermore, lanthanide complexes demonstrate additional peaks at 1268, 1221, and 1160 cm^{-1} corresponding to the triflate ion. Therefore, according to the FT-IR spectra, it is evidenced that the coordination of the lanthanide-ligand complexes was successful. **Figure 35** shows the downfield shift of C=O peak by 38 cm^{-1} for **L1** complexes compared to the ligand. Other spectra are given in the appendix section.

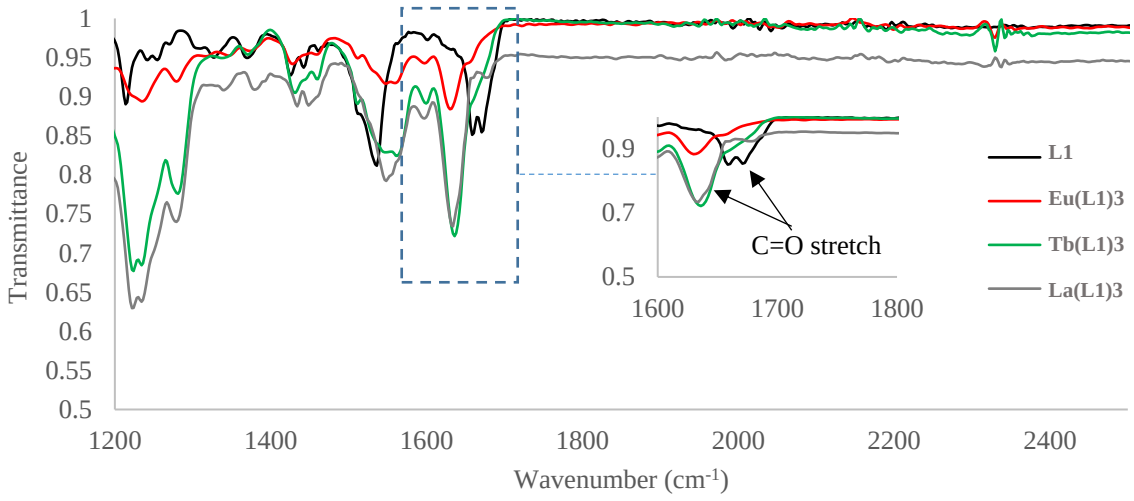

Figure 35: Stacked FT-IR spectra of **L1** ligand and complexes with europium, terbium and lanthanum showing the shift of the C=O stretch by 38 cm^{-1}.

^{1}H NMR spectra of the La(**L1**)$_3$ and La(**L4**)$_3$ complexes were obtained in $CDCl_3$ and a significant peak shift was observed in both spectra when compared to the relevant ligand. **Figure 36** demonstrates the stacked proton NMR of **L4** and La(**L4**)$_3$ complex. The NH proton of La(**L4**)$_3$ complex demonstrates a significant downfield shift by 0.4 ppm, with smaller shifts observed for other protons.

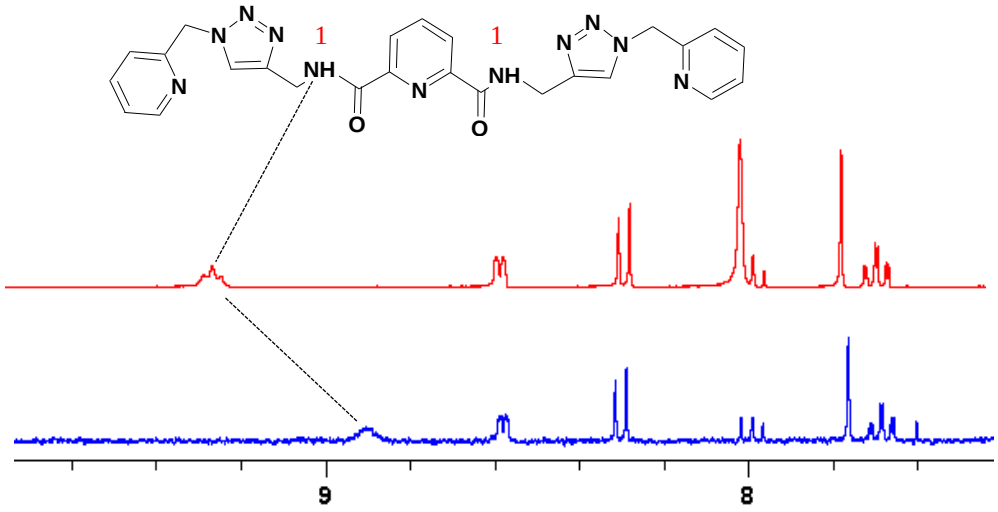

Figure 36: ^{1}HNMR spectrum of **L4** (top) and La(**L4**)$_3$ spectrum (bottom) showing the peak shift of the complex.

The ^{1}H NMR of La(**L5**)$_3$ complex shows 3 significant shifts by 0.1 ppm as shown in **Figure 37** due to the NH peak and the pyridine-H. Complexation of the lanthanide to the ligand is further evidenced by the proton NMR of La complexes.

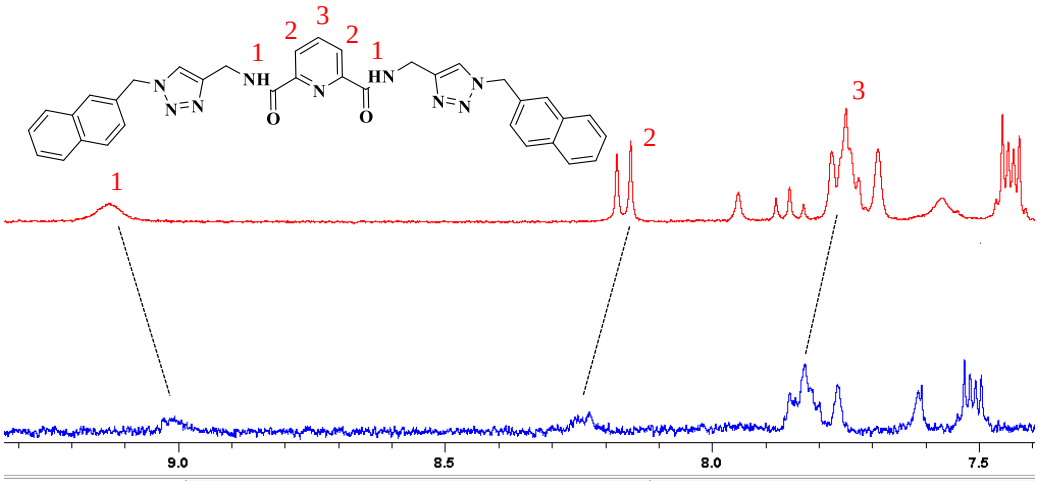

Figure 37: Stacked ^{1}HNMR spectrum of **L1** (top) and La(**L1**)$_3$ spectrum (bottom) showing the peak shift of the complex.

2.4 PHOTOPHYSICAL PROPERTIES OF COMPLEXES

The photophysical properties of complexes Eu(**L1**)$_3$, Tb(**L1**)$_3$, Eu(**L3**)$_3$, Tb(**L3**)$_3$, Eu(**L4**)$_3$, Tb(**L4**)$_3$, Eu(**L5**)$_3$ and Tb(**L5**)$_3$, were evaluated in acetonitrile solutions. The UV/Vis absorption spectrum of the **L1** and **L5** europium complexes were governed by an absorption of the naphthalene π→π* antenna with an absorption maximum (λ_{max}) at 275 nm and by the n→π* transition of the central PDC unit at 225 nm.[52,53] **Figure 38** shows the absorption spectra of **L5** complexes with Eu^{3+}, Tb^{3+}, and La^{3+}.

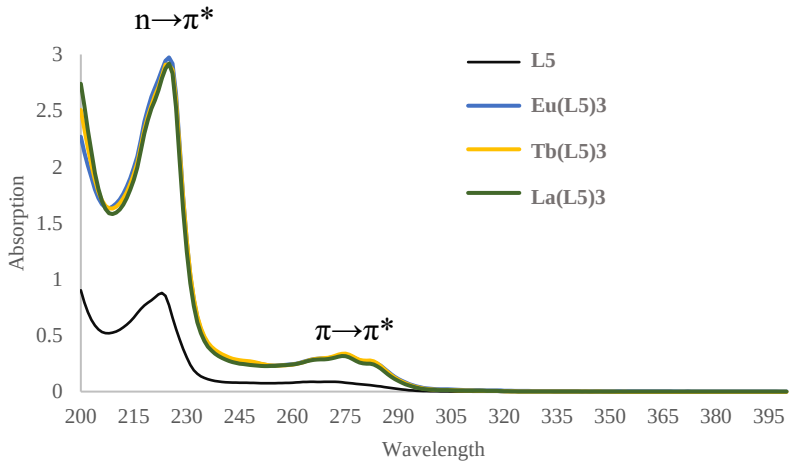

Figure 38: Absorption spectra of **L5** complexes with europium showing the π→π* and n→π* transitions

The ultraviolent spectral range falls between 198 nm- 380 nm and the visible spectral region covers the wavelength range from 380 nm-750 nm. **Figure 39** displays the hypothetical energy diagram showing the possible electronic transitions of a molecule in the UV/Vis region. However, within the UV/Vis spectral range, σ → σ* transition is not possible as it requires to absorb higher energy which does not fall in the UV/Vis range. Therefore, only π → π***** and n → π***** transitions can be observed within the UV/Vis range. According to the energy diagram (**Figure 39**), π → π***** transitions require higher energy. Thus, the π → π***** transitions are stronger than n → π* transitions. However, when the molecule is highly conjugated with pi systems, the gap between the π → π* orbitals become smaller than that of n → π*. Therefore,

in highly conjugated systems such as **L1**-**L6** ligands, $\pi \rightarrow \pi^*$ transition occurs at a longer wavelength and $n \rightarrow \pi^*$ transitions occur at a shorter wavelength as shown in **Figure 38**.

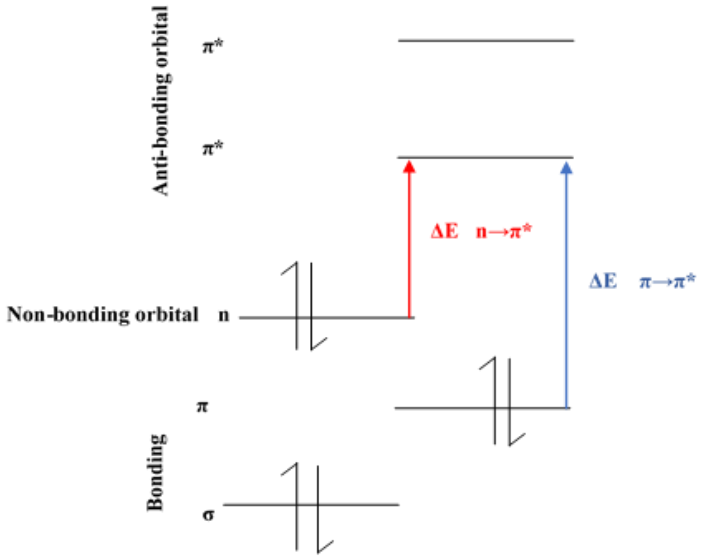

Figure 39: Hypothetical energy diagram showing the possible electronic transitions of a molecule

Emission spectra of complexes were measured in acetonitrile. The PDC-based ligand complexes demonstrate distinctive sharp bands corresponding to the europium-centred emission from $^5D_0$ excited states and terbium-centred emission from $^5D_4$ excited states upon excitation at 281 nm (**Figure 40**).[54] The observation of sensitized emission indicates the successful coordination of lanthanides to the ligand.

Similar emission peaks were observed for other europium and terbium complexes which are given in the appendix.

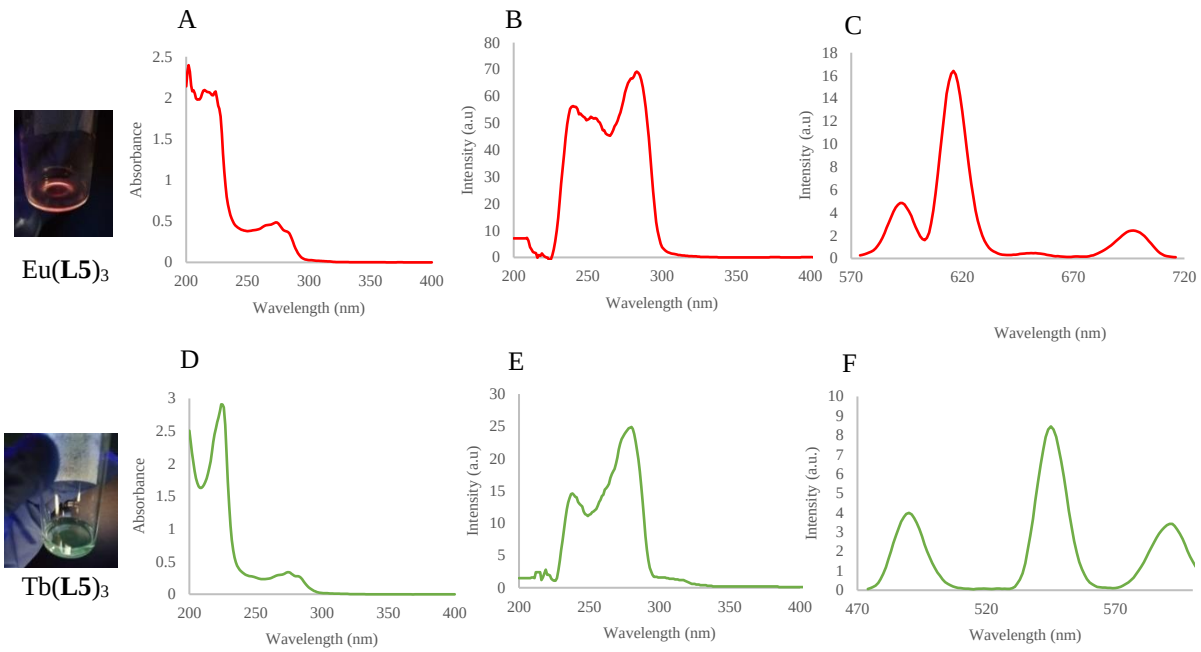

Figure 40: (A,D) The absorption spectrum, (B, E) the excitation spectrum, λ_{em} = 617 nm and (C,F) the phosphorescence emission spectrum, λ_{ex} = 286 nm of of Eu(**L5**)$_3$ and Tb(**L5**)$_3$ complexes in MeCN solution at RT (1 X 10^{-5} M)

Excitation of the naphthalene and pyridyl antenna at 274 nm cause Eu^{3+}-centred luminescence showing an efficient sensitization of the $^5D_0$ excited state following deactivation of the ^7F_J state.[55] As shown in **Figure 41**, line-like emission bands were observed at 582 nm, 595 nm, 615 nm, 650 nm, 705 nm corresponding to the $^5D_0 \rightarrow {}^7F_0$, $^5D_0 \rightarrow {}^7F_1$, $^5D_0 \rightarrow {}^7F_2$, $^5D_0 \rightarrow {}^7F_3$ and $^5D_0 \rightarrow {}^7F_4$ respectively. Most Eu^{3+} complexes show a very weak $^5D_0 \rightarrow {}^7F_0$ transition.[56] According to the Judd-Ofelt theory, the $^5D_0 \rightarrow {}^7F_0$ transition is a forbidden transition. However, it is assumed that this weak transition occurs because of *J*-mixing or the mixing of charge-transfer states of Eu^{3+} with wavefunctions of $4f^6$ energy levels.[57,58] The strongest emission band is observed due to the $^5D_0 \rightarrow {}^7F_2$ transition which causes the red colour of the Eu^{3+} complexes. Moreover, the $^5D_0 \rightarrow {}^7F_2$ transition is known as "hypersensitive-transition" as it is directly dependent upon the ligand.[56] In fluorescence mode, a weak emission due to the naphthalene antenna is observed in the 280- 450 nm region (**Figure 41**).

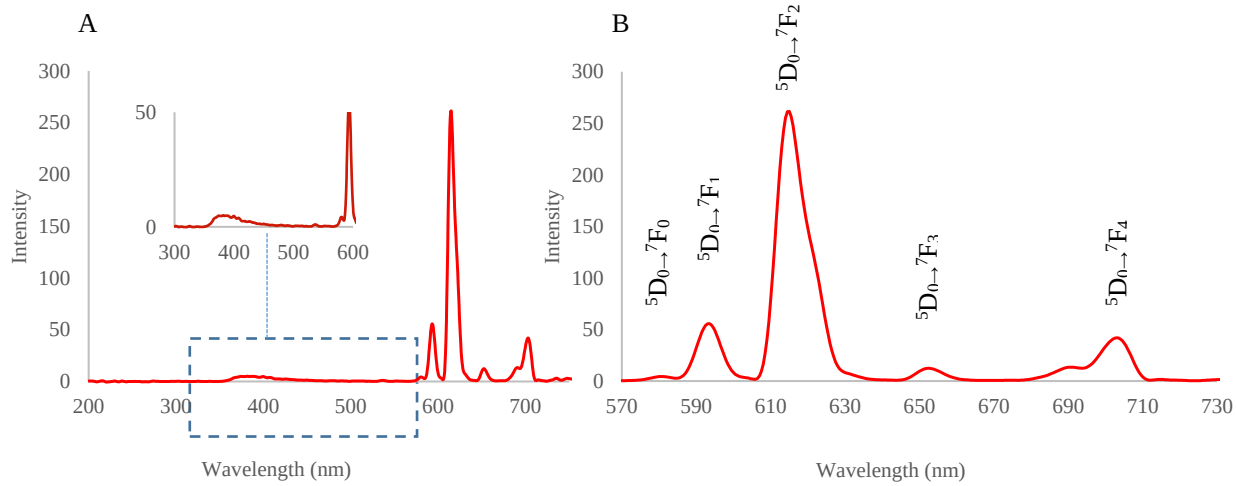

Figure 41: (A) Complete luminescence spectra of Eu(**L5**)$_3$ (B) luminescence spectra of Eu(**L5**)$_3$ showing the $^5D_0 \rightarrow {}^7F_J$ transitions in MeCN at RT (1 X 10^{-5} M, λ_{Exc} = 274 nm)

The characteristic emission bands for Tb(**L5**)$_3$ at excitation wavelength 281 nm, were observed at 492 nm, 545 nm, 587 nm and 623 nm corresponding to the $^5D_4 \rightarrow {}^7F_6$, $^5D_4 \rightarrow {}^7F_5$, $^5D_4 \rightarrow {}^7F_4$, $^5D_4 \rightarrow {}^7F_3$ respectively.[59–61]

The emission spectra of Tb(**L5**)3 is dominated by the $^5D_4 \rightarrow {}^7F_5$ transition at 545 nm. The intense green luminescence is also caused by $^5D_4 \rightarrow {}^7F_5$ transition as shown in **Figure 42**.

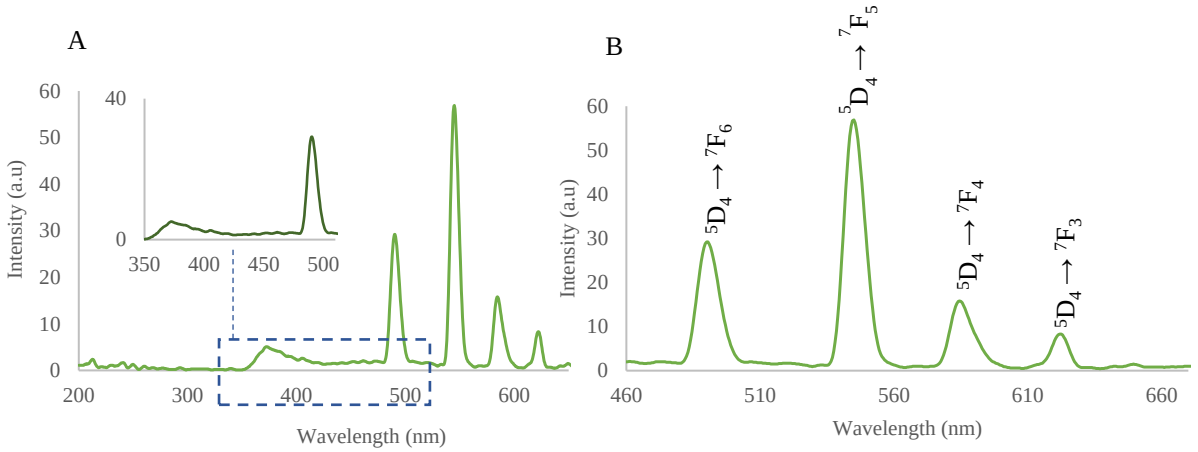

Figure 42: (A) Complete luminescence spectra of Tb(**L5**)$_3$ (B) luminescence spectra of Tb(**L5**)$_3$ showing the $^5D_4 \rightarrow {}^7F_J$ transitions in MeCN at RT (1 X 10^{-5} M, λ_{Exc} = 274 nm)

Figure 41 (A) and **Figure 42** (A) show the emission spectra of Eu(**L5**)$_3$ and Tb(**L5**)$_3$ complexes respectively. When looking at the emission spectra of both Eu(**L5**)$_3$ and Tb(**L5**)$_3$ complexes, a weak emission is observed in the 350 nm- 500 nm region due to a ligand-based residue. This implies that the energy was completely transferred from the π excited state of the ligand to the lanthanide-centred f-excited state.[62] Furthermore, the presence of characteristic emissions bands of Eu^{3+} ($^5D0 \rightarrow 7F_J$, where J =1−4) and Tb^{3+} $^5D_4 \rightarrow {}^7F_J$ where J =6−2) show that the lanthanides are coordinated to the ligands.[63]

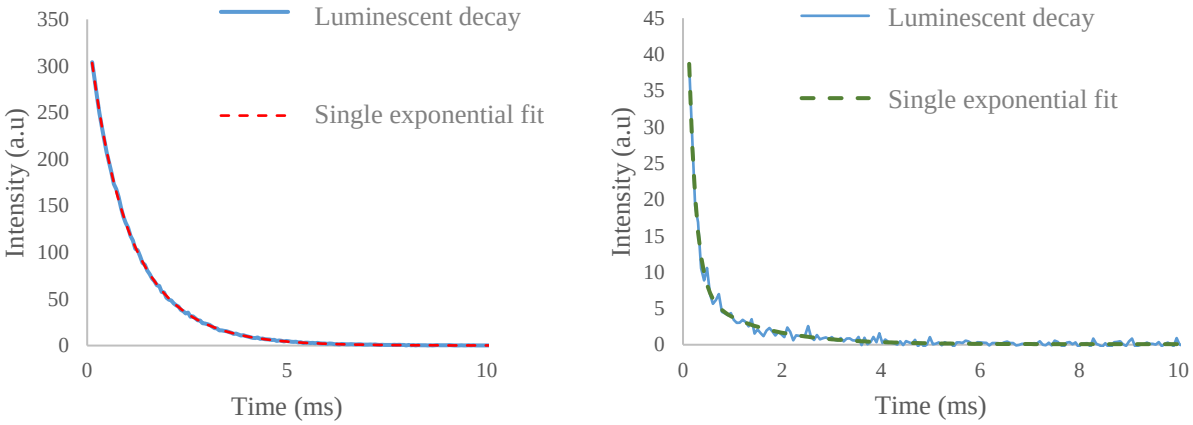

Figure 43: Lifetimes of Eu(**L1**)$_3$ and Tb(**L1**)$_3$ and their corresponding fits. (for Eu λ_{em}=616 nm and for Tb λ= 545 nm)

Lifetime measurements were obtained with exponential components for emission decay of the europium and terbium centred luminescence (**Figure 43**). The ligand nature, solvent and specific geometries around the lanthanide ion affects the luminescence lifetimes of lanthanide complexes.[64] The decay curves were collected in triplicate and the average was taken at λ_{ex} = 274 nm. The average lifetimes of each complex are given in **Table 2**. The excited stated lifetimes of both Eu(**L1**)$_3$ and Tb(**L1**)$_3$ were best fitted to single exponential decay giving τ =1.065 ms and τ = 0.287 ms respectively. It suggests that presence of a single luminescent species. The longest lifetime was observed for Eu(**L1**)$_3$ complex. The complexes Eu(**L4**)$_3$,

Tb(**L4**)$_3$, Eu(**L5**)$_3$ and Tb(**L5**)$_3$ were fitted into a double exponential decay indicating the presence of multiple luminescent components. Literature reveals that similar structures demonstrate Eu^{3+} excited state lifetimes between 0.5 ms and 1.10 ms in acetonitrile.[65]

Table 2: Lifetime measurements of lanthanide complexes.

Lanthanide complex	Average τ (ms)
Eu(**L1**)$_3$	1.065
Tb(**L1**)$_3$	0.287
Eu(**L3**)$_3$	0.250
Tb(**L3**)$_3$	0.134
Eu(**L5**)$_3$	0.229
Tb(**L5**)$_3$	0.260

2.5 MONITORING COMPLEXATION AND SELF-ASSEMBLY STUDIES

2.5.1 Fluorescence Titration of L5 against Eu^{3+} in acetonitrile

The self-assembly studies between **L5** and Eu^{3+} were carried out in acetonitrile solution at room temperature. The changes observed upon titrating **L5** against $Eu(CF_3SO_3)_3 \cdot 6H_2O$ is demonstrated in **Figure 44**. In the emission spectra, the emission maximum was observed at 616 nm for $^5D_0 \rightarrow {}^7F_4$ transition. The addition of Eu^{3+} caused a gradual increase in the emission bands. Changes in the emission peaks were mainly observed at 616 nm. When the Eu^{3+} was added, the increase in emission intensity was first observed at 0.4 equivalents of Eu^{3+}. That indicates that the desired formation of the ligand and metal complex occurs at a stoichiometric ratio of 3:1. The plot started to plateau at the addition of 1.0 equivalent, showing a slower increase of the emission bands after 0.4 equivalent points.

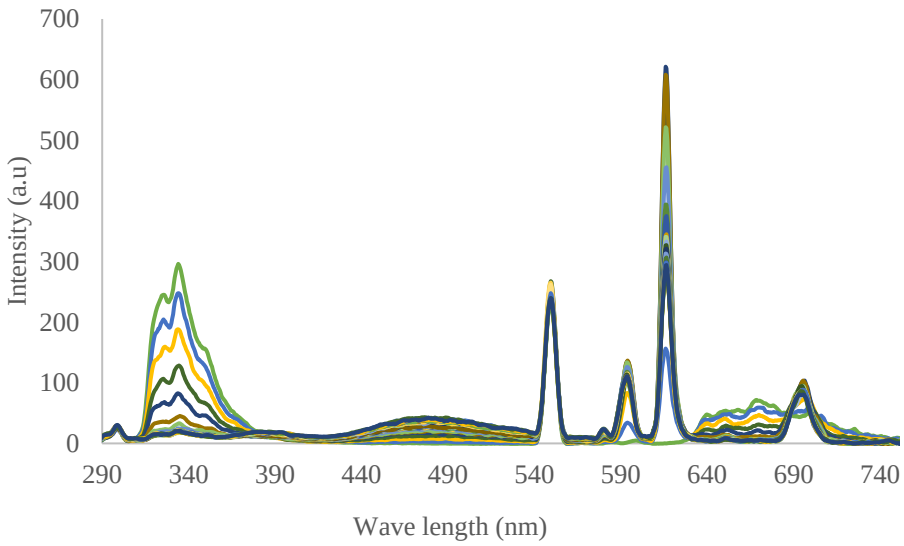

Figure 44: The changes in fluorescence spectra of **L5** (1×10^{-5} M) upon addition of Eu^{3+} triflate in acetonitrile

Emission intensities of $^5D_0 \rightarrow {}^7F_4$ at 616 nm as a function of added Eu^{3+} equivalents are shown in **Figure 45**. It reveals that the emission intensity rapidly increases to maximum at nearly 0.4

equivalents, then decreases gradually and start to plateau after the addition of 1.0 equivalent of Eu^{3+} as would be expected for initial 3:1 binding followed by 2:1 and 1:1 binding.

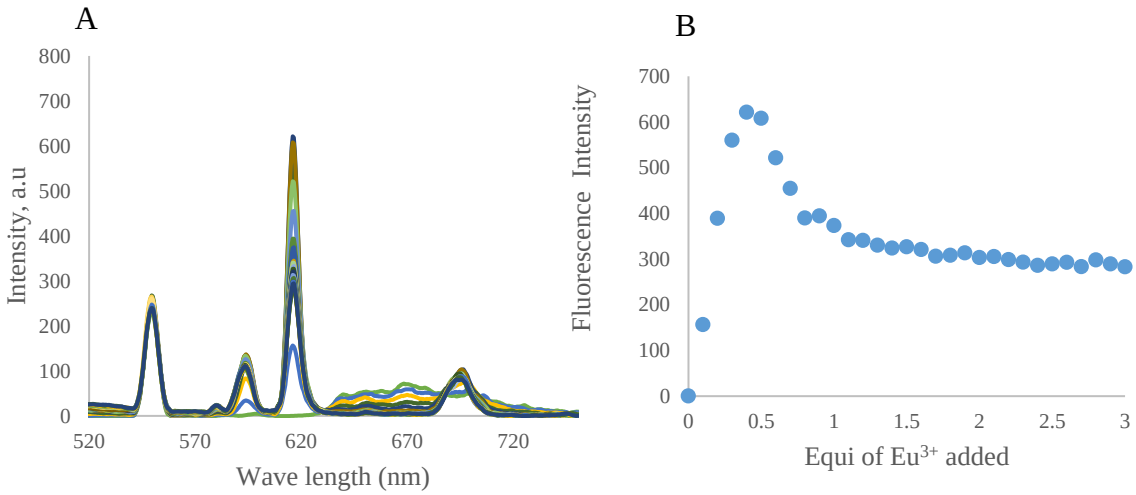

Figure 45: Emission intensities of $^5D_0 \rightarrow {}^7F_4$ at 616 nm as a function of added Eu^{3+} equivalents

In order to acquire a better understanding of the formation of self-assembly complexes, the analysis data was further processed using nonlinear regression analysis (using the ReactLab™ software) and obtained the speciation plot showing in **Figure 46**. The speciation plot confirmed the presence of four species: L, ML, ML2, and ML3. The experimental data was successfully fitted into the software and it obeys the following equilibria and the associated binding constants.

$$Eu + \mathbf{L5} \longleftrightarrow Eu\mathbf{L5} \qquad (\text{Log } \beta_{1:1})$$

$$Eu + 2\mathbf{L5} \longleftrightarrow Eu(\mathbf{L5})_2 \qquad (\text{Log } \beta_{1:2})$$

$$Eu + 3\mathbf{L5} \longleftrightarrow Eu(\mathbf{L5})_3 \qquad (\text{Log } \beta_{1:3})$$

Figure 46 shows the speciation distribution plot of this titration. According to that, the percentage yield of $Eu(\mathbf{L5})_3$ formation at 0.3 equivalents of Eu^{3+} is 55.7%. In addition to the desired 1:3 stoichiometry, 1:1 and 1:2 ratios are also formed at the same time. Hence, $Eu(\mathbf{L5})_2$ was formed giving a percentage yield of 59.3% whereas Eu**L5** gave a percentage yield of

75.6% at 0.5 and 1.0 equivalents respectively. From the analysis of **L5**, binding constants were obtained as 8.497, 16.009 and 22.550 for Eu**L5**, Eu(**L5**)$_2$ and Eu(**L5**)$_3$ respectively. The binding constants obtained from the emission titration (**Table 3**) are consistent with the values found for similar structures according to literature.[66]

Table 3: Binding constants and % formation of species obtained for **L5** vs Eu^{3+} from fluorescence titration

Binding Constants		±	Percentage formation of species
Log $\beta_{1:1}$	8.5	± 0.081	55.7 %
Log $\beta_{1:2}$	16.0	± 0.147	59.3 %
Log $\beta_{1:3}$	22.5	± 0.195	75.6 %

According to the speciation distribution plot, all species were present in the solution until the end of the titration. At the end, the Eu(**L5**) (1:1) complex was present in 95% whereas Eu(**L5**)$_2$ and Eu(**L5**)$_3$ were present in 4.2% and 0.1% respectively.

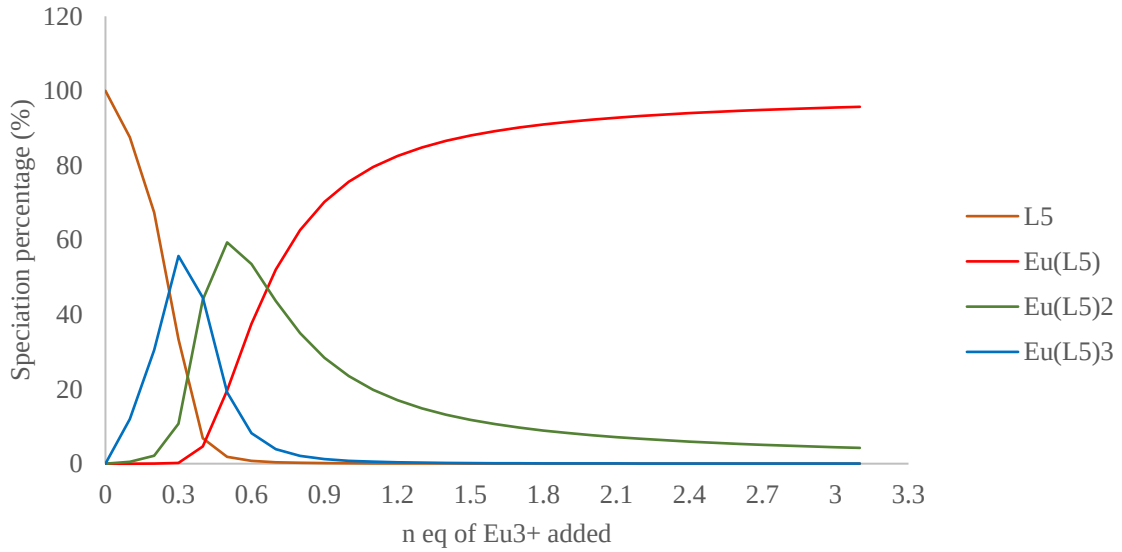

Figure 46: Speciation-distribution plot obtained from fitting the experimental data of the emission spectrum of **L5**, using ReactLab™ upon addition of Eu^{3+} triflate in CH_3CN. (RT= 25^0C, [Eu^{3+} triflate] = 0.05mM)

As shown in **Figure 45** (A), monitoring the shifts in the ligand-centred emission during the titration was difficult as the ligand fluorescence was poor.

The emission bands of Eu^{3+} due to the transition of $^5D_0 \rightarrow {}^7F_J$ (where J= 1,2,3,4) occurred when the ligand was excited at 274 nm. Therefore, it indicates that the Eu: **L5** assemblies are formed upon addition of Eu^{3+}. The emission bands at 594 nm and 695 nm due to the transition $^5D_0 \rightarrow {}^7F_{1,4}$ showed an increase in the intensity up to 0.4 equivalents addition of Eu^{3+} and started to plateau afterwards with each addition. But monitoring the emission band at 616 nm due to $^5D_0 \rightarrow {}^7F_2$ was clear as it gradually increased up to 0.4 equivalents addition and after that, with each addition, the increase in intensity dropped due to the saturation of luminescence intensity.

2.5.2 UV Titration of L5 against Eu^{3+} in acetonitrile.

The UV titration of **L5** against Eu^{3+} was carried out in acetonitrile solution at 25˚C. As shown in **Figure 47**, the absorption spectrum of **L5** demonstrated two maxima at 224 nm and 274 nm. Each addition of 0.1 equivalents of Eu^{3+} resulted in hyperchromicity.[67] It was expected to obtain a similar result as those obtained for Eu^{3+} emission. Unfortunately, the experimental data was unable to be fitted into the ReactLab™ software package. However, when the absorbance at 274 nm was plotted against the Eu^{3+} equivalents added, it showed a sudden increase at 0.5 and started to decrease gradually and began to plateau after 1 equivalent of Eu^{3+} addition. That indicates the potential ability of the ligand and the lanthanide to self-assemble.

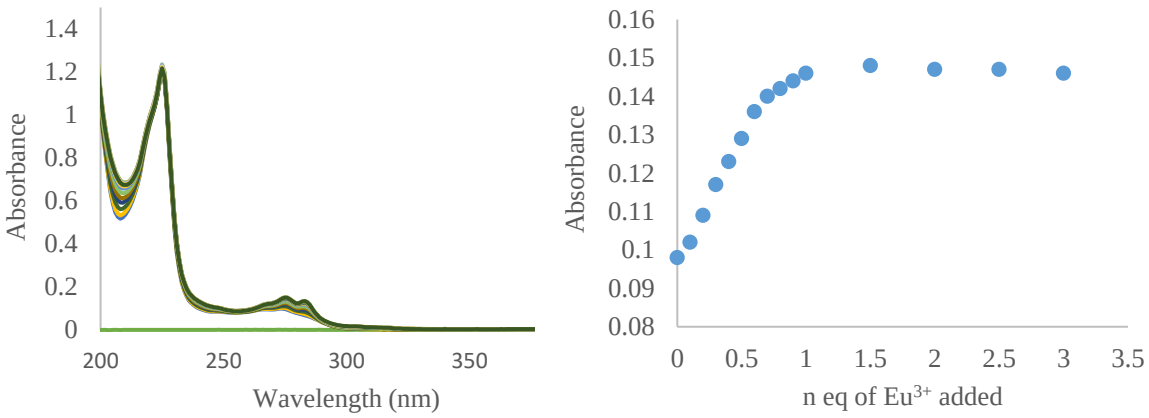

Figure 47: Absorption spectrum of **L5** (1×10^{-5} M) upon addition of Eu^{3+} triflate in acetonitrile at 274 nm.

CHAPTER 3: CONCLUSION, CHALLENGES AND FUTURE WORK

3.1 CONCLUSION AND CHALLENGES

The primary objectives of this research project were as follows;

- Synthesis and characterization of new symmetrical and asymmetrical 2,6-pyridinedicarboxamide-1,2,3 triazole ligand systems.
- Complexation of synthesized ligands with europium, terbium and lanthanum ions.
- Characterization of the lanthanide complexes.
- Determining the photophysical properties and carrying out complexation and self-assembly studies of the synthesized ligands with europium and terbium.
- Obtaining single crystals of the lanthanide complexes.

At the end of the research year, many of the stated objectives were able to be fulfilled. Four symmetrical ligand systems (**L1**-**L4**) and two asymmetrical ligand systems (**L4** and **L6**) were successfully synthesized. All synthesized ligands were characterized by ^{1}H NMR, ^{13}C NMR, and FT-IR, however only **L1**, **L4**, **L5** and **L6** were characterized by mass spectrometry due to solubility issues. Several attempts were made to dissolve **L2** and **L3** in different solvent systems at a concentration of 1 x 10^{-5} moldm^{-3}. **L3** was dissolved in ethanol at 60^{0} C, but it eventually crashed out at room temperature therefore **L3** could not be analysed by mass spectrometry.

Ligands **L1**, **L3**, **L4** and **L5** were successfully complexed with europium, terbium and lanthanum. However, complexation of **L2** was unsuccessful due to its low solubility. Structural analysis of FT-IR demonstrates that the ligands were coordinated with the lanthanide ions. The brightest visible luminescence was observed in **L4** complexes. Moreover, the ^{1}HNMR spectra of lanthanum complexes show that the coordination with the lanthanum ion was successful.

The UV analyses of the complexes also confirm that the ligands are coordinated to the lanthanide ion at a ratio of 3:1.

Both europium and terbium complexes of **L1**, **L4**, and **L5** present strong photoemission of red and green in solution. Successful coordination of the ligand to the lanthanide ions was further evidenced by photophysical studies. Photophysical data of complexes demonstrated the presence of the characteristic emission bands of europium and terbium ions.

Complexation and self-assembly studies of **L5** ligand with Eu^{3+} using UV-Vis and fluorescence spectroscopic titrations show that the expected 3:1 ligand: lanthanide ratio is observed and the bulky triazole substituents do not affect complex formation. This is important as it will allow us to move on to more complex and larger ligands that incorporate amino acids/peptides. The speciation plot obtained by the Reactlab software showed the formation of Eu(**L5**)$_3$ complex in 55.7% yield.

Several attempts were made to obtain single crystals of the complexes through vapor diffusion methods in three different solvent systems. Unfortunately, no single crystals were obtained, with all complexes being isolated as powders.

3.2 FUTURE WORK

Future work includes developing and characterizing additional ligand systems based on PDC-triazole scaffolds and their complexation with different lanthanide ions. Additionally, preparing multi-metallic structures (e.g. Ln-Zn) using **L4** where the pyridine ring would act as a secondary coordination site for transition metals.

Moreover, amino acids can be incorporated onto the amino group of the ligand for biological (imaging) and sensing applications as shown in **Figure 48**. Linking two ligands through a suitable linker/ spacer would open up new possibilities to assemble helical systems for

enhanced luminescent properties and construction of larger more complex metallosupramolecular assemblies.

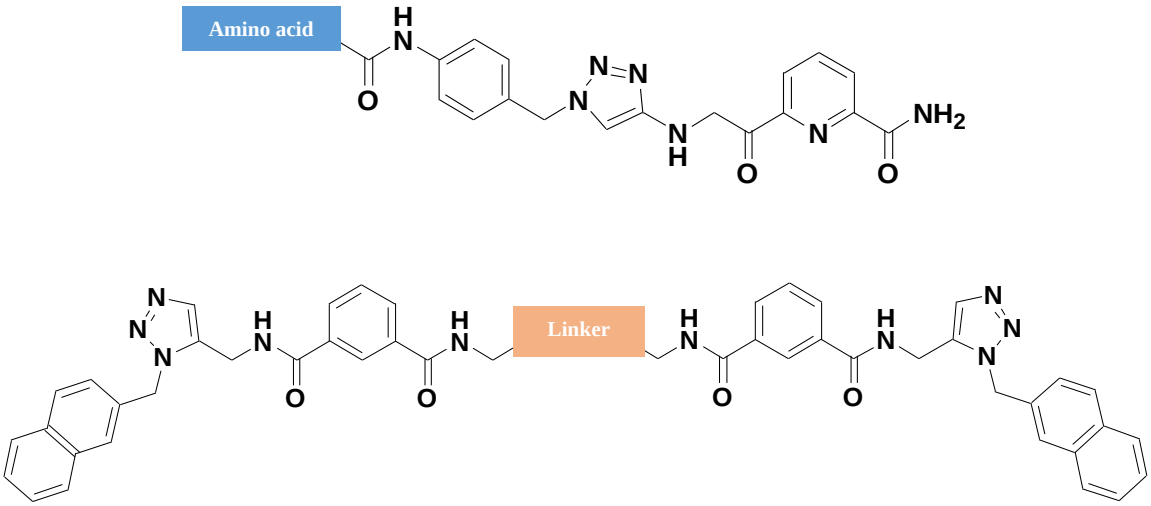

Figure 48: Incorporating amino acids onto the amino group of the ligand for biological (imaging) and sensing applications (top). Linking two ligands through a linker to assemble helical systems for enhanced luminescent properties and construction of larger more complex metallosupramolecular assemblies (bottom).

CHAPTER 4: EXPERIMENTAL

4.1 GENERAL REMARKS

All chemicals including the primary starting materials Pyridine 2-6-dicarboxylic acid, 2,6-Pyridinedicarbonyl dichloride and other reagents were commercially purchased, and analytical grade solvents were used for all reactions hence further purification was not needed. The solvents used for UV and, fluorescence studies were of HPLC grade whereas LC-MS grade solvents were used for mass spectrometric analysis. All glassware was rinsed with acetone, further cleaned in laboratory glassware washer and dried in the oven. Glassware used for complexation was used directly after purchase. Prior to the mass spectroscopy analysis, glassware was rinsed with distilled water, millipore water and oven dried.

Newly synthesized ligands were characterized by ^{1}H NMR, ^{13}C NMR, and FTIR. Ln-Ligand complexes were characterized by FTIR, UV, and fluorometer. Nuclear Magnetic Resonance characterization was carried out on a Bruker 300 spectrometer in commercially available deuterated solvents and the data were further processed using TopSpin 4.0.6 software. δ values were recorded in ppm referring to $SiMe_4$ (= 0 ppm) and the reference signal of the solvent used. Melting points of the synthesized compounds were determined on melting point apparatus. Neat solid samples of both ligands and complexes were analysed with a Bruker's ALPHA FT-IR spectrometer and data were processed on OPUS spectroscopy software. The infrared spectra were recorded in cm^{-1} and plotted on Excel. The local minima points of the FTIR spectra were integrated using a Microsoft Excel formula for better accuracy.

UV spectra were studied on Shimadzu UV-Vis spectrometer. Fluorescence emission spectra of lanthanide complexes and self-assembly studies were carried out with an RF-6000 Spectro fluorophotometer. Phosphorescence studies and lifetime measurements were measured with an

Agilent Cary Eclipse Fluorescence Spectrophotometer. Preparation of solutions of both ligands and complexes for photophysical studies was carried out in HPLC grade acetonitrile at a concentration of 0.00001 M. All data were collected as a comma-separated-values (.CSV) file and plotted on Excel.

Ligands **L1**- **L6** were synthesized according to copper(I)-catalysed alkyne-azide cycloaddition in a mixture of DMF: H_2O (4:1) as the solvent. Sodium azide is known to be a hazardous and a deadly chemical as it rapidly reacts with water and acids to produce a toxic gas. Therefore, when handling NaN_3, safety precautions were strictly followed. Use of a metal spatula was always avoided while it was always measured into a clean and dry glassware. NaN_3 was added at last into the other reactants and always carried out inside the fume hood. When synthesising N^2,N^6-Di-2-propyn-1-yl-2,6-pyridinedicarboxamide, the reaction was carried out in DCM for the ease of removing the solvent, however, in literature DMF has been used as the solvent for this reaction.[68] All of the bis-ligands were obtained as a white colour solid while in literature it is mentioned that L2 was obtained as a pale-yellow colour solid.[68] It was observed that the pale-yellow colour was due to the excess Cu^{2+} ions. Therefore, EDTA solution in NH_4OH was used to remove the excess Cu^{2+} bound to the ligand.

For complexation reactions, Terbium (III) tris(trifluromethanesulfate), Europium (III) tris(trifluromethanesulfate) and Lanthunum(III) tris(trifluromethanesulfate) were commercially purchased as the lanthanide metal salts. Complexation reactions were carried out in a microwave reactor. Ligands and the lanthanide salt of interest were initially sonicated to get a clear solution of the Metal-ligand complex. Then the reactions were performed under microwave irradiation for 30 minutes in analytical grade solvents. The resulting clear solution was split into three vials and subjected to vapour diffusion in diethyl ether jars. The solid complexes appeared as oil-like substances and were scraped off the glass surface and analysed.

4.2 SYNTHESIS OF LIGANDS

4.2.1 Symmetrical / Bis-systems

Synthesis of N^2,N^6-Di-2-propyn-1-yl-2,6-pyridinedicarboxamide

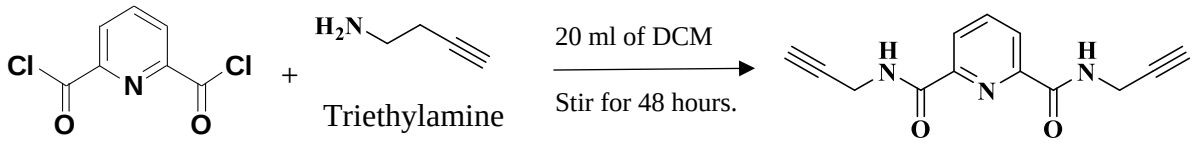

Propargyl amine (0.313 ml, 4.9 mmol) and Triethylamine (1.80 ml, 13.0 mmol) were dissolved in 20 mL DCM and cooled in an ice bath. 2,6-Pyridinedicarbonyl dichloride (500 mg, 2.45 mmol) was slowly added into the cool suspension of Propargyl amine and Triethylamine. The reaction mixture was left to stir for 48 hours. This was then washed with HCl (1 M, 20 mL), $NaHCO_3$ (1 M, 20 mL) and water. The organic layer was evaporated using the rotary evaporator under 832atm at 40°C. A pale white colour solid (333 mg, 63.0%) was collected. Melting Point 185.4°C (Decom. colourless to brown), ^{1}H NMR (300 MHz, $CDCl_3$), δ= 8.37 (2H, d, J=7.8 Hz, Pyridine-2H), δ = 8.02 (1H, t, J=7.5 Hz, Pyridine-H), δ = 7.96 (2H, s, NH), δ =4.31 (4H, dd, J=2.6 Hz, 3.2 Hz, NH-CH_2), δ = 2.28 (2H, t, 4.7 Hz, C-CH), ^{13}C NMR (75 MHz, $CDCl_3$,), δ=163.15, 148.39, 139.20, 125.61, 79.25, 71.89, 29.29

Synthesis of L1

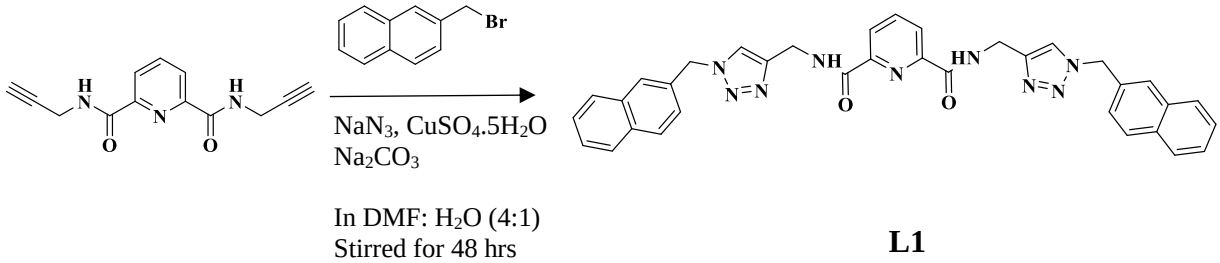

L1

N^2,N^6-Di-2-propyn-1-yl-2,6-pyridinedicarboxamide (200 mg, 0.419 mmol) was dissolved in DMF/ H_2O (4:1, 20 mL). NaN_3 (2.2 eq, 0.0599g, 0.92 mmol), $CuSO_4.5H_2O$ (0.4 eq, 0.041 g, 0.16 mmol), Ascorbic acid (2.2 eq, 0.162 g, 0.419 mmol), 2-(Bromomethyl)naphthalene (2.0 eq, 0.185 g, 0.838 mmol) were then added in to the reaction mixture. The reaction mixture was stirred for 48 hours. Then EDTA (50 ml, 0.1 M) was added into the pale-yellow colour reaction mixture. A white colour precipitate was formed upon addition of EDTA. The precipitate was then filtered off on to a filter paper followed by a water and ether wash to wash off excess DMF. The resulting precipitate was left to dry overnight. Yield (0.422 g, 82.74%), Melting point 131.4 ^{0}C, LRMS (ESI^+) (m/z) calculated for $(C_{35}H_{29}N_9O_2 + Na)^+$ 630.23 found 630.2 and $(C_{35}H_{29}N_9O_2 + K)^+$ 646.21 found 646.2, ^{1}H NMR (300 MHz, DMSO-d_6), δ=9.8609 (2H, t, J=6 Hz, NH), δ= 8.1306 (3H, m, Pyridine), δ= 8.1058 (2H, s, triazole), δ= 7.8556 (8H, m, naphthalene H), δ= 7.4969 (4H, m, naphthalene H), δ=7.4142 (2H, d, J=3.0 Hz, naph H), δ= 5.7145 (4H, s, CH_2), δ= 4.5854 (4H, d, J= 6.0 Hz, NH-CH_2), ^{13}C NMR (75 MHz, DMSO) δ= 163.6, 148.9, 145.6, 139.9, 134.0, 133.1, 132.9, 128.9, 128.0, 127.4, 127.0, 126.9, 126.2, 123.7, 53.3, 34.9, IR U/cm^{-1} : 3470, 3382, 3278, 3121, 3078, 3055, 1670, 1658, 1632, 1601, 1536, 1460, 1442, 1426, 1370, 1326, 1309.7, 1270, 1254, 1242, 1213, 1173, 1142, 1117, 1075, 1054, 1026, 1020, 999, 981, 964, 946, 930, 901.7, 891.5, 883.3, 875.2, 852.7, 836.4, 824.2, 787, 767, 748, 730, 701, 677, 646, 640, 618.1, 593, 565, 542, 534, 514, 493, 473, 426, UV/Vis (Acetonitrile) λ_{max} (ε), 222 = 112,000 $Lmol^{-1}cm^{-1}$, 265 = 13,190 $Lmol^{-1}cm^{-1}$, 274 = 13,470 $Lmol^{-1}cm^{-1}$, 286 = 9200 $Lmol^{-1}cm^{-1}$

Synthesis of L2

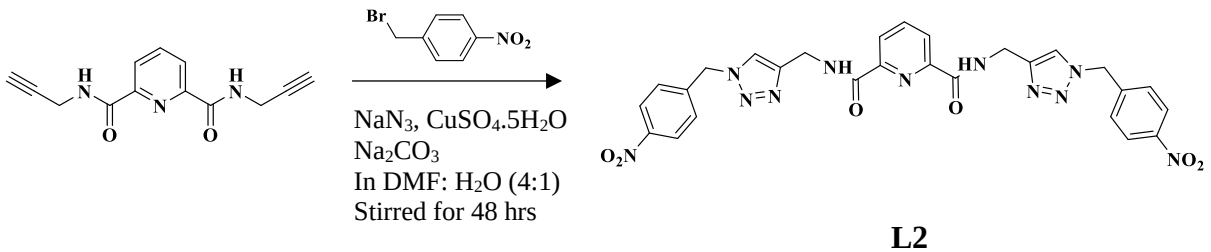

L2

N^2,N^6-Di-2-propyn-1-yl-2,6-pyridinedicarboxamide (100 mg, 0.47 mmol) was dissolved in DMF/ H_2O (4:1, 20 mL). NaN_3 (0.122g, 0.94 mmol), $CuSO_4.5H_2O$ (0.75 g, 0.75 mmol), ascorbic acid (0.165 g, 0.47 mmol), nitro benzyl bromide (0.213g, 0.47 mmol) were then added. The reaction mixture was stirred for 48 hours. Then EDTA (50 ml, 0.1 M) was added into the reaction mixture. The precipitate was then filtered off on to a filter paper followed by a water and ether wash to get rid of the excess DMF. The precipitate was left to dry overnight. A white colour precipitate was collected. It was kept in a desiccator overnight for further drying to obtain a dry powder. Yield (0.196 g, 79.1%), Melting point 234.2^0 C, ^{1}H NMR (300 MHz, DMSO, ppm), δ= 9.92 (2H, t, J=6.19 Hz, NH), δ= 8.24 (3H, m, Pyridine), δ= 8.21 (4H, m, Benzene H), δ= 8.12 (2H, s, Triazole), δ= 7.54 (4H, d, Benzene H), δ=5.72 (4H, s, CH), δ= 4.62 (4H, d, J= 6.1, NH-CH_2), ^{13}C NMR (75 MHz, DMSO, ppm) δ= 163.6, 148.9, 147.6, 145.8, 143.9, 140.1, 129.5, 124.9, 124.0, 81.5, 28.5, IR U/cm^{-1} : 3362, 3264, 3133, 1667, 1603, 1516, 1444, 1426, 1389, 1340, 1297, 1248, 1230, 1218, 1169, 1149, 1122, 1106, 1077, 1053, 1034, 1016, 1000, 969, 940, 902, 871, 847, 804, 792, 763, 730, 712, 683, 647, 634, 561, 534, 524, 508, 486, 465

Synthesis of L3

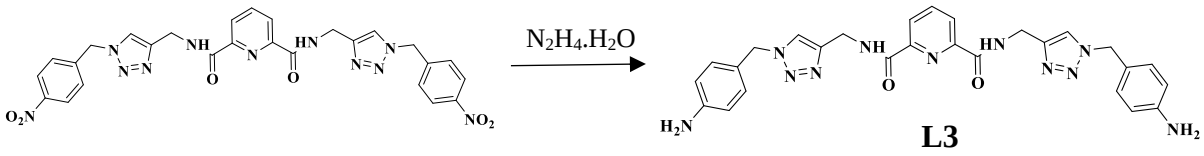

L2 (200 mg) was mixed with excess hydrazine hydrate (4-5 drops), 50 mg of Pd/C and refluxed at 60^0C for 4 hours in ethanol as the solvent. Pd/C was filtered off and the filtrate was evaporated *in vacuo* at 40^0 C, 175 mbar and kept in a desiccator for further drying. The white precipitate was then collected. (Yield 162 mg, 90 %), ^{1}H NMR (300 MHz, DMSO), δ= 9.8442 (2H, t, J=6.03 Hz, NH), δ= 8.1352 (3H, m, Pyridine), δ= 7.8787 (2H, s, Triazole), δ= 7.0118 (2H, d, , J=8.40 Hz Benzene H), δ= 6.4917 (2H, d, , J=8.40 Hz Benzene H), δ=5.2990 (4H, s, CH), δ= 4.5532 (4H, d, J= 6.0, NH-CH_2), ^{13}C NMR (75 MHz, DMSO) δ= 163.6, 148.9, 145.4, 140.0, 129.8, 124.9, 122.9, 114.1, 53.2, 34.8 , IR U/cm^{-1}: 3403, 3329, 3247, 3125, 2993, 2921, 2852, 2729, 2674, 2627, 2570, 2562, 2548, 2525, 2519, 2495, 2446, 2417, 2379, 2348, 2334, 2323, 2311, 2299, 2291, 1658, 1616, 1536, 1518, 1454, 1442, 1430, 1371, 1332, 1312, 1299, 1269, 1226, 1216, 1177, 1128, 1085, 1071, 1063, 1053, 1042, 1022, 1002, 975, 947, 936, 926, 916, 845, 828, 802, 775, 747, 704, 681, 665, 651, 539, 510, 490, 449, 428, 406, UV/Vis (Acetonitrile) λ_{max} (ε), 200 = 70,100 $Lmol^{-1}cm^{-1}$, 248 = 23,700 $Lmol^{-1}cm^{-1}$, 278 = 4900 $Lmol^{-1}cm^{-1}$, 285 = 4300 $Lmol^{-1}cm^{-1}$

Synthesis of L4

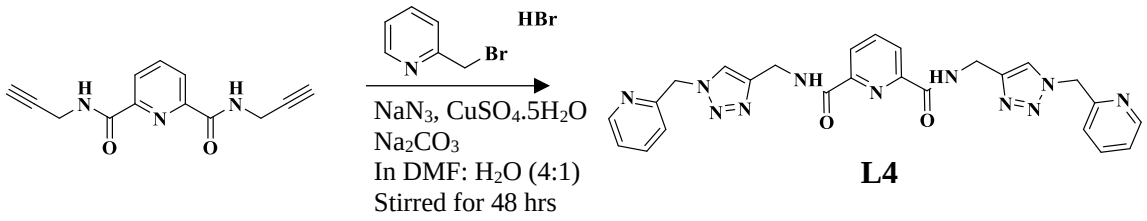

L4

N^2,N^6-Di-2-propyn-1-yl-2,6-pyridinedicarboxamide (200 mg, 0.82 mmol) was dissolved in DMF/ H_2O (4:1, 20 mL). NaN_3 (2.1 eq, 0.1131g, 1.72 mmol), $CuSO_4.5H_2O$ (0.4 eq, 0.025 g, 0.328 mmol), Ascorbic acid (2.1 eq, 0.306 g, 1.72 mmol), 2-(Bromomethyl)pyridine hydrobromide (2.1 eq, 0.440 g, 1.72 mmol) were then added in to the reaction mixture and stirred for 48 hours at room temperature. Then EDTA (50 ml, 0.5 M) was added into the reaction mixture. The precipitate was then filtered off on to a filter paper followed by a water and ether wash to get rid of excess DMF solvent. The precipitate was left to dry overnight. A white colour precipitate was collected. Yield (0.220 g, 52.1%), Melting point 291.4 ^{0}C, LRMS (ESI^+) (m/z) calculated for $(C_{25}H_{23}N_{11}O_2 + Na)^+$ 532.2 found 532.2 and calculated for $(C_{25}H_{23}N_{11}O_2 + K)^+$ 548.2 found 548.0, ^{1}H NMR (300 MHz, DMSO), δ= 9.9108 (2H, t, J=6.06 Hz, NH), δ= 8.511 (2H, d, J = 4.0 Hz, Pyridine-H), δ= 8.1560 (3H, m, DPA Pyridine-H), δ= 8.07 (2H, s, Triazole), δ= 7.72 (2H, td, J=7.70, 5.91 1.80, Pyridine-H), δ=7.31 (2H, dd, J = 4.96, 1.79 Hz, Pyridine-H), δ= 7.2703 (2H, d, J= 7.79, Pyridine-H), δ=5.6732 (4H, s, CH_2), δ=4.6205 (4H, d, J = 5.6, NH-CH_2), ^{13}C NMR (75 MHz, DMSO, ppm), δ= 163.6, 155.5, 149.8, 148.9, 145.4, 140.0, 1377, 124.9, 124.3, 123.7, 122.2, 54.7, 34.9, IR U/cm^{-1} : 3353, 3145, 3085, 3004, 1699.3, 1668.7, 1609.6, 1595.3, 1587.1, 1572.8, 1552.4, 1528.0, 1499.4, 1491.2, 1472.9, 1456.6, 1438.2, 1405.6, 1364.8, 1328.0, 1309.7, 1126.1, 1097.5, 1071.0, 1056.7, 1013.9, 997.6, 973.1, 932.3, 887.4, 871.1, 850.7, 828.2, 805.8, 773.2, 752.8, 722.2, 707.9, 671.2, 652.8, 593.6, 554.9, 536.5, 528.4, 518.2, 501.8, 493.7, 454.9, 430.4, 416.2, UV/Vis (Acetonitrile) λ_{max} (ε), 200 = 47,300 $Lmol^{-1}cm^{-1}$, 222 = 27,400 $Lmol^{-1}cm^{-1}$, 274 = 7410 $Lmol^{-1}cm^{-1}$, 282 = 5560 $Lmol^{-1}cm^{-1}$

4.2.2 Asymmetrical / Mono-systems

Synthesis of Pyridine-2,6-dicarboxylicmonobenzyl ester

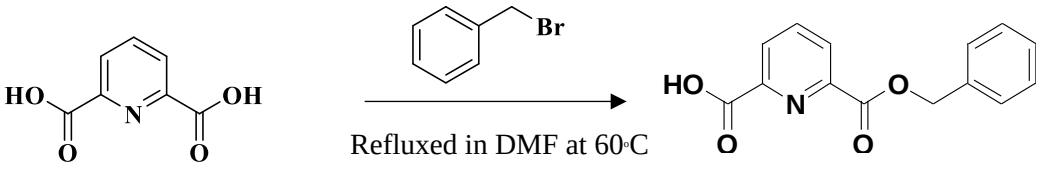

2,6-pyridinedicarboxylic acid (2 g, 0.012 mol), was added in to a 250 mL round bottom flask and into that oven-dried $NaHCO_3$ (1g, 0.012 mol, 1eq) was added followed by 100 mL of dry DMF. The solution was stirred at 60^oC under N_2 gas for 30 minutes. To the stirring colourless suspension, benzyl bromide (1.43 mL, 0.012 mol, 1eq) was added and refluxed at 60^oC for 48 hours. After 48 hours the reaction mixture was diluted with 150 mL of H_2O and neutralized with saturated $NaHCO_3$ solution. Diester side product was extracted with diethyl ether (2 x 100 mL). Then the aqueous layer was acidified with Conc. HCl solution until the pH ≈ 3 and extracted with ethyl acetate (4 x 50 mL). Ethyl acetate layers were combined, dried over $MgSO_4$ and removed the solvent *in vacuo* at 40^oC, 240atm. The resulting white colour solid was dissolved in 50 mL of dichloromethane and washed with water (2 x 100 mL), brine (NaCl, 100 mL) and the DCM layer was dried over $MgSO_4$ and the organic solvent was removed *in vacuo* at 40° C, 800atm.[69] The resulting white colour solid was left to dry in air. Yield (0.862 g, 28.0%), ^1H NMR (300 MHz, DMSO), δ= 7.48 (3H, m, Pyridine-H), δ= 7.32 (5H, m, benzyl group-H), δ=5.42 (2H, s, O-CH_2)

Synthesis of 6-Prop-2-ynylcarbamoyl-pyridine-2-carboxylic acid benzyl ester

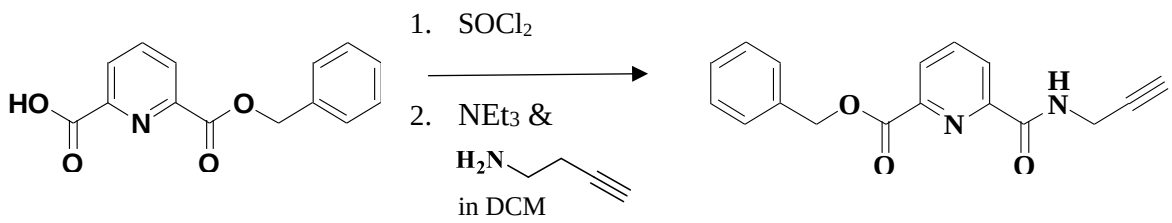

Mono-protected Pyridine-2,6-dicarboxylicmonobenzyl ester (500 mg) was weighed into a round bottom flask and dissolved in 20 mL of dry dichloromethane. It was stirred at 60^{o}C for 15 minutes under N_2 gas. Into the stirred solution added 1 mL of $SOCl_2$ and refluxed for 5 hours. To a stirred cooled solution of propargyl amine (0.149 ml, 0.00194 mol, 1.1eq) and triethylamine (0.86 ml, 13.0 mmol, 5.30eq) was dissolved in 20 mL DCM and cooled in an ice bath. 2,6-Pyridinedicarbonyl dichloride (500 mg, 2.45 mmol, 1eq) was dissolved in 20 mL of DCM and was slowly added into the cool suspension of propargyl amine and triethylamine. The reaction mixture was stirred at room temperature for 48 hours. After 18 hours the DCM layer was washed with 1 M HCl, 1 M $NaHCO_3$ and water respectively. The DCM layer was dried over $MgSO_4$ and evaporated *in vacuo*. It resulted in a brown oil-like substance and needed further drying overnight to obtain a dark brown colour solid. Yield (392mg, 73.4%), ^{1}H NMR (300 MHz, DMSO), δ= 8.25 (3H, m, Pyridine-H), δ= 8.00 (1H, t, J= 7.4 Hz, NH) δ= 7.36 (5H, m, benzyl group-H), δ= 5.48 (2h, s, O-CH_2), δ= 4.29 (2H, d, J = 2.64, NH-CH_2),

Synthesis of 6-{[1-(4-Nitro-benzyl)-1H-[1,2,3]triazol-4-ylmethyl]-carbamoyl}-pyridine-2-carboxylic acid benzyl ester

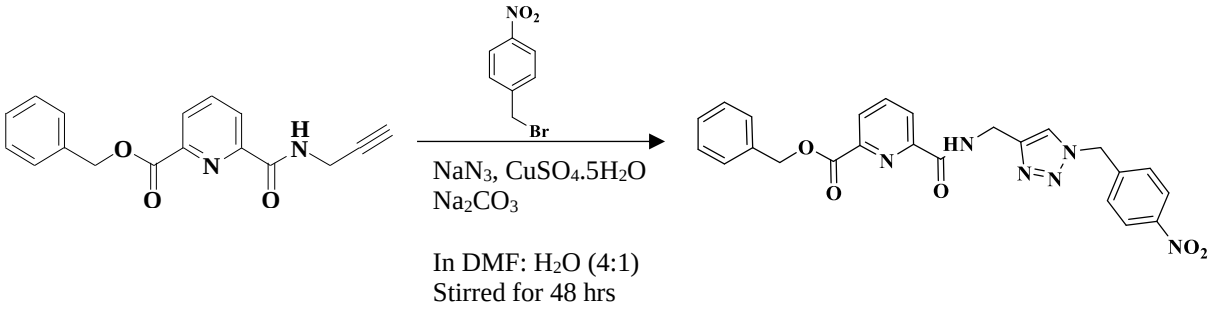

6-Prop-2-ynylcarbamoyl-pyridine-2-carboxylic acid benzyl ester (500 mg, mmol) was dissolved in DMF/ H_2O (4:1, 20 mL). NaN_3 (0.132 g, mmol, 1.2eq), $CuSO_4.5H_2O$ (0.084 g, mmol, 0.2 eq), ascorbic acid (0.357 g, mmol, 1.2eq), 4-Nitrobenzyl bromide (0.438 g, mmol, 1.2eq) and Na_2CO_3 were then added. The reaction mixture was stirred for 48 hours. Then EDTA (50 ml, 0.5 M) was added into the reaction mixture and a white colour precipitate was formed in the solution. Then the precipitate was filtered off on to a filter paper using vacuum filtration method. This was then washed with water and diethyl ether to remove excess solvent residues and left to dry overnight. Yield (0.496 g, 61.5%), ^{1}H NMR (300 MHz, DMSO), δ= 9.0758 (1H, t, J=6.03 Hz, NH), δ= 8.2046 (5H, m, benzene), δ=8.1298 (1H, s, Triazole), δ=7.4926 (4H, m, nitro-benzene), δ= 7.3122 (3H, m, Pyridine H), δ= 5.753 (2H, s, , O-CH_2), δ=5.4346 (2H, s, N-CH), δ= 4.5532 (4H, d, J= 6.0, NH-CH_2), IR U/cm^{-1} : 3517, 3321, 3113, 3066, 2927, 2851, 1724, 1677, 1607, 1585, 1571, 1534, 1512, 1446, 1434, 1391, 1381, 1348, 1316, 1297, 1257, 1240, 1218, 1169, 1146, 1130, 1110, 1077, 1046, 1028, 1008, 983, 949, 940, 916, 906, 875, 859, 842, 808, 787, 755, 732, 720, 679, 657, 647, 630, 581, 522, 503, 489, 475, 463, 443, 422

Synthesis of Pyridine-2,6-dicarboxylic acid 2-amide 6-prop-2-ynylamide

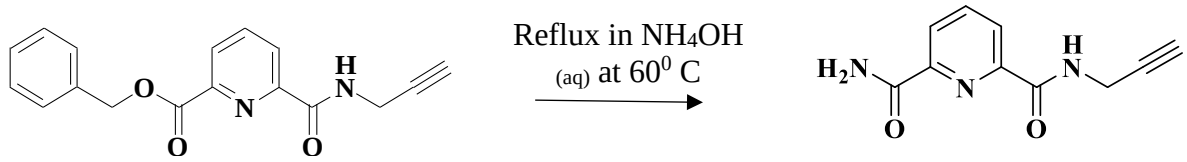

6-Prop-2-ynylcarbamoyl-pyridine-2-carboxylic acid benzyl ester (500 mg) was refluxed in NH_4OH solution for 12 hours at 60^0 C. Resulting solution was left to evaporate and dissolved in DCM. The DCM layer was separated with distilled water and the water layer was evaporated in the rotary evaporator to obtain a white colour compound. This was repeated if the resulting solid contained a yellow colour residue. Yield (0.122 g, 34.7%), 1H NMR (300 MHz, $CDCl_3$), δ= 8.4 (2H, d, J=8.0 Hz, Pyridine-2H), δ = 8.06 (1H, t, J=7.7 Hz, Pyridine-H), δ = 7.88 (1H, s, NH_2), δ = 7.60 (1H, s, NH_2), δ = 5.76 (1H, s, NH), δ =4.33 (2H, dd, J=2.5 Hz, 3.1 Hz, NH-CH_2), δ = 2.32 (1H, t, 2.59 Hz, C-CH), δ = 2.28 (2H, t, 2.6 Hz, C-CH)

Synthesis of L5

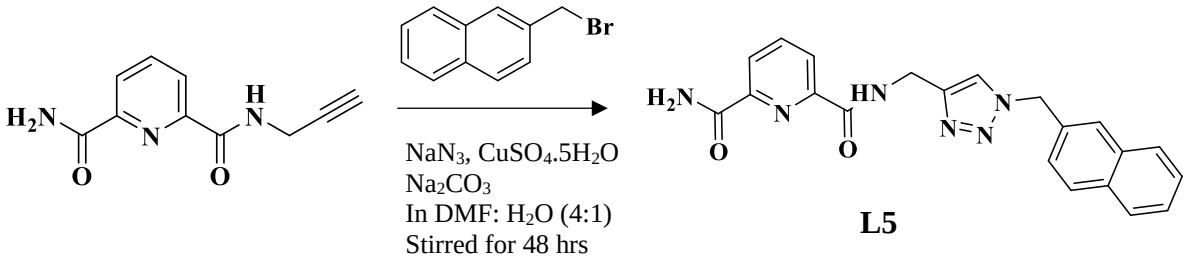

L5

Pyridine-2,6-dicarboxylic acid 2-amide 6-prop-2-ynylamide (150 mg, 0.73 mmol) was dissolved in DMF/ H_2O (4:1, 20 mL). NaN_3 (1.2 eq, 0.057 g, 0.876 mmol), $CuSO_4.5H_2O$ (0.2 eq, 0.036 g, 0.147 mmol), ascorbic acid (1.2 eq, 0.155 g, 0.73 mmol), Na_2CO_3 (3 eq, 0.234 g, 2.19 mmol) and 2-(Bromomethyl)naphthalene (1.2 eq, 234.6 g, 0.73 mmol) were then added in to the reaction mixture and stirred for 48 hours at room temperature. The reaction mixture turned into a pale-yellow colour solution overt time. After 48 hours, added EDTA (20 mL, 0.5 moldm^{-3}) and no precipitation was formed. The solution was stirred vigorously with DCM in a magnetic stirrer for a couple of minutes. Then the DCM layer was separated and further washed with water, dried over Na_2SO_4, evaporated *in vacuo*. Yield (0.142 g, 49.8%), LRMS (ESI$^+$) (m/z) calculated for $(C_{21}H_{18}N_6O_2 + Na)^+$ 409.1 found 409.2 and calculated for $(C_{25}H_{23}N_{11}O_2 + K)^+$ 425.5 found 425.0, ^{1}H NMR (300 MHz, DMSO) , δ= 9.88 (1H, t, J=6.0 Hz, NH), δ=8.90 (1H, s, NH_2), δ= 8.15 (3H, m, Pyridine), 8.1058 (2H, s, triazole), δ= 7.86 (4H, m, naphthalene H) δ= 7.7 (1H, s, NH_2), δ= 7.50 (2H, m, naphthalene H), δ=7.43 (2H, d, J=3.0, naphthalene H), δ= 5.73 (4H, s, CH_2), δ= 4.57 (4H, d, J= 6.0 Hz, NH-CH_2), ^{13}C NMR (75 MHz, DMSO, ppm), δ= 165.7, 163.7, 149.4, 148.9, 145.6, 139.8, 134.0, 133.2, 133.1, 132.9, 128.9, 128.2, 128.0, 127.4, 127.0, 126.9, 124.7, 124.7, 123.7, 53.3, 34.9, IR U/cm^{-1}: 3408, 3316, 3125, 3060, 2960, 2936, 2325, 2206, 2094, 1990, 1925, 1868, 1802, 1780, 1688, 1669, 1650, 1585, 1454, 1365, 1317, 1287, 1262, 1247, 1220, 1176, 1136, 1127, 1080, 1053, 1009, 1000, 969, 936, 901, 867, 736, 688, 557, 431, UV/Vis (Acetonitrile) λmax (ε), 222 = 87,740 Lmol^{-1}cm^{-1}, 265 = 8680 Lmol^{-1}cm^{-1}, 274 = 8710 Lmol^{-1}cm^{-1}

Synthesis of L6

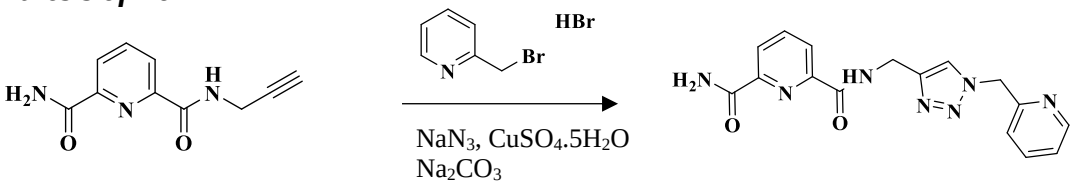

L6

Pyridine-2,6-dicarboxylic acid 2-amide 6-prop-2-ynylamide (100 mg, 0.49 mmol) was dissolved in DMF/ H_2O (4:1, 20 mL). NaN_3 (1.2 eq, 0.038 g, 0.588 mmol), $CuSO_4.5H_2O$ (0.2 eq, 0.024 g, 0.098 mmol), Ascorbic acid (1.2 eq, 0.104 g, 0.588 mmol), Na_2CO_3 (3 eq, 0.156 g, 1.47 mmol) 2-(Bromomethyl)pyridine hydrobromide (1.2 eq, 234.6 g, 0.73 mmol) were then added in to the reaction mixture and stirred for 48 hours at room temperature. Reaction mixture was turned into a pink colour solution and turned in to dark reddish-brown colour solution over the time period of 48 hours. There was no precipitate formed upon addition of EDTA (20 ml, 0.5 M). Into that, added DCM and the reaction mixture was stirred vigorously in a magnetic stirrer for a couple of minutes. The DCM layer was then separated out and washed with distilled water. The aqueous layer was then evaporated *in vacuo* and the resulting white colour solid was left to dry overnight in a desiccate. Yield (140.0 mg, 84.3%), LRMS (ESI^+) (m/z) calculated for $(C_{16}H_{15}N_7O_2 + Na)^+$ 360.3 found 360.0 and calculated for $(C_{16}H_{15}N_7O_2 + K)^+$ 376.4 found 375.9, ^1H NMR (300 MHz, DMSO), δ= 9.84 (1H, t, J=6.0 Hz, NH), δ= 8.45 (1H, d, J = 4.0 Hz, Pyridine-H), δ= 8.08 (3H, m, DPA Pyridine-H), δ= 8.00 (1H, s, Triazole), δ= 7.21 (2H, m, Pyridine-H), δ=5.61 (2H, s, CH_2), δ=4.52 (2H, d, J = 6.1 Hz, NH-CH_2), ^{13}C NMR (75 MHz, DMSO, ppm), δ= 39, 40.7, 122.7, 123.7, 124.3,124.7, 137.8, 139.8, 148.9, 149.4, 149.8, 155.5, 163.6, 165.7, 207.1, IR U/cm^{-1}: 3402, 3333, 3247, 3124, 3077, 3027, 2316, 2199, 2123, 1981, 1934, 1903, 1657, 1612, 1553, 1535, 1518, 1475, 1441, 1392, 1357, 1313, 1292, 1225, 1178, 1127, 1053, 1019, 1001, 975, 957, 940, 920, 890, 845, 815, 775, 746, 703, 681, 663, 650, 538, 511, 492, 442, 428, 412, UV/Vis (Acetonitrile) λmax (ε), 222 = 37,150 $Lmol^{-1}cm^{-1}$, 265 = 15,700 $Lmol^{-1}cm^{-1}$, 274 = 10,500 $Lmol^{-1}cm^{-1}$, 280 = 7570 $Lmol^{-1}cm^{-1}$

4.3 SYNTHESIS OF LANTHANIDE COMPLEXES

4.3.1 Synthesis of L1 complexes with Eu^{3+}, Tb^{3+} and La^{3+}

Synthesis of L1Eu^{3+} complex

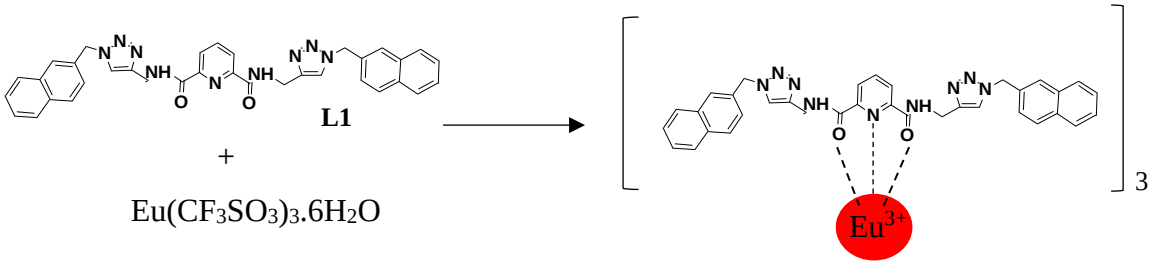

L1 ligand (40 mg, 0.065 mmol) and $Eu(CF_3SO_3)_3.6H_2O$ (0.33 eq, 15.3 mg, 0.021 mmol) were dissolved in 10 mL of DCM: MeOH (8:2) mixture in a glass vial, then sonicated at 40^0 C until a clear solution was obtained. Then the reaction mixture was heated under microwave irradiation for 30 minutes. The resulting solution was split into 3 glass vials and subjected to vapour diffusion in diethyl ether. Resulting glass-like substances were scraped off the glass surface as a white powder and analysed.

IR U/cm^{-1} : 3054, 2330, 2301, 2287, 2268, 2258, 2250, 2238, 2226, 2213, 2201, 2175, 2162, 2154, 2140, 2136, 2128, 2120, 2111, 2105, 2097, 2085, 2073, 2052, 1654, 1630, 1597, 1561, 1546, 1512, 1459, 1428, 1375, 1346, 1318, 1308, 1279, 1236, 1224, 1197, 1163, 1153, 1126, 1077, 1049, 1028, 1002, 977, 969, 965, 924, 916, 900, 859, 840, 820, 806, 785, 771, 755, 734, 716, 683, 663, 655, 647, 632, 610, 594, 573, 565, 559, 549, 539, 516, 488, 473, 455, 445, 437, 426, 416, 402

Synthesis of L1.Tb^{3+} complex

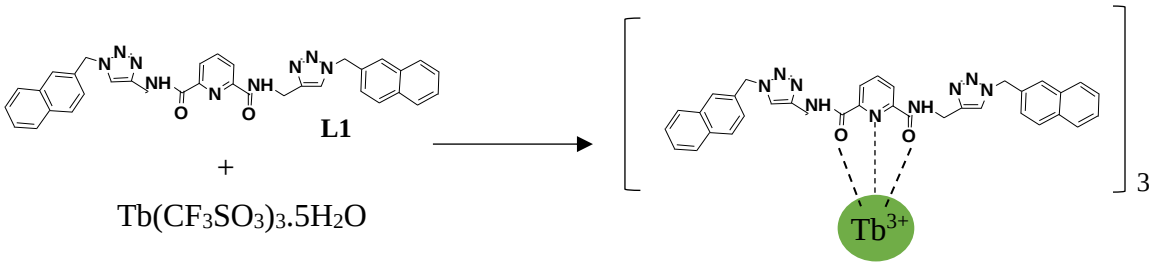

L1 ligand (40 mg, 0.065 mmol) and $Tb(CF_3SO_3)_3.5H_2O$ (0.33 eq, 15.5 mg, 0.021 mmol) were dissolved in 10 mL of DCM: MeOH (8:2) mixture in a glass vial, then sonicated at 40^0 C until a clear solution was obtained. Then the reaction mixture was heated under microwave irradiation for 30 minutes. The resulting solution was split into 3 glass vials and subjected to vapour diffusion in diethyl ether. Resulting glass-like substances were scraped off the glass surface as a white powder and analysed.

IR U/cm^{-1} : 3321, 3313, 3295, 3272, 3246, 3219, 3174, 3140, 3129, 3115, 3089, 3054, 2330, 2297, 2287, 2273, 2262, 2238, 2232, 2220, 2209, 2189, 2179, 2166, 2148, 2136, 2120, 2109, 2097, 2089, 2081, 2052, 2042, 2020, 2013, 1993, 1985, 1979, 1965, 1950, 1926, 1918, 1897, 1879, 1873, 1863, 1850, 1832, 1803, 1791, 1775, 1752, 1744, 1726, 1636, 1599, 1563, 1548, 1512, 1461, 1430, 1371, 1281, 1234, 1224, 1161, 1128, 1053, 1028, 967, 902, 883, 861, 840, 818, 785, 755, 732, 679, 669, 659, 634, 573, 534, 516, 473, 414

Synthesis of L1La^{3+} complex

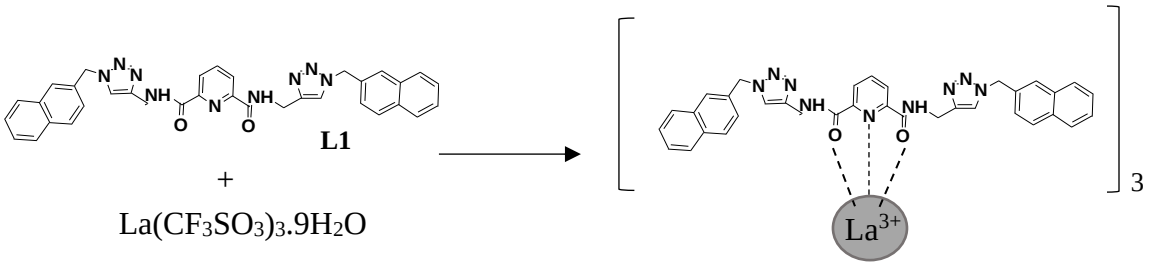

L1 ligand (40 mg, 0.065 mmol) and La(CF_3SO_3)$_3$.9H_2O (0.33 eq, 16.2 mg, 0.021 mmol) were dissolved in 10 mL of DCM: MeOH (8:2) mixture in a glass vial, then sonicated at 40^0 C until a clear solution was obtained. Then the reaction mixture was heated under microwave irradiation for 30 minutes. The resulting solution was split into 3 glass vials and subjected to vapour diffusion in diethyl ether. Resulting glass-like substances were scraped off the glass surface as a white powder and analysed.

IR U/cm^{-1} : 3682, 3643, 3560, 3272, 3142, 3111, 3089, 3058, 3025, 2985, 2352, 2346, 2330, 2297, 2266, 2248, 2232, 2211, 2197, 2175, 2136, 2118, 2109, 2103, 2095, 2077, 2042, 2022, 1991, 1977, 1944, 1916, 1865, 1842, 1805, 1783, 1748, 1716, 1634, 1597, 1546, 1432, 1371, 1279, 1222, 1161, 1065, 1028, 967, 900, 861, 840, 818, 785, 755, 679, 634, 571, 516, 473, 428

4.3.2 Synthesis of L3 complexes with Eu^{3+}, Tb^{3+} and La^{3+}

Synthesis of L3Eu^{3+} complex

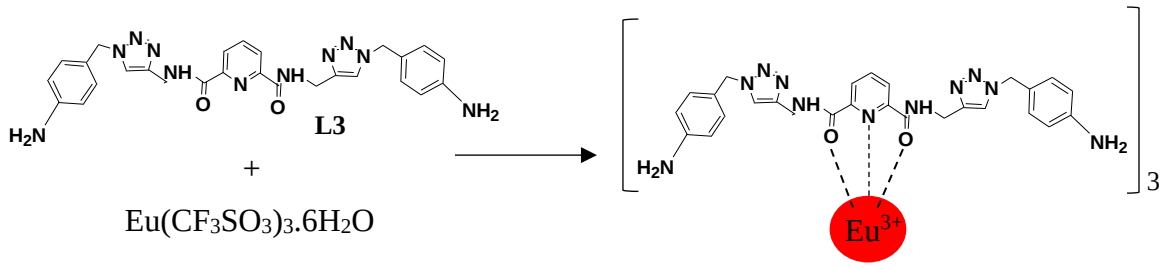

L3 ligand (40 mg, 0.074 mmol) and $Eu(CF_3SO_3)_3.6H_2O$ (0.33 eq, 17.3 mg, 0.024 mmol) were dissolved in 10 mL of in THF: Ethanol (1:1) mixture in a glass vial, then sonicated at 40° C until a clear solution was obtained. Then the reaction mixture was heated under microwave irradiation for 30 minutes. The resulting solution was split into 3 glass vials and subjected to vapour diffusion in diethyl ether. Resulting glass-like substances were scraped off the glass surface as a white powder and analysed.

IR U/cm^{-1} : 3455, 3358, 3140, 3088, 2987, 2351, 2343, 2330, 2282, 2194, 2114, 1984, 1925, 1632, 1563, 1519, 1459, 1447, 1434, 1380, 1339, 1275, 1237, 1224, 1161, 1076, 1056, 1027, 874, 837, 819, 781, 755, 723, 689, 669, 635, 573, 544, 516, 497, 411

Synthesis of L3Tb^{3+} complex

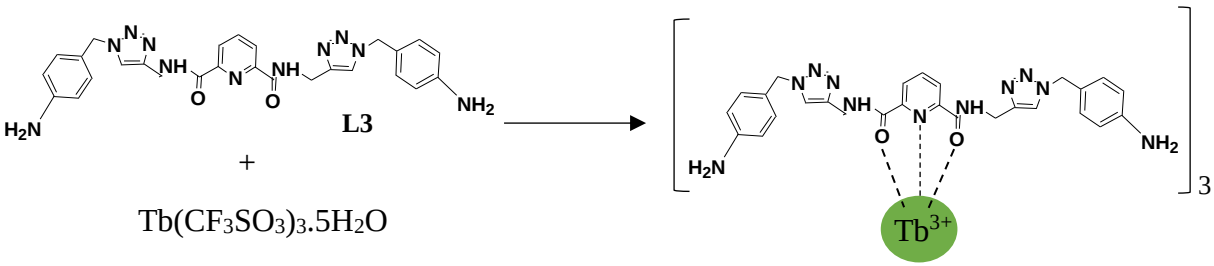

L3 ligand (40 mg, 0.074 mmol) and $Tb(CF_3SO_3)_3.5H_2O$ (0.33 eq, 17.5 mg, 0.024 mmol) were dissolved in 10 mL of in THF: Ethanol (1:1) mixture in a glass vial, then sonicated at 40° C until a clear solution was obtained. Then the reaction mixture was heated under microwave irradiation for 30 minutes. The resulting solution was split into 3 glass vials and subjected to vapour diffusion in diethyl ether. Resulting glass-like substances were scraped off the glass surface as a white powder and analysed.

IR U/cm^{-1}: 3454, 3448, 3431, 3354, 3321, 3305, 3288, 3244, 3144, 3101, 3089, 3074, 3044, 3027, 3007, 2952, 2397, 2373, 2360, 2350, 2338, 2315, 2285, 2271, 2252, 2236, 2217, 2203, 2191, 2164, 2144, 2113, 2079, 2054, 2003, 1979, 1958, 1940, 1934, 1926, 1918, 1885, 1863, 1840, 1820, 1795, 1767, 1738, 1716, 1628, 1546, 1520, 1440, 1328, 1277, 1222, 1157, 1061, 1026, 934, 922, 904, 898, 836, 781, 749, 724, 704, 687, 677, 657, 632, 571, 539, 514, 498, 457, 428, 410

Synthesis of L3La^{3+} complex

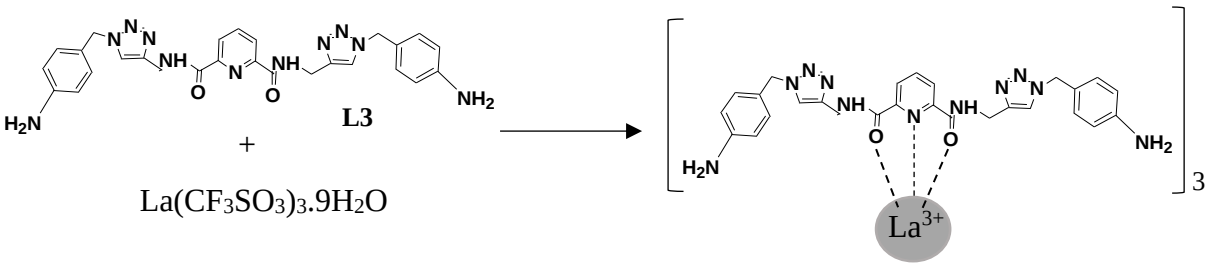

L3 ligand (40 mg, 0.074 mmol) and La(CF_3SO_3)$_3$.9H_2O (0.33 eq, 18.3 mg, 0.024 mmol) were dissolved in 10 mL of in THF: Ethanol (1:1) mixture in a glass vial, then sonicated at 40° C until a clear solution was obtained. Then the reaction mixture was heated under microwave irradiation for 30 minutes. The resulting solution was split into 3 glass vials and subjected to vapour diffusion in diethyl ether. Resulting glass-like substances were scraped off the glass surface as a white powder and analysed.

IR U/cm^{-1}: 3272, 3142, 3113, 3084, 3021, 2703, 2685, 2544, 2534, 2501, 2487, 2468, 2434, 2407, 2368, 2356, 2344, 2330, 2301, 2281, 2262, 2250, 2236, 2207, 2197, 2191, 2171, 2148, 2138, 2113, 2099, 2083, 2073, 2026, 2007, 1987, 1958, 1944, 1924, 1907, 1875, 1854, 1834, 1818, 1805, 1795, 1761, 1746, 1738, 1730, 1718, 1714, 1634, 1595, 1546, 1479, 1459, 1436, 1322, 1277, 1222, 1161, 1100, 1055, 1026, 1002, 871, 802, 753, 722, 632, 571, 514, 473, 461, 428

4.3.3 Synthesis of L4 complexes with Eu^{3+}, Tb^{3+} and La^{3+}

Synthesis of L4Eu^{3+} complex

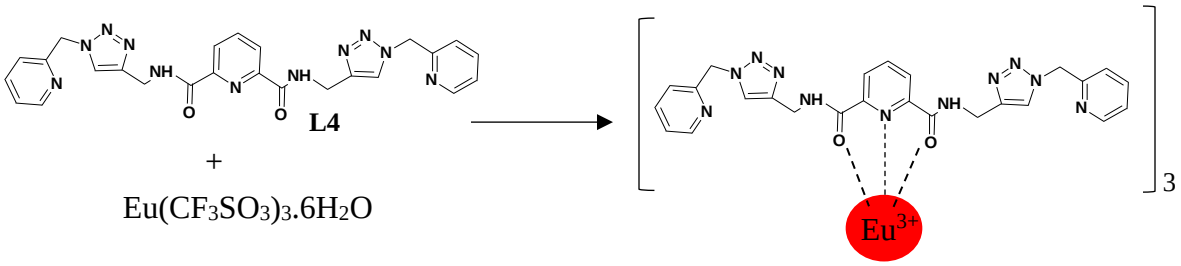

L4 ligand (40 mg, 0. 0785 mmol) and $Eu(CF_3SO_3)_3.6H_2O$ (0.35 eq, 19.4 mg, 0.027 mmol) were dissolved in 10 mL of in THF: Methanol (4:1) mixture in a glass vial, then sonicated at 40° C until a clear solution was obtained. Then the reaction mixture was heated under microwave irradiation for 30 minutes. The resulting solution was split into 3 glass vials and subjected to vapour diffusion in diethyl ether. Resulting glass-like substances were scraped off the glass surface as a white powder and analysed.

IR U/cm^{-1}: 3444, 3297, 3140, 3088, 2987, 2324, 2111, 1990, 1633, 1596, 1562, 1520, 1460, 1435, 1379, 1339, 1276, 1237, 1223, 1161, 1076, 1055, 1027, 875, 839, 781, 755, 722, 334, 572, 515

Synthesis of L4Tb^{3+} complex

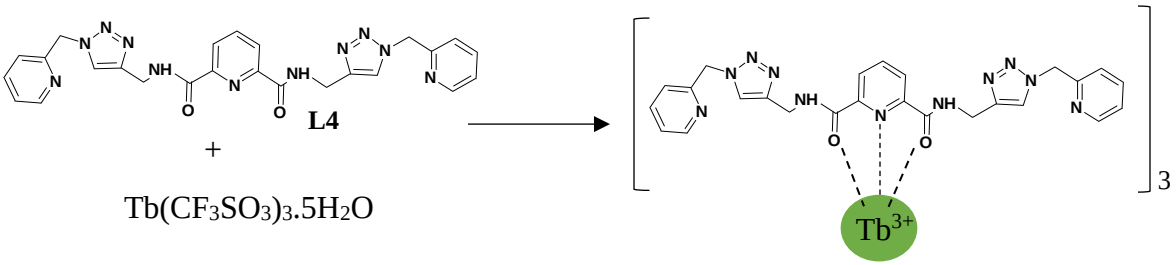

L4 ligand (40 mg, 0. 0785 mmol) and $Tb(CF_3SO_3)_3.5H_2O$ (0.35 eq, 19.6 mg, 0.027 mmol) were dissolved in 10 mL of in THF: Methanol (4:1) mixture in a glass vial, then sonicated at 40° C until a clear solution was obtained. Then the reaction mixture was heated under microwave irradiation for 30 minutes. The resulting solution was split into 3 glass vials and subjected to vapour diffusion in diethyl ether. Resulting glass-like substances were scraped off the glass surface as a white powder and analysed.

IR U/cm^{-1}: 3643, 3274, 3142, 3084, 3017, 2972, 2927, 2679, 2660, 2603, 2568, 2552, 2536, 2519, 2509, 2491, 2485, 2464, 2454, 2432, 2395, 2383, 2348, 2322, 2301, 2287, 2262, 2224, 2209, 2191, 2146, 2109, 2020, 2013, 1981, 1911, 1887, 1869, 1856, 1834, 1805, 1787, 1746, 1726, 1634, 1595, 1548, 1432, 1373, 1334, 1279, 1224, 1161, 1049, 1028, 971, 900, 863, 840, 818, 787, 755, 683, 634, 571, 516, 473, 432

Synthesis of L4La^{3+} complex

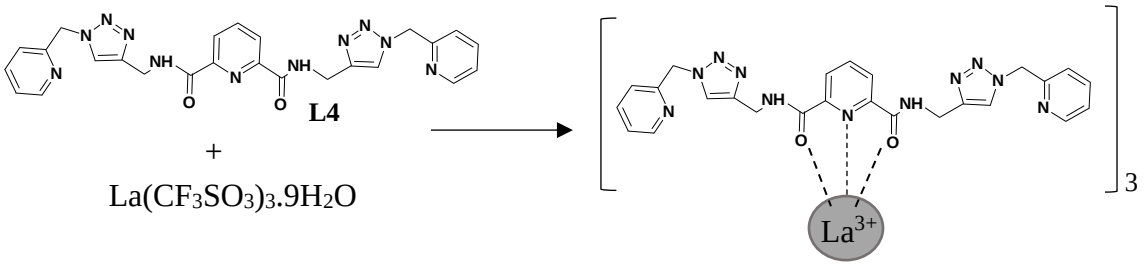

L4 ligand (40 mg, 0. 0785 mmol) and $La(CF_3SO_3)_3.9H_2O$ (0.35 eq, 20.5 mg, 0.027 mmol) were dissolved in 10 mL of in THF: Methanol (4:1) mixture in a glass vial, then sonicated at 40° C until a clear solution was obtained. Then the reaction mixture was heated under microwave irradiation for 30 minutes. The resulting solution was split into 3 glass vials and subjected to vapour diffusion in diethyl ether. Resulting glass-like substances were scraped off the glass surface as a white powder and analysed.

IR $\tilde{U}/cm^{-1}$: 3690, 3674, 3272, 3142, 3113, 3084, 3021, 1634, 1595, 1546, 1479, 1459, 1436, 1322, 1277, 1222, 1161, 1100, 1055, 1026, 1002, 871, 802, 753, 722, 632, 571, 514, 473, 461, 428

4.3.4 Synthesis of L5 complexes with Eu^{3+}, Tb^{3+} and La^{3+}

Synthesis of L5Eu^{3+} complex

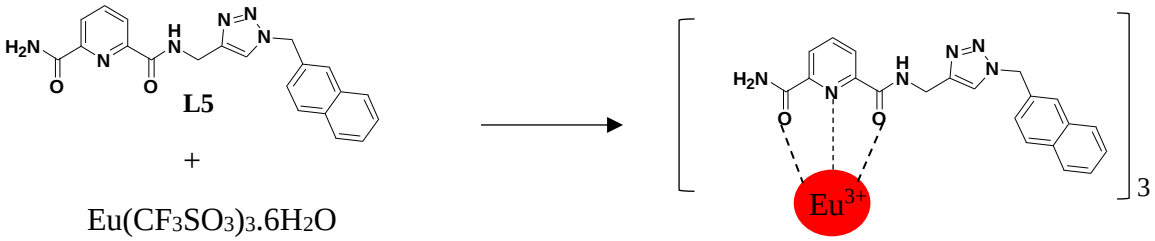

L5 ligand (40 mg, 0. 103 mmol) and $Eu(CF_3SO_3)_3.6H_2O$ (0.35 eq, 25.6 mg, 0.036 mmol) was dissolved in 10 mL of in DCM: Methanol (3:7) mixture in a glass vial, then sonicated at 40° C until a clear solution was obtained. Then the reaction mixture was heated under microwave irradiation for 30 minutes. The resulting solution was split into 3 glass vials and subjected to vapour diffusion in diethyl ether. Resulting glass-like substances were scraped off the glass surface as a white powder and analysed.

IR U/cm^{-1}: 3314, 3125, 3076, 3059, 3019, 2986, 2960, 2935, 2884, 2853, 2766, 2725, 2654, 2647, 2609 2594 2566 2558 2527 2474 2464 2427 2405 2372 2348, 2337, 2288, 2235, 2215, 2207, 2125, 2099, 2011, 1991, 1984, 1954, 1925, 1895, 1868, 1844, 1835, 1829, 1801, 1793, 1778, 1750, 1742, 1733, 1668, 1650, 1585, 1566, 1552, 1523, 1509, 1454, 1430, 1387, 1366, 1328, 1260, 1246, 1223, 1168, 1136, 1126, 1079, 1052, 1030, 1009, 968, 950, 936, 901, 885, 864, 844, 824, 781, 764, 736, 662, 634, 616, 556, 534, 516, 487, 473, 430, 422, 403

Synthesis of L5Tb^{3+} complex

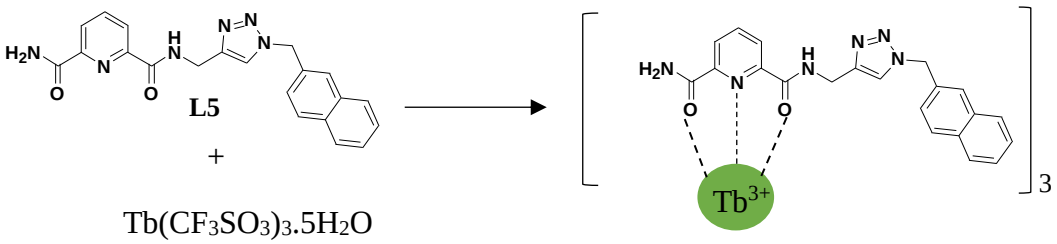

L5 ligand (40 mg, 0. 103 mmol) and $Tb(CF_3SO_3)_3.5H_2O$ (0.35 eq, 25.8 mg, 0.036 mmol) were dissolved in 10 mL of in DCM: Methanol (3:7) mixture in a glass vial, then sonicated at 40° C until a clear solution was obtained. Then the reaction mixture was heated under microwave irradiation for 30 minutes. The resulting solution was split into 3 glass vials and subjected to vapour diffusion in diethyl ether. Resulting glass-like substances were scraped off the glass surface as a white powder and analysed.

IR U/cm^{-1}: 3314, 3127, 2996, 2988, 2935, 2858, 2666, 2564 2539 2527 2511 2503 2496 2474 2462 2450 2439 2405 2382 2323, 2315, 2303, 2290, 2270, 2250, 2237, 2227, 2217, 2205, 2195, 2174, 2168, 2099, 2044, 2025, 2011, 1991, 1984, 1966, 1962, 1935, 1925, 1909, 1895, 1868, 1858, 1844, 1838, 1829, 1823, 1801, 1791, 1780, 1772, 1762, 1756, 1750, 1740, 1668, 1638, 1585, 1566, 1527, 1511, 1452, 1432, 1387, 1350, 1240, 1223, 1166, 1128, 1079, 1064, 1052, 1028, 966, 901, 883, 864, 844, 824, 783, 756, 681, 660, 634, 618, 573, 534, 516, 473, 430, 420, 405

Synthesis of L5La^{3+} complex

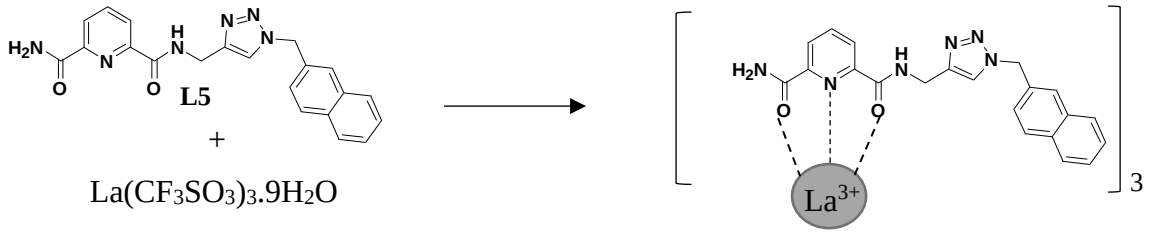

L5 ligand (40 mg, 0. 103 mmol) and $La(CF_3SO_3)_3.9H_2O$ (0.35 eq, 27.1 mg, 0.036 mmol) were dissolved in 10 mL of in DCM: Methanol (3:7) mixture in a glass vial, then sonicated at 40° C until a clear solution was obtained. Then the reaction mixture was heated under microwave irradiation for 30 minutes. The resulting solution was split into 3 glass vials and subjected to vapour diffusion in diethyl ether. Resulting glass-like substances were scraped off the glass surface as a white powder and analysed.

IR U/cm^{-1}: 3314, 3125, 3086, 3078, 2988, 2962, 2937, 2774, 2609 2576 2564 2547 2539 2521 2511 2503 2484 2472 2462 2450 2439 2427 2382 2350, 2325, 2315, 2301, 2268, 2258, 2250, 2235, 2227, 2217, 2205, 2195, 2166, 2123, 2101, 2042, 2031, 2011, 1991, 1966, 1956, 1935, 1925, 1909, 1895, 1844, 1825, 1803, 1778, 1650, 1585, 1525, 1452, 1430, 1389, 1368, 1236, 1226, 1175, 1136, 1128, 1079, 1052, 1028, 1009, 968, 936, 901, 883, 866, 844, 824, 781, 764, 736, 634, 616, 577, 558, 534, 516, 487, 471, 424, 405

4.4 SELF-ASSEMBLY STUDIES OF L5 AGAINST $Eu(CF_3SO_3)_3.6H_2O$

4.4.1 Preparation of solutions

A solution of **L5** in acetonitrile was prepared. **L5** ligand (10.2 mg, 0.0263 mmol) was carefully weighed into a clean vial. It was then dissolved in 4.0 mL of DCM and 9.1980 mL of methanol to prepare a stock solution of 2 x 10^{-3} M. It was further diluted to make a solution of 1 x 10^{-3} M in acetonitrile. Similarly, $Eu(CF_3SO_3)_3.6H_2O$ (10.4 mg, 0.0147 mmol) was weighed into a clean vial and dissolved in 2.941 mL of acetonitrile to make a stock solution of Eu^{3+} ion. It was further diluted in acetonitrile to make a solution of 1 x 10^{-3} M. Solvent volumes were measured using micropipettes for better accuracy.

4.4.2 UV-Vis/ Fluorescence Titration of L5 against $Eu(CF_3SO_3)_3.6H_2O$

From the **L5** (1 x 10^{-3} M) solution, 30 µL was pipetted into a 3 mL quartz cuvette containing 2.97 mL of acetonitrile to prepare a 1 x 10^{-5} M solution of **L5**. Then 0.1 equivalents of Eu^{3+} ion solution was titrated into the cuvette by adding 3 µL from Eu^{3+} stock solution (1 x 10^{-3} M). After each addition, the absorbance and fluorescence intensity were recorded using the UVProbe and LabSolutions RF software respectively. The process was repeated to obtain a second set of data for better accuracy.

REFERENCES

(1) Bünzli, J. C. G. Lanthanide Photonics: Shaping the Nanoworld. *Trends Chem.* **2019**, *1* (8), 751–762. https://doi.org/10.1016/j.trechm.2019.05.012.

(2) Cotton, S. *Lanthanide and Actinide Chemistry*; 2006. https://doi.org/10.1002/0470010088.

(3) Barry, D. E.; Caffrey, D. F.; Gunnlaugsson, T. Lanthanide-Directed Synthesis of Luminescent Self-Assembly Supramolecular Structures and Mechanically Bonded Systems from Acyclic Coordinating Organic Ligands. *Chem. Soc. Rev.* **2016**, *45* (11), 3244–3274. https://doi.org/10.1039/c6cs00116e.

(4) Taylor S.R. Abundance of Chemical Elements in the Continental Crust : A New Table. *Geochim. Cosmochim. Acta* **1964**, *28*, 1273–1285.

(5) Pallares, R. M.; Abergel, R. J. Transforming Lanthanide and Actinide Chemistry with Nanoparticles. *Nanoscale* **2020**, *12* (3), 1339–1348. https://doi.org/10.1039/c9nr09175k.

(6) Kitchen, J. A.; Gunnlaugsson, T. Lanthanides: Supramolecular Chemistry. In *Encyclopedia of Inorganic and Bioinorganic Chemistry*; 2012. https://doi.org/10.1002/9781119951438.eibc2048.

(7) Binnemans, K. Lanthanide-Based Luminescent Hybrid Materials. *Chem. Rev.* **2009**, *109* (9), 4283–4374. https://doi.org/10.1021/cr8003983.

(8) Bradberry, S. J.; Savyasachi, A. J.; Martinez-Calvo, M.; Gunnlaugsson, T. Development of Responsive Visibly and NIR Luminescent and Supramolecular Coordination Self-Assemblies Using Lanthanide Ion Directed Synthesis. *Coord. Chem. Rev.* **2014**, *273–274*, 226–241. https://doi.org/10.1016/j.ccr.2014.03.023.

(9) DOSSANTOS, C.; HARTE, A.; QUINN, S.; GUNNLAUGSSON, T. Recent Developments in the Field of Supramolecular Lanthanide Luminescent Sensors and Self-Assemblies. *Coord. Chem. Rev.* **2008**, *252* (23–24), 2512–2527. https://doi.org/10.1016/j.ccr.2008.07.018.

(10) Ruiz-Medina, A.; Llorent-Martinez, E. J.; Ortega-Barrales, P.; Cordova, M. L. F. De. Lanthanide-Sensitized Luminescence as a Promising Tool in Clinical Analysis. *Appl. Spectrosc. Rev.* **2011**, *46* (7), 561–580.

https://doi.org/10.1080/05704928.2011.600401.

(11) Charbonniere, L. J. Luminescent Lanthanide Labels. *Curr. Inorg. Chem.* **2011**, *1* (1), 2–16. https://doi.org/10.2174/1877945x11101010002.

(12) Wales, D. J.; Kitchen, J. A. Surface-Based Molecular Self-Assembly: Langmuir-Blodgett Films of Amphiphilic Ln(III) Complexes. *Chem. Cent. J.* **2016**, *10* (1), 1–8. https://doi.org/10.1186/s13065-016-0224-6.

(13) Kornblatt, A. N.; Urband, P. H.; Steere, A. C. Arthritis Caused by Borrelia Burgdorferi in Dogs. *J. Am. Vet. Med. Assoc.* **1985**, *186* (9), 960–964.

(14) Lakowicz, J. R. *Principles of Fluorescence Spectroscopy*; 2006. https://doi.org/10.1007/978-0-387-46312-4.

(15) Xu, L.; Feng, L.; Han, Y.; Jing, Y.; Xian, Z.; Liu, Z.; Huang, J.; Yan, Y. Supramolecular Self-Assembly Enhanced Europium(Iii) Luminescence under Visible Light. *Soft Matter* **2014**, *10* (26), 4686–4693. https://doi.org/10.1039/c4sm00335g.

(16) Crosby, G. A.; Whan, R. E.; Freeman, J. J. Spectroscopic Studies of Rare Earth Chelates. *J. Phys. Chem.* **1962**, *66* (12), 2493–2499. https://doi.org/10.1021/j100818a041.

(17) Latva, M.; Takalob, H.; Mukkala, V. M.; Matachescu, C.; Rodríguez-Ubis, J. C.; Kankare, J. Correlation between the Lowest Triplet State Energy Level of the Ligand and Lanthanide(III) Luminescence Quantum Yield. *J. Lumin.* **1997**, *75* (2), 149–169. https://doi.org/10.1016/S0022-2313(97)00113-0.

(18) Amoroso, A. J.; Pope, S. J. A. Using Lanthanide Ions in Molecular Bioimaging. *Chem. Soc. Rev.* **2015**, *44* (14), 4723–4742. https://doi.org/10.1039/c4cs00293h.

(19) Bünzli, J. C. G. Lanthanide Luminescence: From a Mystery to Rationalization, Understanding, and Applications. *Handb. Phys. Chem. Rare Earths* **2016**, *50*, 141–176. https://doi.org/10.1016/bs.hpcre.2016.08.003.

(20) Hasegawa, Y.; Kitagawa, Y.; Nakanishi, T. Effective Photosensitized, Electrosensitized, and Mechanosensitized Luminescence of Lanthanide Complexes /639/638/439/943 /639/638/911 Review-Article. *NPG Asia Mater.* **2018**, *10* (4), 52–70. https://doi.org/10.1038/s41427-018-0012-y.

(21) An, B. L.; Huang, X. Di; Zhang, J. M.; Zhu, X. Y.; Xu, J. Q. Synthesis and Strong Luminescence of Water Soluble Lanthanide Complexes Sensitized by a New Tridentate Organic Ligand. *J. Lumin.* **2017**, *187*, 340–346. https://doi.org/10.1016/j.jlumin.2017.03.043.

(22) Pearson, R. G. Hard and Soft Acids and Bases. *J. Am. Chem. Soc.* **1963**, *85* (22), 3533–3539. https://doi.org/10.1021/ja00905a001.

(23) Andres, J.; Chauvin, A. S. Energy Transfer in Coumarin-Sensitised Lanthanide Luminescence: Investigation of the Nature of the Sensitiser and Its Distance to the Lanthanide Ion. *Phys. Chem. Chem. Phys.* **2013**, *15* (38), 15981–15994. https://doi.org/10.1039/c3cp52279b.

(24) Speldrich, M.; van Leusen, J.; Kögerler, P. CONDON 3.0: An Updated Software Package for Magnetochemical Analysis-All the Way to Polynuclear Actinide Complexes. *J. Comput. Chem.* **2018**, 2133–2145. https://doi.org/10.1002/jcc.25389.

(25) Tanase, S.; Gallego, P. M.; de Gelder, R.; Fu, W. T. Synthesis, Crystal Structure and Photophysical Properties of Europium(III) and Terbium(III) Complexes with Pyridine-2,6-Dicarboxamide. *Inorganica Chim. Acta* **2007**, *360* (1), 102–108. https://doi.org/10.1016/j.ica.2006.07.115.

(26) Kitchen, J. A. Lanthanide-Based Self-Assemblies of 2,6-Pyridyldicarboxamide Ligands: Recent Advances and Applications as next-Generation Luminescent and Magnetic Materials. *Coordination Chemistry Reviews*. Elsevier B.V. 2017, pp 232–246. https://doi.org/10.1016/j.ccr.2017.01.012.

(27) Albrecht, M. “Let’s Twist Again” - Double-Stranded, Triple-Stranded, and Circular Helicates. *Chem. Rev.* **2001**, *101* (11), 3457–3497. https://doi.org/10.1021/cr0103672.

(28) Hamacek, J.; Besnard, C.; Mehanna, N.; Lacour, J. Tripodal Europium Complex with Triangulenium Dye: A Model Bifunctional Metallo-Organic System. *Dalton. Trans.* **2012**, *41* (22), 6777–6782. https://doi.org/10.1039/c2dt12332k.

(29) Stomeo, F.; Lincheneau, C.; Leonard, J. P.; O’Brien, J. E.; Peacock, R. D.; McCoy, C. P.; Gunnlaugsson, T. Metal-Directed Synthesis of Enantiomerially Pure Dimetallic Lanthanide Luminescent Triple-Stranded Helicates. *J. Am. Chem. Soc.* **2009**, *131* (28), 9636–9637. https://doi.org/10.1021/ja9032204.

(30) Jonathan A. Kitchen and Philip A. Gale 4.1. *Chirality in Supramolecular Assemblies*; 2017.

(31) Cotton, S. A. Establishing Coordination Numbers for the Lanthanides in Simple Complexes. *Comptes Rendus Chim.* **2005**, *8* (2), 129–145. https://doi.org/10.1016/j.crci.2004.07.002.

(32) Cotton, S. A.; Harrowfield, J. M. Lanthanides: Coordination Chemistry. *Encycl. Inorg. Bioinorg. Chem.* **2012**. https://doi.org/10.1002/9781119951438.eibc2062.

(33) Byrne, J. P.; Kitchen, J. A.; Gunnlaugsson, T. The Btp [2,6-Bis(1,2,3-Triazol-4-Yl)Pyridine] Binding Motif: A New Versatile Terdentate Ligand for Supramolecular and Coordination Chemistry. *Chem. Soc. Rev.* **2014**, *43* (15), 5302–5325. https://doi.org/10.1039/c4cs00120f.

(34) Himo, F.; Lovell, T.; Hilgraf, R.; Rostovtsev, V. V.; Noodleman, L.; Sharpless, K. B.; Fokin, V. V. Copper(I)-Catalyzed Synthesis of Azoles. DFT Study Predicts Unprecedented Reactivity and Intermediates. *J. Am. Chem. Soc.* **2005**, *127* (1), 210–216. https://doi.org/10.1021/ja0471525.

(35) Crowley, J. D.; Bandeen, P. H.; Hanton, L. R. A One Pot Multi-Component CuAAC "Click" Approach to Bidentate and Tridentate Pyridyl-1,2,3-Triazole Ligands: Synthesis, X-Ray Structures and Copper(II) and Silver(I) Complexes. *Polyhedron* **2010**, *29* (1), 70–83. https://doi.org/10.1016/j.poly.2009.06.010.

(36) Elliott, P. I. P. Organometallic Complexes with 1,2,3-Triazole-Derived Ligands. *Organomet. Chem.* **2014**, *39*, 1–25. https://doi.org/10.1039/9781849737692-00001.

(37) Bünzli, J. C. G. Review: Lanthanide Coordination Chemistry: From Old Concepts to Coordination Polymers. In *Journal of Coordination Chemistry*; 2014; Vol. 67, pp 3706–3733. https://doi.org/10.1080/00958972.2014.957201.

(38) Kilbourn, B. T. Metallurgical Applications of Yttrium and the Lanthanides. *Jom* **1988**, *40* (5), 22–25. https://doi.org/10.1007/BF03258906.

(39) Kilbourn, B. T. The Role of the Lanthanides in Applied Catalysis. *J. Less-Common Met.* **1986**, *126* (C), 101–106. https://doi.org/10.1016/0022-5088(86)90254-7.

(40) Bünzli, J. C. G. Rising Stars in Science and Technology: Luminescent Lanthanide Materials. *Eur. J. Inorg. Chem.* **2017**, *2017* (44), 5058–5063.

https://doi.org/10.1002/ejic.201701201.

(41) Hagan, A. K.; Zuchner, T. Lanthanide-Based Time-Resolved Luminescence Immunoassays. *Anal. Bioanal. Chem.* **2011**, *400* (9), 2847–2864. https://doi.org/10.1007/s00216-011-5047-7.

(42) Zhu, X.; Su, Q.; Feng, W.; Li, F. Anti-Stokes Shift Luminescent Materials for Bio-Applications. *Chem. Soc. Rev.* **2017**, *46* (4), 1025–1039. https://doi.org/10.1039/c6cs00415f.

(43) Cordina, N. M.; Sayyadi, N.; Parker, L. M.; Everest-Dass, A.; Brown, L. J.; Packer, N. H. Reduced Background Autofluorescence for Cell Imaging Using Nanodiamonds and Lanthanide Chelates. *Sci. Rep.* **2018**, *8* (1), 1–14. https://doi.org/10.1038/s41598-018-22702-1.

(44) Petoud, S.; Cohen, S. M.; Bünzli, J. C. G.; Raymond, K. N. Stable Lanthanide Luminescence Agents Highly Emissive in Aqueous Solution: Multidentate 2-Hydroxyisophthalamide Complexes of Sm3+, Eu 3+, Tb3+, Dy3+. *J. Am. Chem. Soc.* **2003**, *125* (44), 13324–13325. https://doi.org/10.1021/ja0379363.

(45) Zukerman-Schpector, J.; Haiduc, I.; Tiekink, E. R. T. *Supramolecular Self-Assembly of Transition Metal Carbonyl Molecules Through M-CO(Lone Pair)...π(Arene) Interactions*; 2012; Vol. 60. https://doi.org/10.1016/B978-0-12-396970-5.00002-5.

(46) Whitesides, G. M.; Boncheva, M. Proceedings of the National Academy of Sciences of the United States of America 2002 WhitesidesBeyond Molecules Self-Assembly of Mesoscopic. **2002**, *99* (8), 1–6.

(47) Vermonden, T.; de Vos, W. M.; Marcelis, A. T. M.; Sudhölter, E. J. R. 3-D Water-Soluble Reversible Neodymium(III) and Lanthanum(III) Coordination Polymers. *Eur. J. Inorg. Chem.* **2004**, *2004* (14), 2847–2852. https://doi.org/10.1002/ejic.200400098.

(48) Gautam R. Desiraju. Chemistry Beyond the Molecule. *Nature.* **2001**, *412* (July), 397–400.

(49) Wen, M. J.; Jackson, M. T.; Garner, C. M. A Quantitative Study of Vapor Diffusions for Crystallizations: Rates and Solvent Parameter Changes. *Dalton. Trans.* **2019**, *48* (30), 11575–11582. https://doi.org/10.1039/c8dt01891j.

(50) Bünzli, J. C. G. Benefiting from the Unique Properties of Lanthanide Ions. *Acc. Chem.*

Res. **2006**, *39* (1), 53–61. https://doi.org/10.1021/ar0400894.

(51) Al, O.; Jeong, H.; Koo, B. H.; Lee, C. G. Mössbauer Spectra of MnFe. **2010**, *4*, 1129–1132. https://doi.org/10.1007/s11771.

(52) Barry, D. E.; Kitchen, J. A.; Albrecht, M.; Faulkner, S.; Gunnlaugsson, T. Near Infrared (NIR) Lanthanide Emissive Langmuir-Blodgett Monolayers Formed Using Nd(III) Directed Self-Assembly Synthesis of Chiral Amphiphilic Ligands. *Langmuir* **2013**, *29* (36), 11506–11515. https://doi.org/10.1021/la402274s.

(53) Kotova, O.; Blasco, S.; Twamley, B.; O'Brien, J.; Peacock, R. D.; Kitchen, J. A.; Martínez-Calvo, M.; Gunnlaugsson, T. The Application of Chiroptical Spectroscopy (Circular Dichroism) in Quantifying Binding Events in Lanthanide Directed Synthesis of Chiral Luminescent Self-Assembly Structures. *Chem. Sci.* **2015**, *6* (1), 457–471. https://doi.org/10.1039/c4sc02474e.

(54) Gassner, A. L.; Duhot, C.; Bünzli, J. C. G.; Chauvin, A. S. Remarkable Tuning of the Photophysical Properties of Bifunctional Lanthanide Tris(Dipicolinates) and Its Consequence on the Design of Bioprobes. *Inorg. Chem.* **2008**, *47* (17), 7802–7812. https://doi.org/10.1021/ic800842f.

(55) Kitchen, J. A.; Barry, D. E.; Mercs, L.; Albrecht, M.; Peacock, R. D.; Gunnlaugsson, T. Circularly Polarized Lanthanide Luminescence from Langmuir-Blodgett Films Formed from Optically Active and Amphiphilic Eu III-Based Self-Assembly Complexes. *Angew. Chemie - Int. Ed.* **2012**, *51* (3), 704–708. https://doi.org/10.1002/anie.201106863.

(56) Binnemans, K. Interpretation of Europium(III) Spectra. *Coordination Chemistry Reviews*. Elsevier B.V. 2015, pp 1–45. https://doi.org/10.1016/j.ccr.2015.02.015.

(57) Chen, X. Y.; Liu, G. K. The Standard and Anomalous Crystal-Field Spectra of Eu3+. *J. Solid State Chem.* **2005**, *178* (2 SPEC. ISS.), 419–428. https://doi.org/10.1016/j.jssc.2004.09.002.

(58) Parchur, A. K.; Ningthoujam, R. S. Behaviour of Electric and Magnetic Dipole Transitions of Eu3+, 5D0 → 7F0 and Eu-O Charge Transfer Band in Li+ Co-Doped YPO4:Eu3+. *RSC Adv.* **2012**, *2* (29), 10859–10868. https://doi.org/10.1039/c2ra22144f.

(59) Han, M.; Zhang, H. Y.; Yang, L. X.; Jiang, Q.; Liu, Y. A Reversible Luminescent Lanthanide Switch Based on a Dibenzo[24]-Crown-8 - Dipicolinic Acid Conjugate. *Org. Lett.* **2008**, *10* (24), 5557–5560. https://doi.org/10.1021/ol802376k.

(60) Yoon, M. S.; Santra, M.; Ahn, K. H. Preparation of Luminescent Lanthanide Polymers by Ring-Opening Metathesis Polymerization. *Tetrahedron Lett.* **2015**, *56* (41), 5573–5577. https://doi.org/10.1016/j.tetlet.2015.08.042.

(61) Jones, G.; Vullev, V. I. Medium Effects on the Photophysical Properties of Terbium(III) Complexes with Pyridine-2,6-Dicarboxylate. *Photochem. Photobiol. Sci.* **2002**, *1* (12), 925–933. https://doi.org/10.1039/b206370k.

(62) Gallardo, H.; Conte, G.; Bortoluzzi, A. J.; Bechtold, I. H.; Pereira, A.; Quirino, W. G.; Legnani, C.; Cremona, M. Synthesis, Structural Characterization, and Photo and Electroluminescence of a Novel Terbium(III) Complex: {Tris(Acetylacetonate) [1,2,5]Thiadiazolo[3,4- f][1,10]Phenanthroline}terbium(III). *Inorganica Chim. Acta* **2011**, *365* (1), 152–158. https://doi.org/10.1016/j.ica.2010.09.003.

(63) Tigaa, R. A.; Lucas, G. J.; De Bettencourt-Dias, A. ZnS Nanoparticles Sensitize Luminescence of Capping-Ligand-Bound Lanthanide Ions. *Inorg. Chem.* **2017**, *56* (6), 3260–3268. https://doi.org/10.1021/acs.inorgchem.6b02638.

(64) Gregório, T.; Leão, J. D. M.; Barbosa, G. A.; Ramos, J. D. L.; Om Kumar Giese, S.; Briganti, M.; Rodrigues, P. C.; De Sá, E. L.; Viana, E. R.; Hughes, D. L.; et al. Promoting a Significant Increase in the Photoluminescence Quantum Yield of Terbium(III) Complexes by Ligand Modification. *Inorg. Chem.* **2019**, *58* (18), 12099–12111. https://doi.org/10.1021/acs.inorgchem.9b01397.

(65) Johnson, K. R.; De Bettencourt-Dias, A. 1O2 Generating Luminescent Lanthanide Complexes with 1,8-Naphthalimide-Based Sensitizers. *Inorg. Chem.* **2019**, *58* (19), 13471–13480. https://doi.org/10.1021/acs.inorgchem.9b02431.

(66) Kitchen, J. A.; Barry, D. E.; Mercs, L.; Albrecht, M.; Peacock, R. D.; Gunnlaugsson, T. Circularly Polarized Lanthanide Luminescence from Langmuir-Blodgett Films Formed from Optically Active and Amphiphilic Eu III-Based Self-Assembly Complexes. *Angew. Chemie - Int. Ed.* **2012**, *51* (3), 704–708. https://doi.org/10.1002/anie.201106863.

(67) Lincheneau, C.; Destribats, C.; Barry, D. E.; Kitchen, J. A.; Peacock, R. D.; Gunnlaugsson, T. Lanthanide Directed Self-Assembly Synthesis and Photophysical Evaluation of Chiral Eu(Iii) Luminescent “Half-Helicates.” *Dalton. Trans.* **2011**, *40* (45), 12056–12059. https://doi.org/10.1039/c1dt11225b.

(68) Lal, K.; Kaushik, C. P.; Kumar, K.; Kumar, A.; Qazi, A. K.; Hamid, A.; Jaglan, S. One-Pot Synthesis and Cytotoxic Evaluation of Amide-Linked 1,4-Disubstituted 1,2,3-Bistriazoles. *Med. Chem. Res.* **2014**, *23* (11), 4761–4770. https://doi.org/10.1007/s00044-014-1038-5.

(69) Galanti, A.; Kotova, O.; Blasco, S.; Johnson, C. J.; Peacock, R. D.; Mills, S.; Boland, J. J.; Albrecht, M.; Gunnlaugsson, T. Exploring the Effect of Ligand Structural Isomerism in Langmuir–Blodgett Films of Chiral Luminescent EuIIISelf-Assemblies. *Chem. - A Eur. J.* **2016**, *22* (28), 9709–9723. https://doi.org/10.1002/chem.201600560.

APPENDIX

NMR spectra of synthesised ligands.

^{1}HNMR Spectrum of **L1**

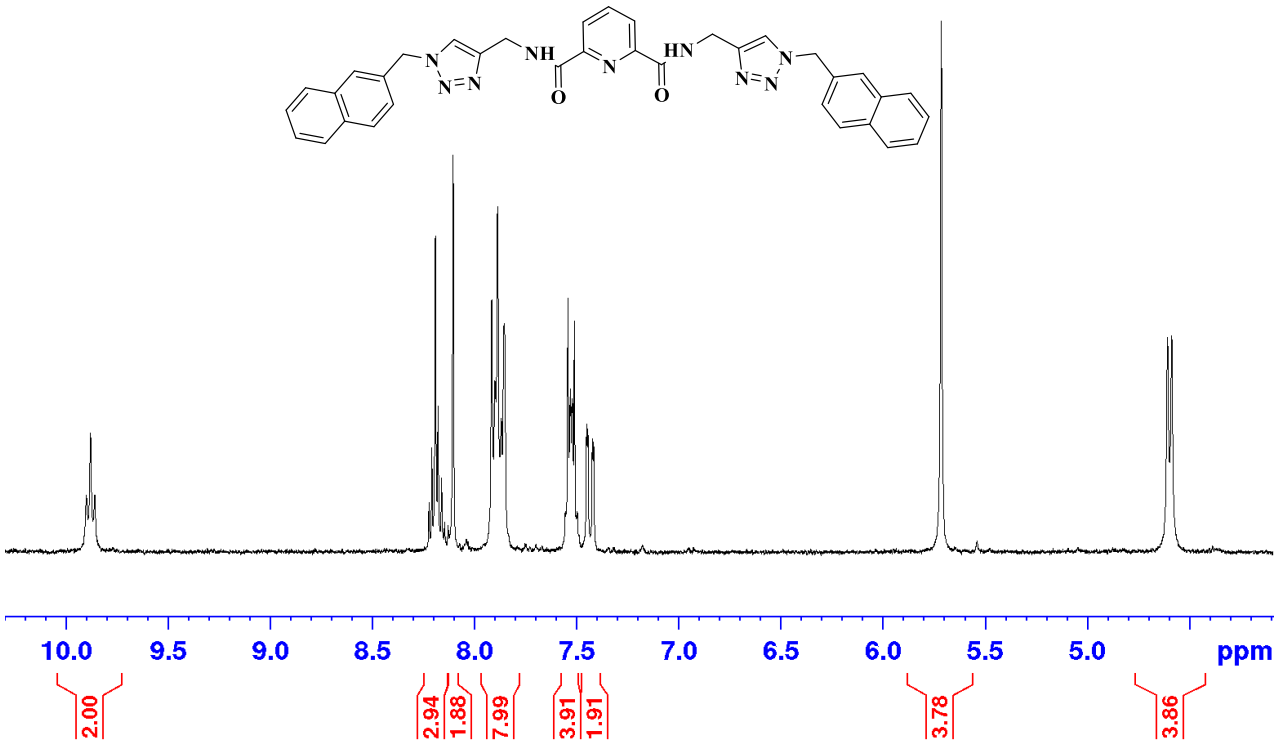

^{13}C NMR Spectrum of **L1**

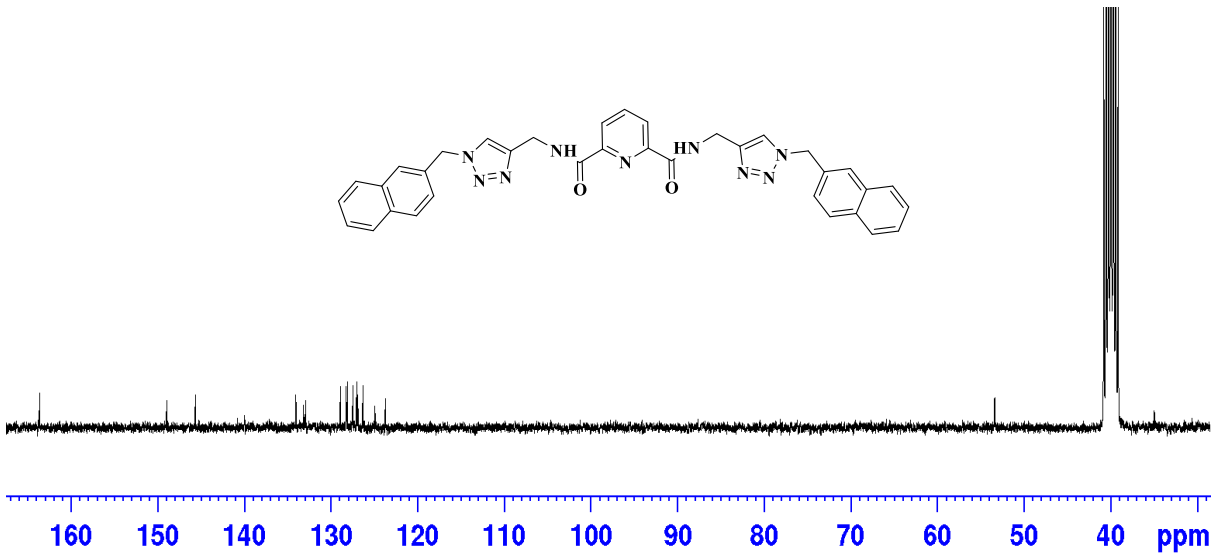

[1]HNMR Spectrum of **L2**

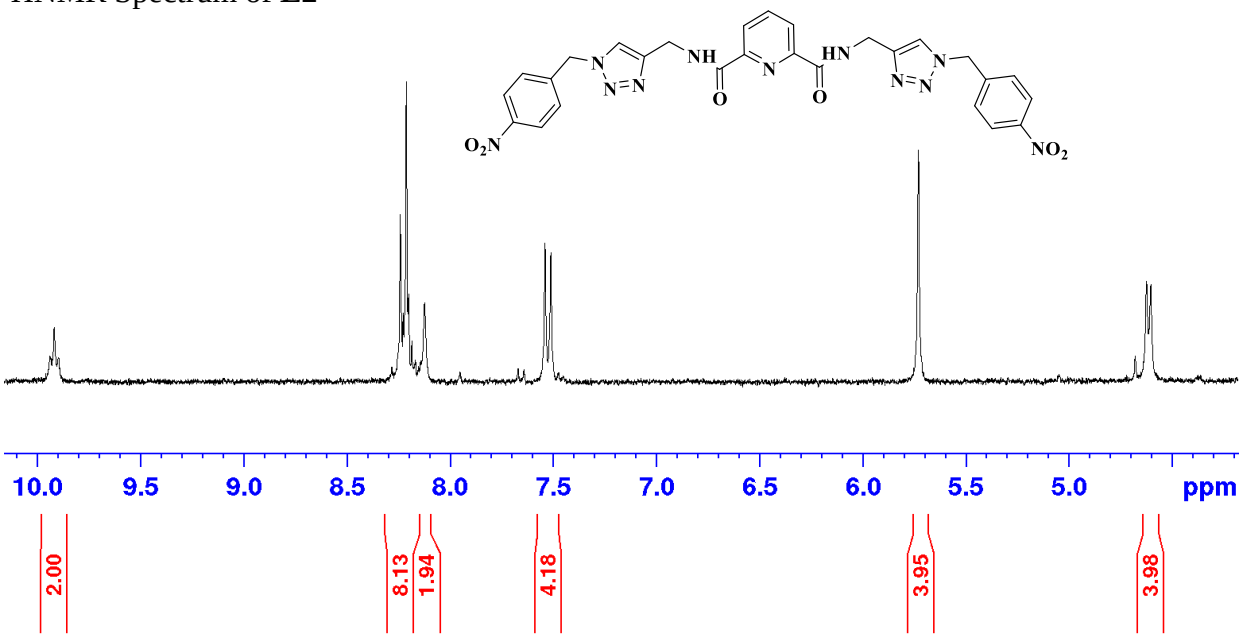

[13]C NMR Spectrum of **L2**

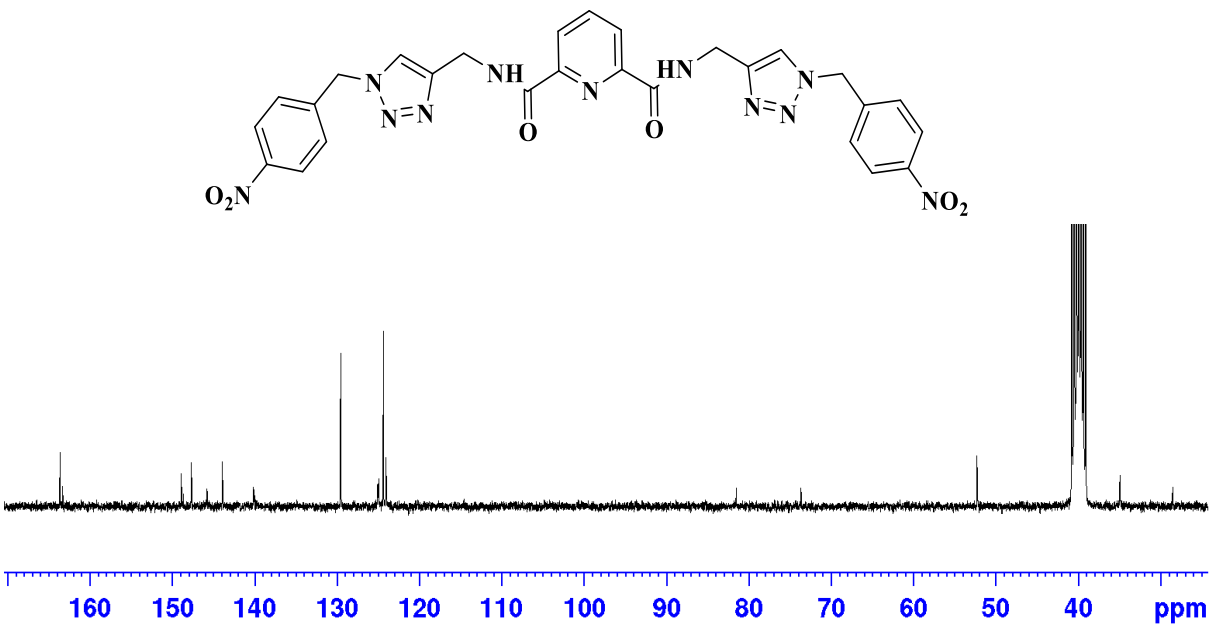

^{1}HNMR Spectrum of **L3**

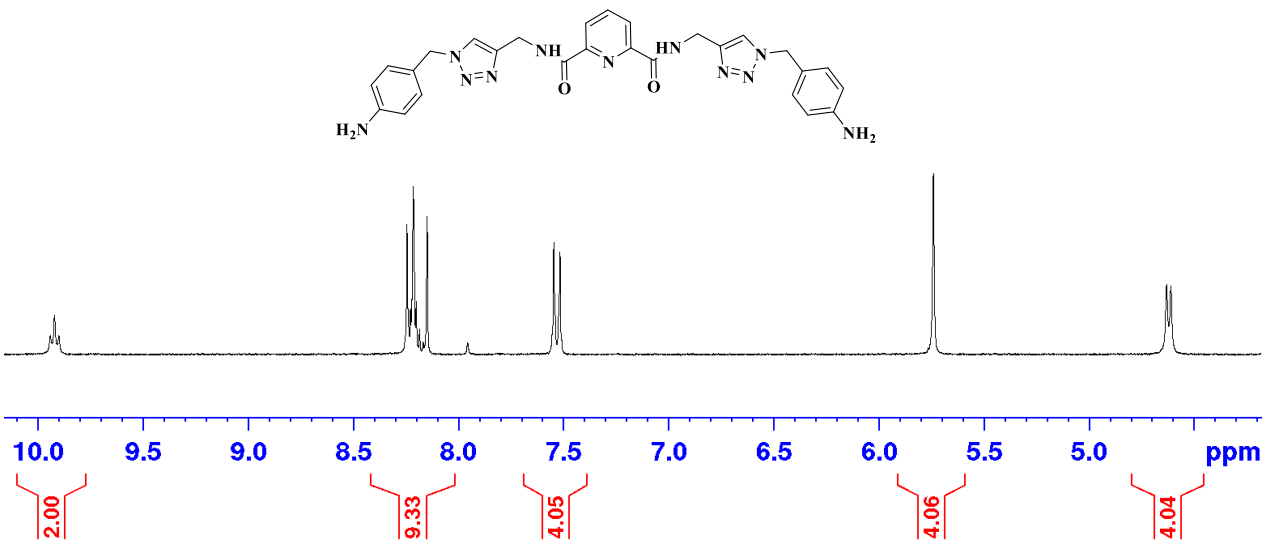

^{13}C NMR Spectrum of **L3**

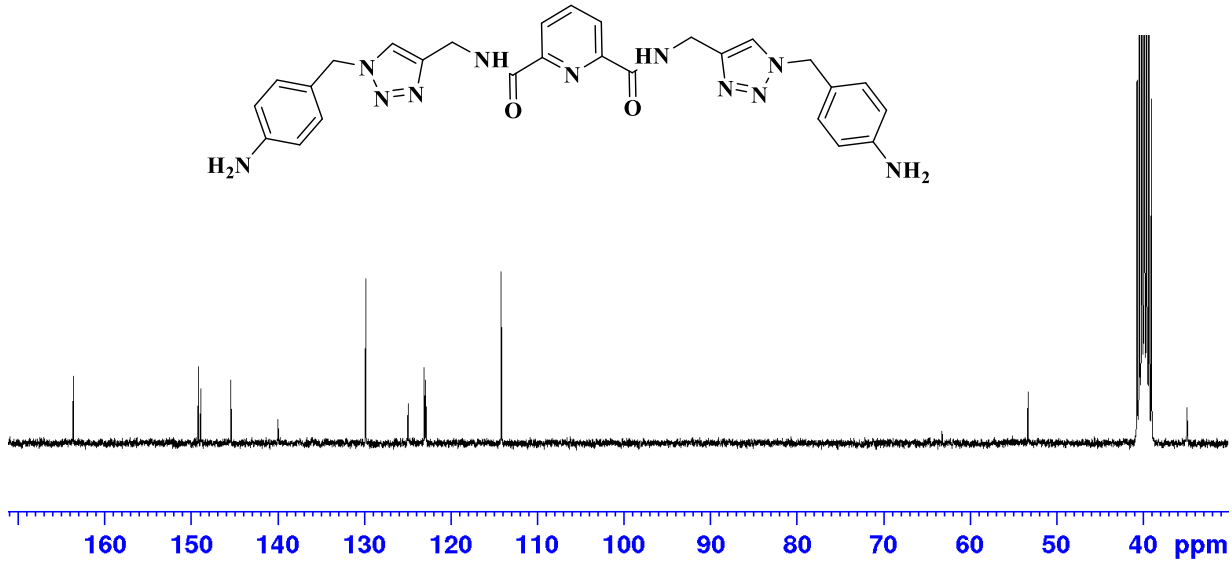

[1]HNMR Spectrum of **L4**

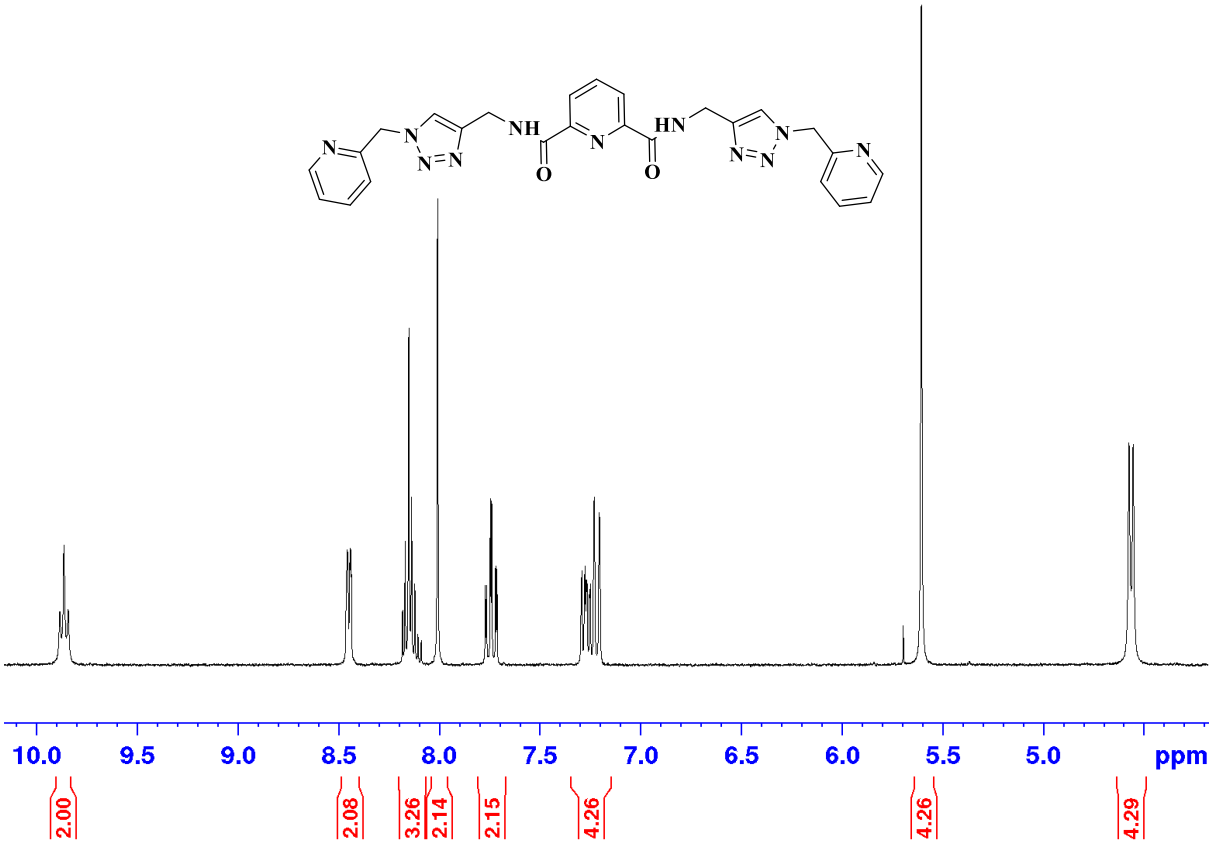

[13]C NMR Spectrum of **L4**

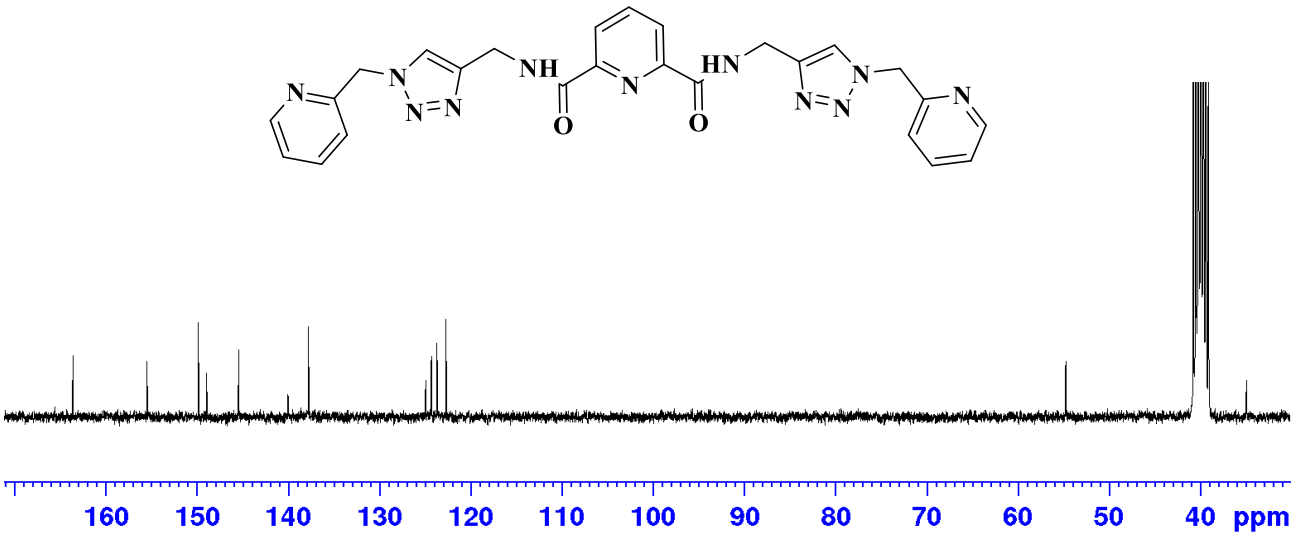

[1]HNMR Spectrum of **L5**

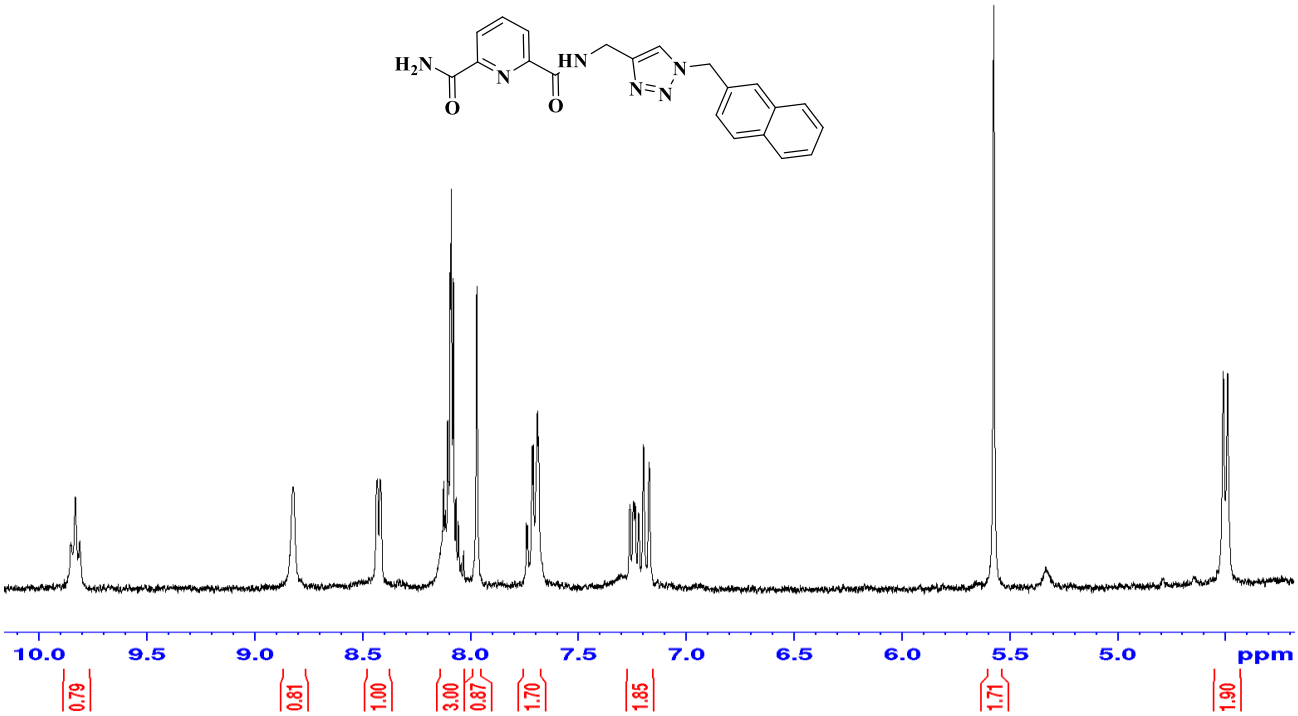

[13]C NMR Spectrum of **L5**

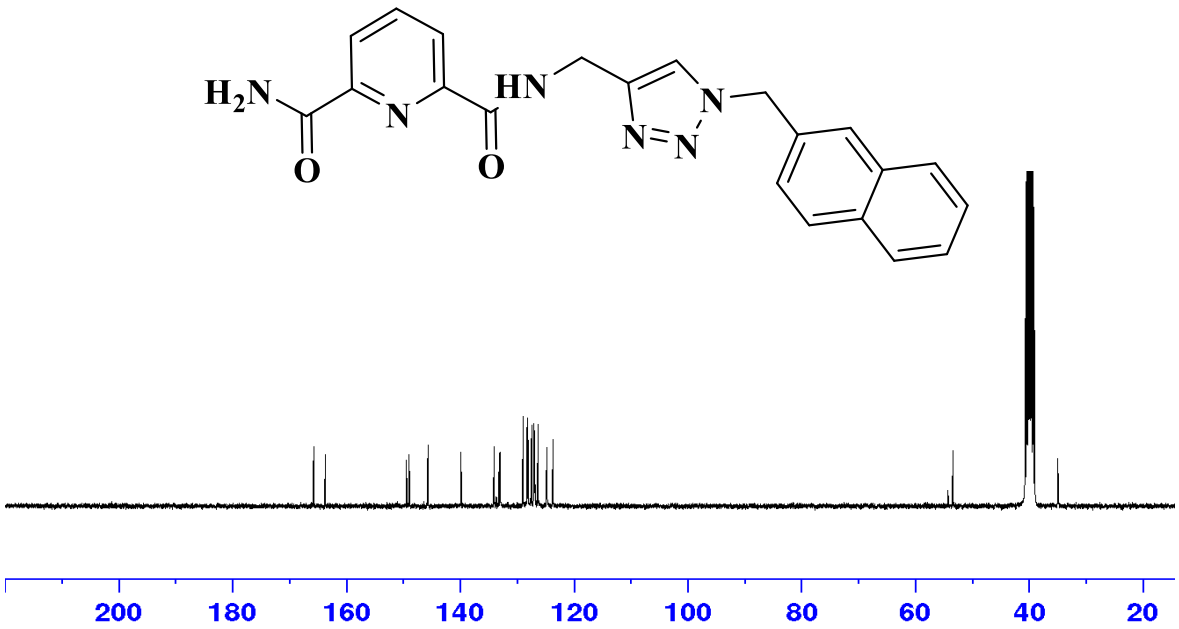

[1]HNMR Spectrum of **L6**

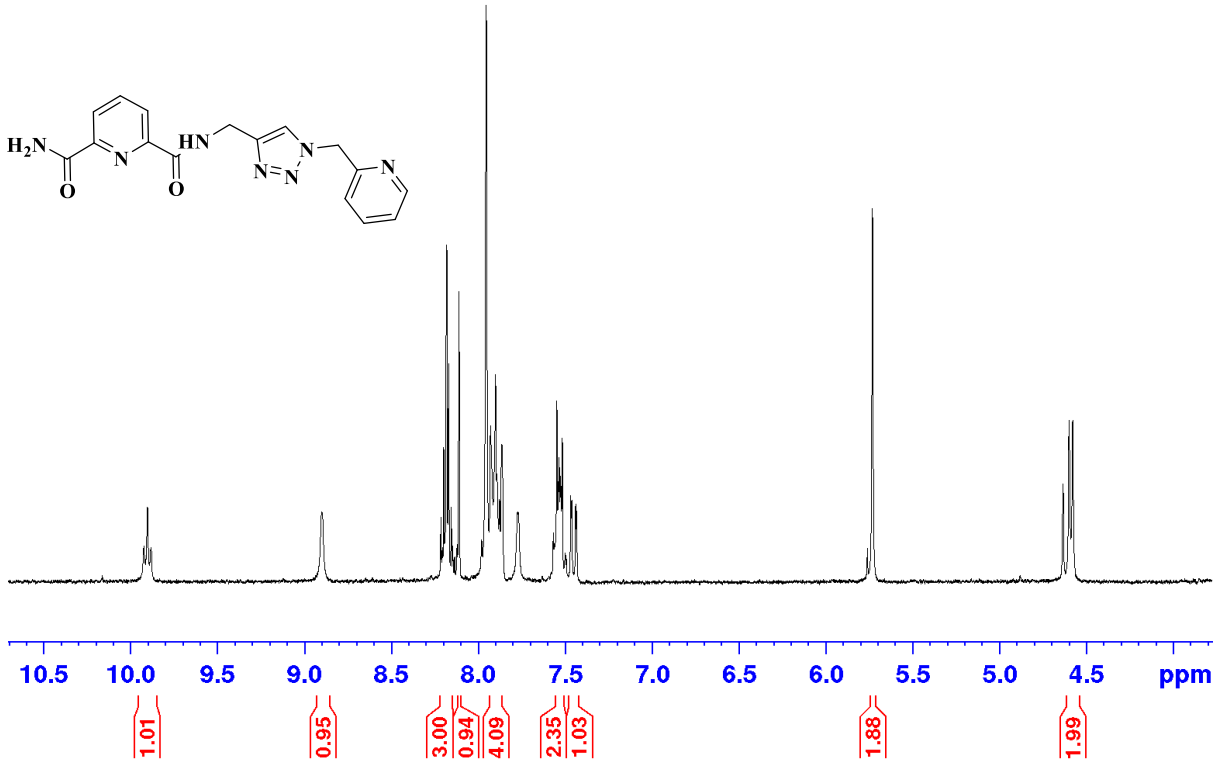

[13]C NMR Spectrum of **L6**

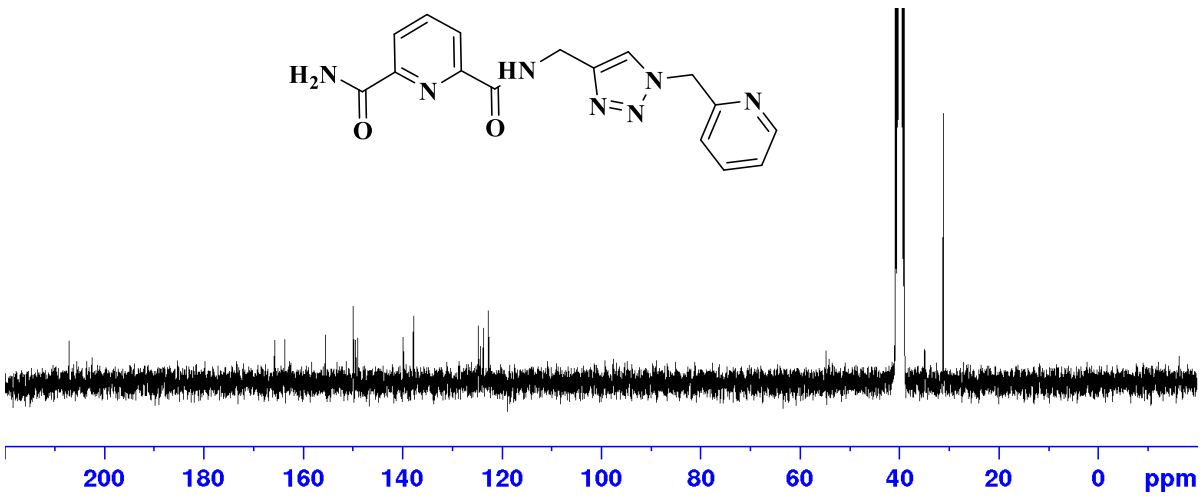

^{1}HNMR Spectrum of deprotected mono alkyne

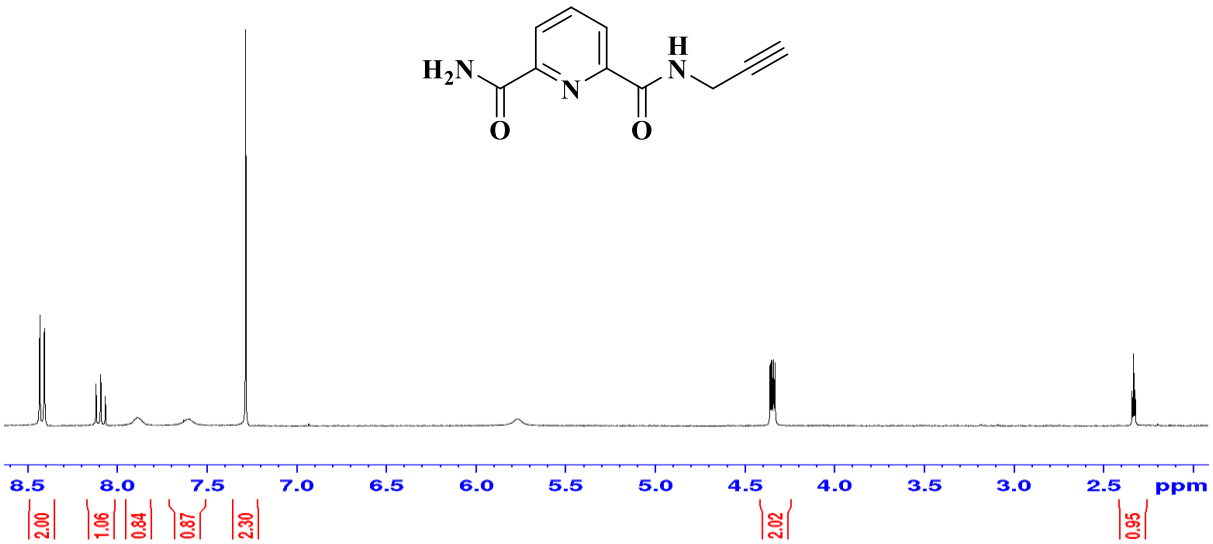

^{1}HNMR Spectrum of *N*^{2},*N*^{6}*-Di-2-propyn-1-yl-2,6-pyridinedicarboxamide*

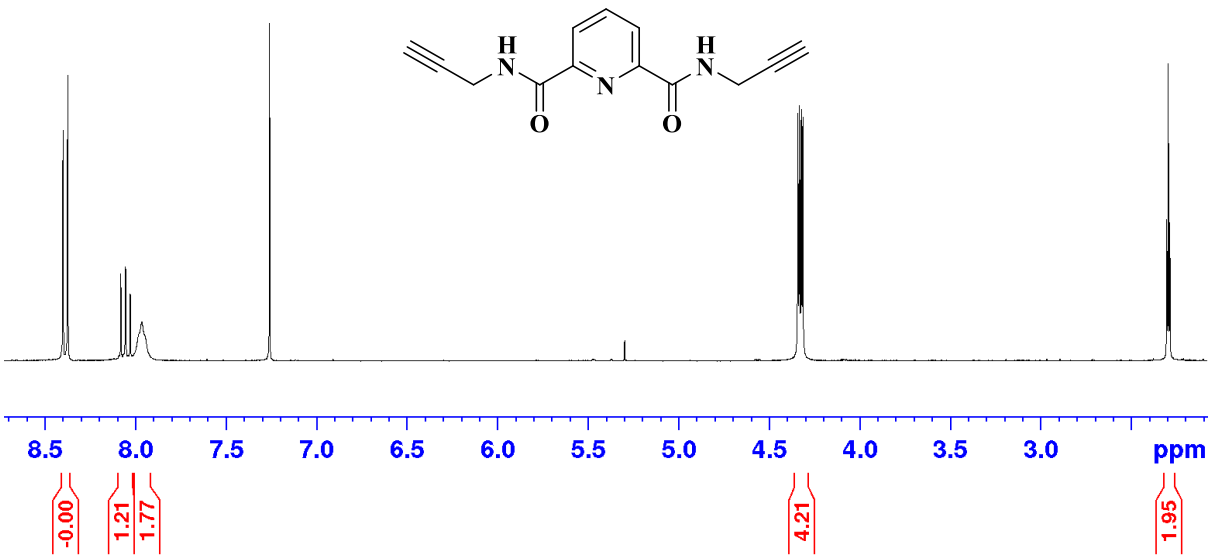

^{13}C NMR Spectrum of N^2,N^6-Di-2-propyn-1-yl-2,6-pyridinedicarboxamide

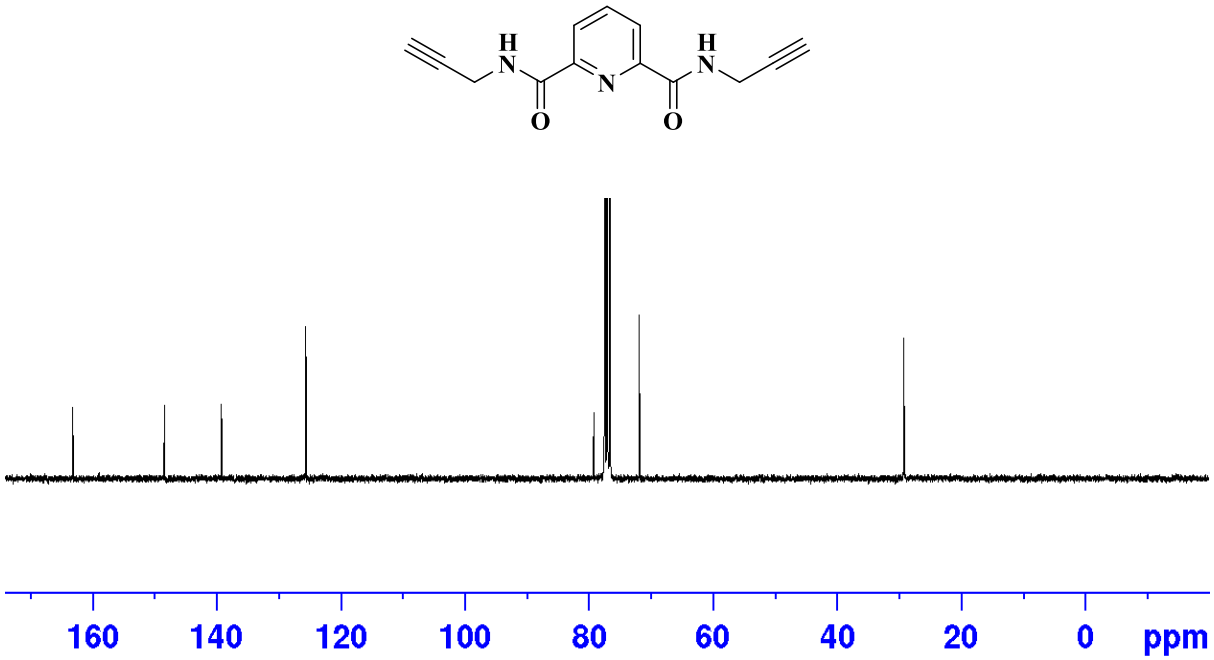

^{1}HNMR Spectrum of *Pyridine-2,6-dicarboxylicmonobenzyl ester*

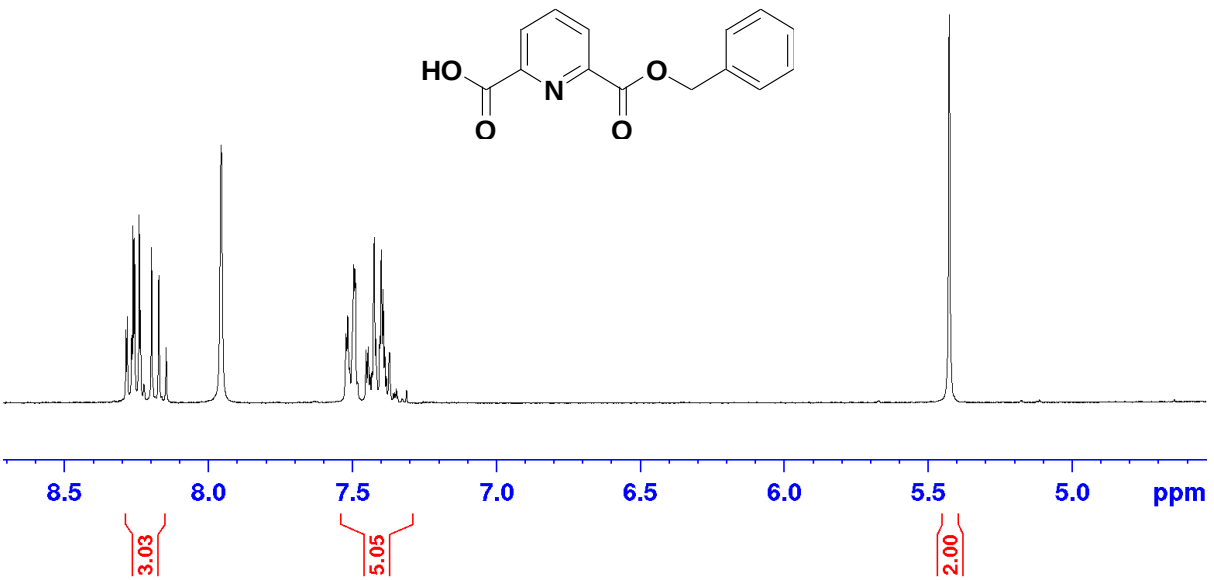

[1]HNMR Spectrum of *6-Prop-2-ynylcarbamoyl-pyridine-2-carboxylic acid benzyl ester*

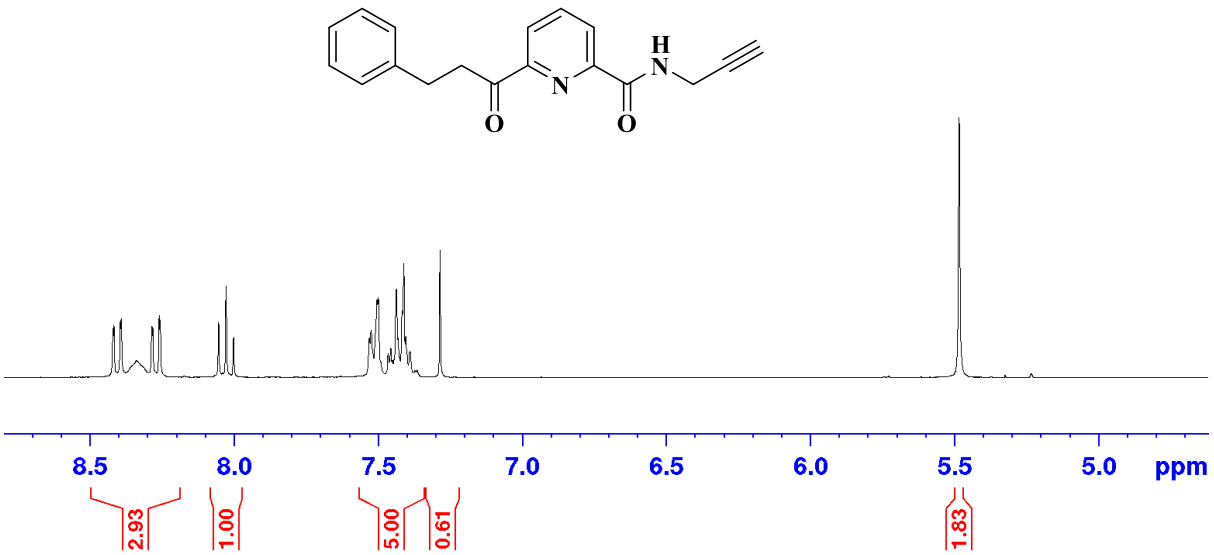

[13]C NMR Spectrum of *6-Prop-2-ynylcarbamoyl-pyridine-2-carboxylic acid benzyl ester*

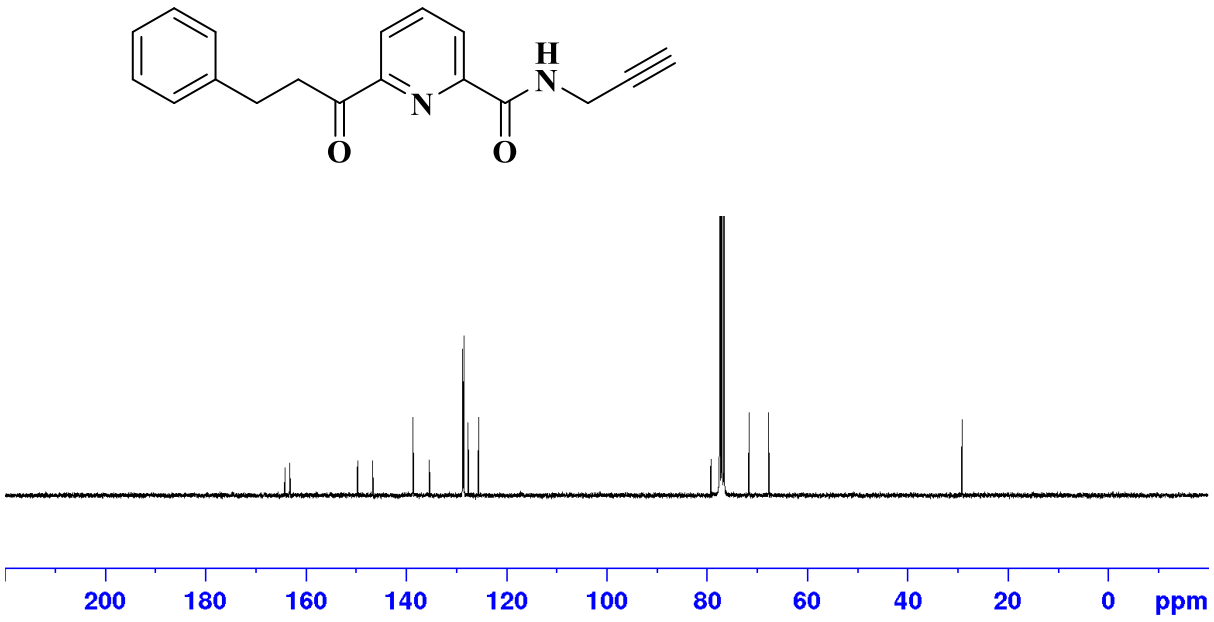

[1]HNMR Spectrum of *Mono-NO_2* ligand

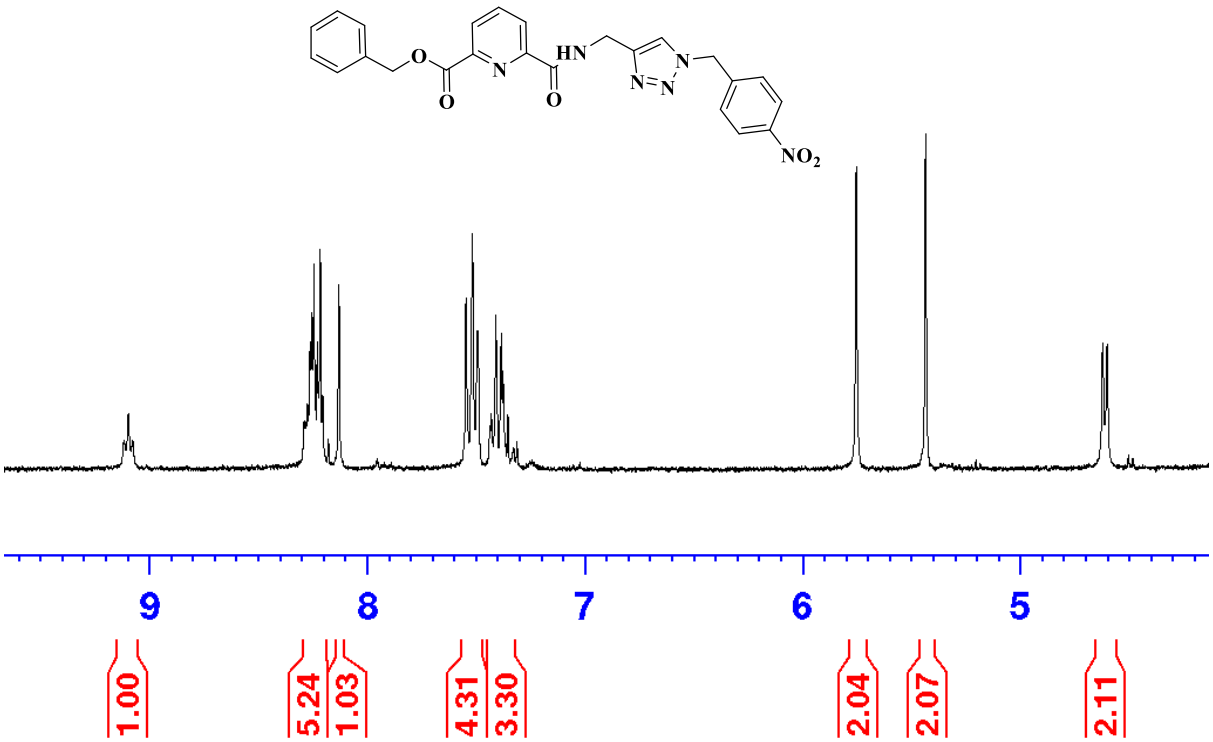

FTIR spectra of ligands.

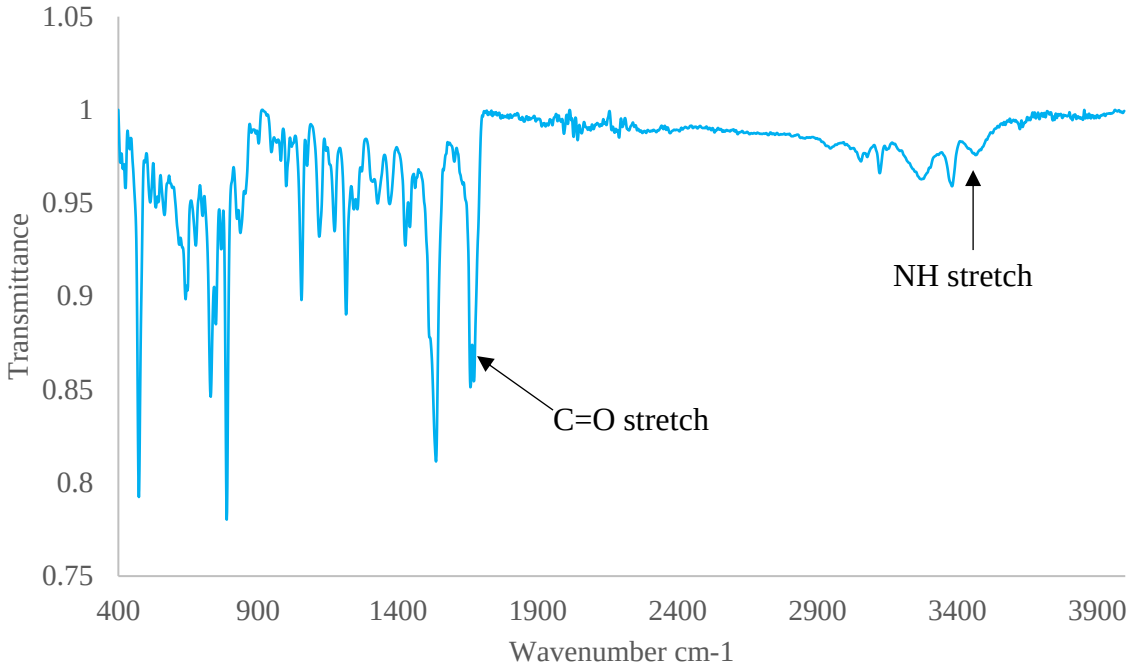

FT-IR spectra of **L1** showing the characteristic C=O stretch and NH stretch of the triazole at 1658 cm-1 and .3470 cm^{-1} respectively.

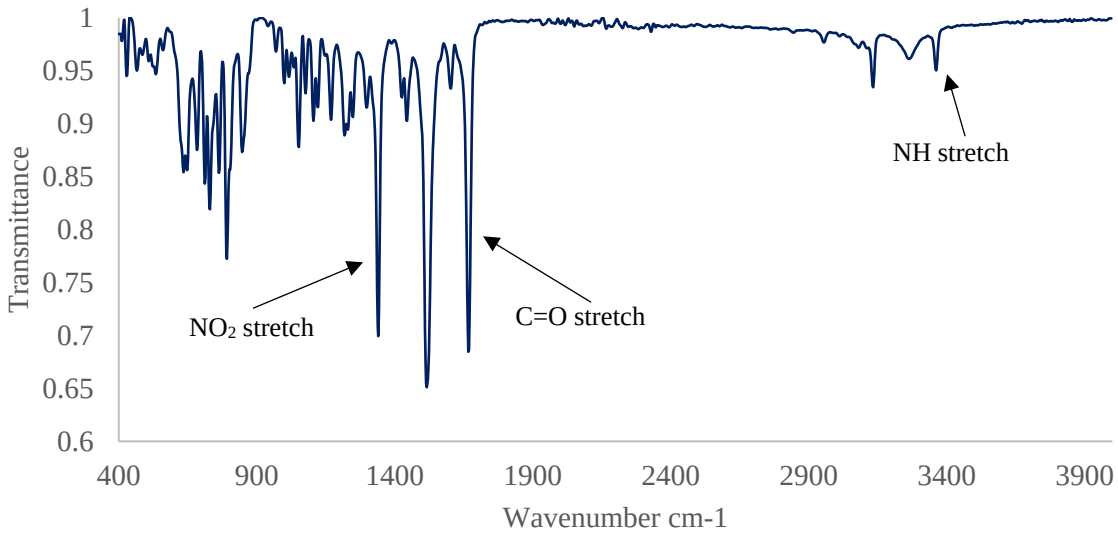

FT-IR spectra of **L2** showing the characteristic C=O, NO_2 and NH stretch of the triazole at 1668 cm^{-1}, 1338 cm^{-1} and 3357 cm^{-1} respectively.

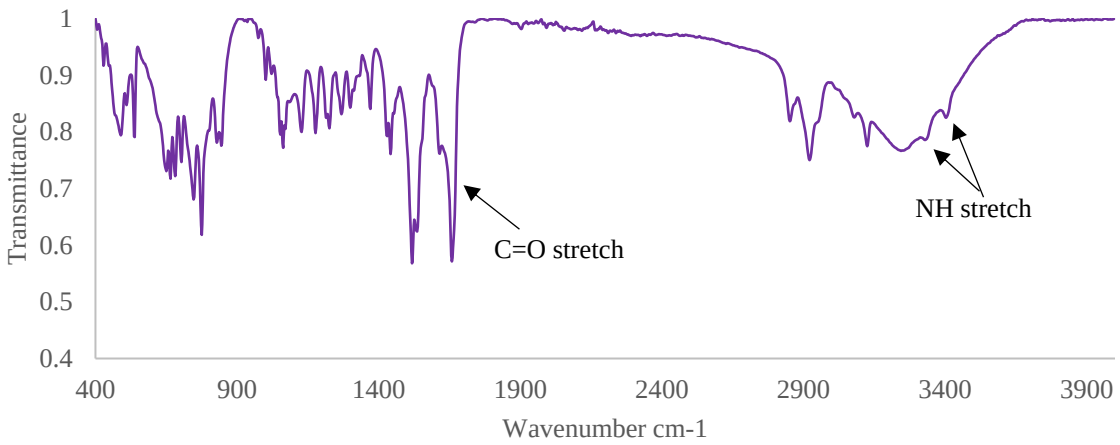

FT-IR spectra of **L3** showing the characteristic C=O, and NH stretches due to the amino group (1^0 amine) at 1660 cm^{-1}, 3337 cm^{-1} and 3404 cm^{-1} respectively.

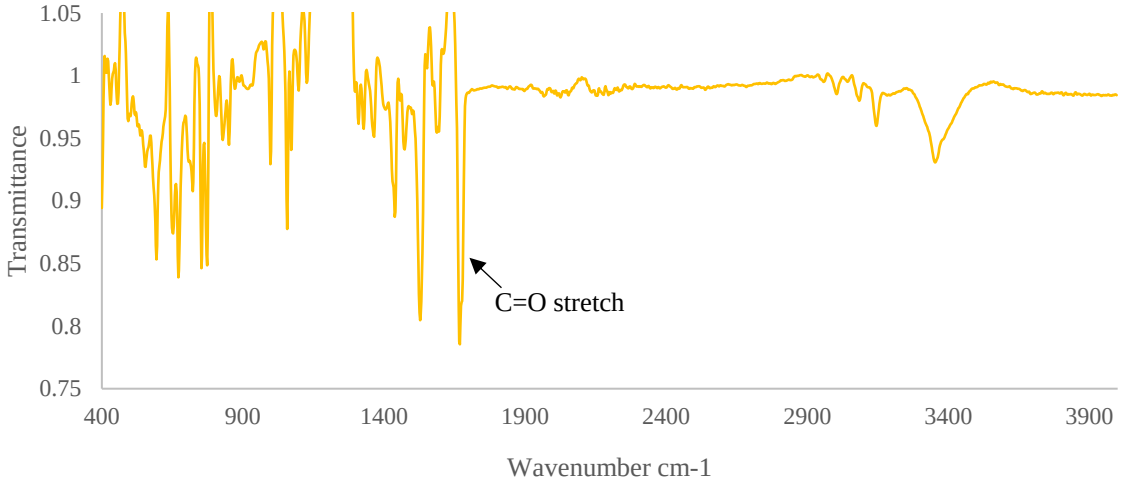

FT-IR spectra of **L4** showing the characteristic C=O, stretch 1668 cm^{-1}.

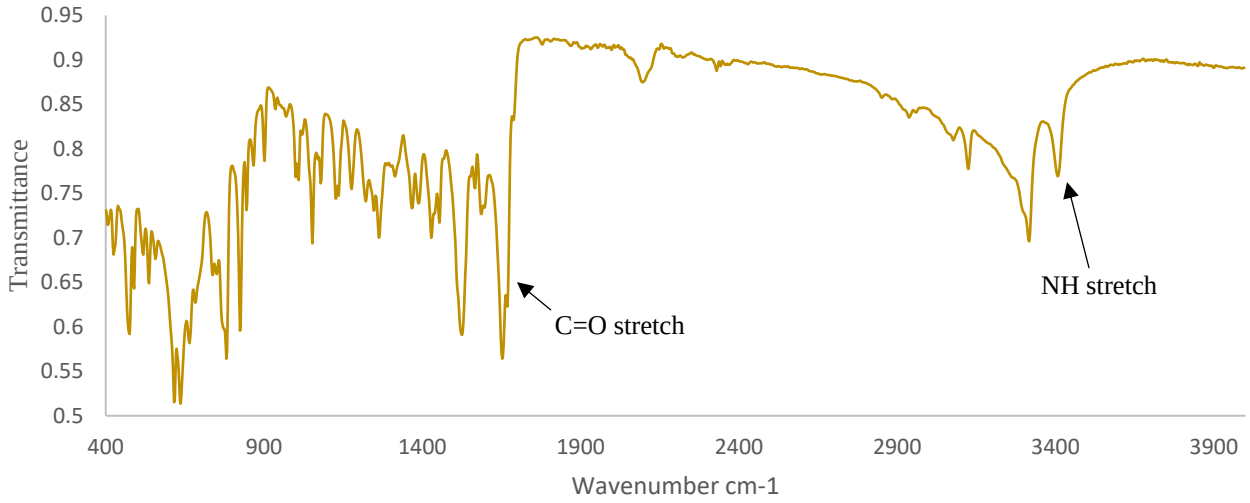

FT-IR spectra of **L5** showing the characteristic C=O and NH (triazole) stretches 1654 cm^{-1} and 3410 cm^{-1} respectively.

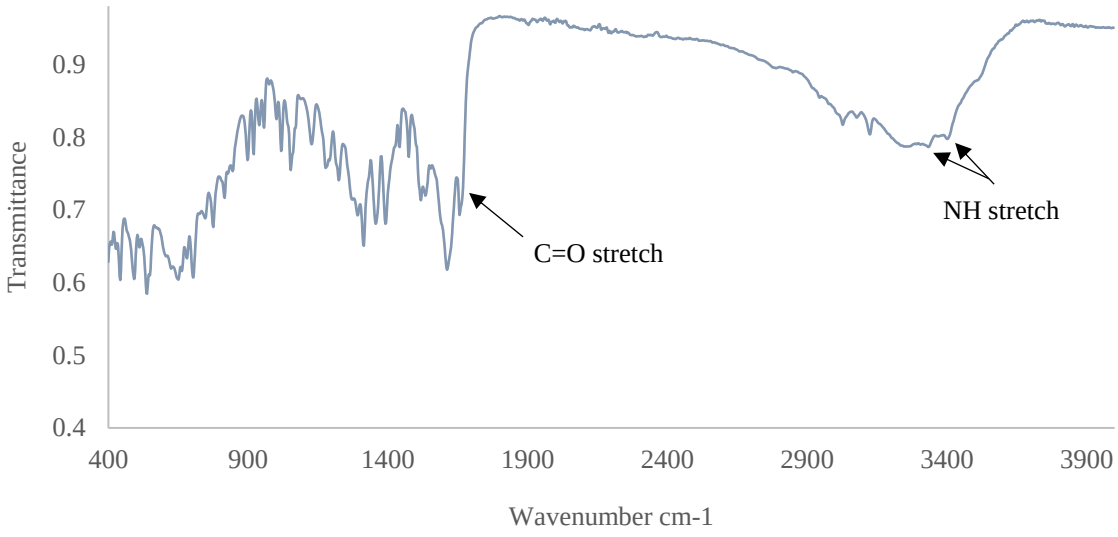

FT-IR spectra of **L5** showing the characteristic C=O and NH stretches 1658 cm^{-1}, 3331 cm^{-1} and 3404 cm^{-1} respectively.

FTIR spectra of complexes

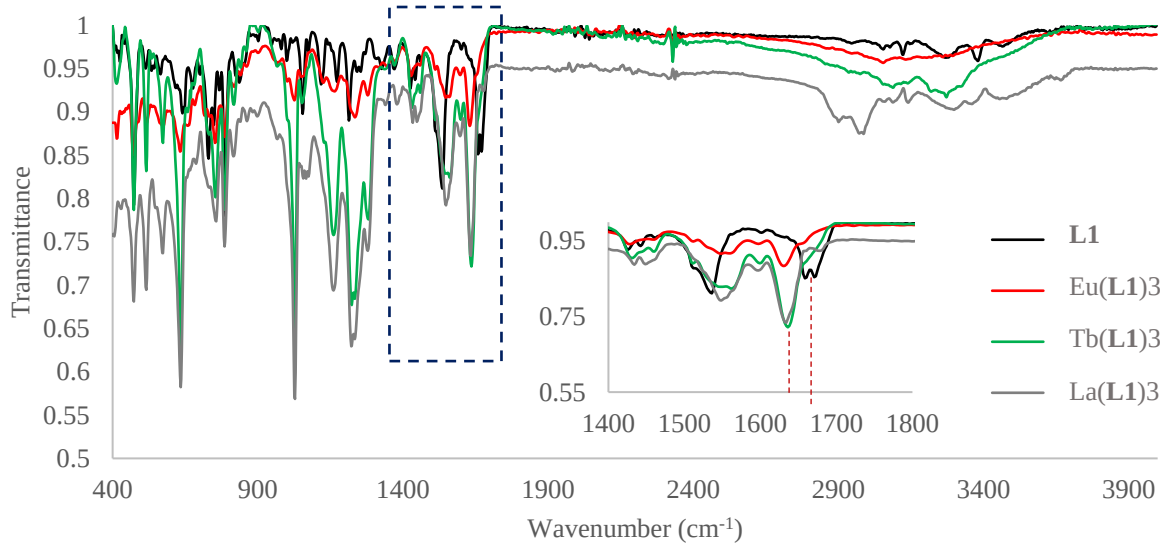

Stacked FT-IR spectra of **L1** and **L1** complexes (Eu, Tb and La) showing the peak shift around 1600 cm^{-1}.

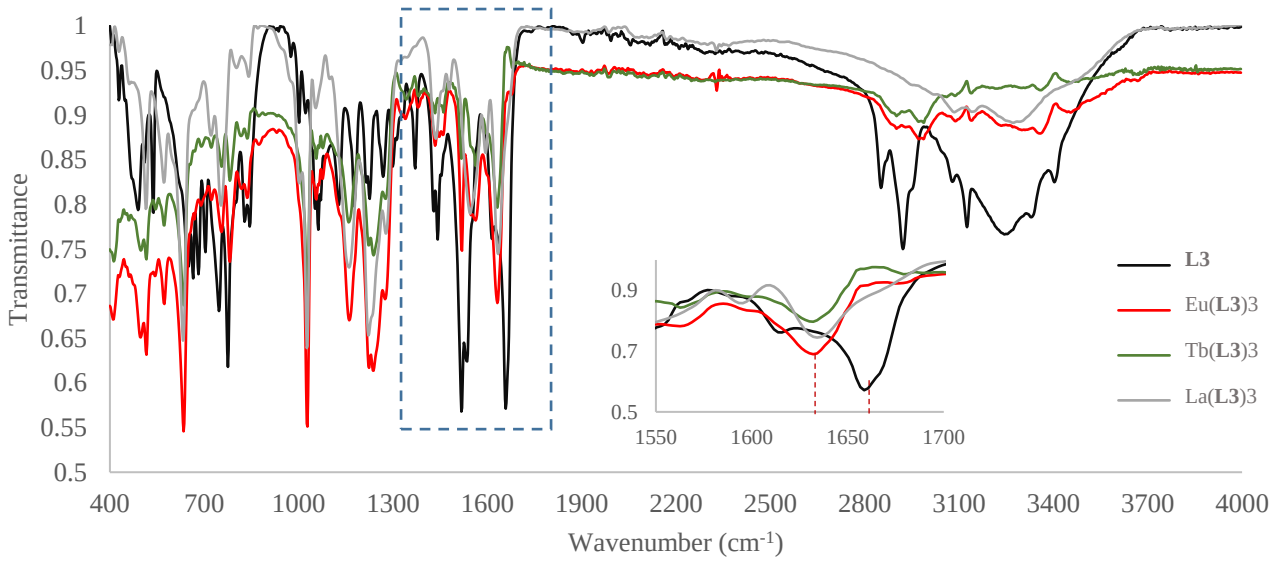

Stacked FT-IR spectra of **L3** and **L3** complexes (Eu, Tb and La) showing the peak shift around 1600 cm^{-1}.

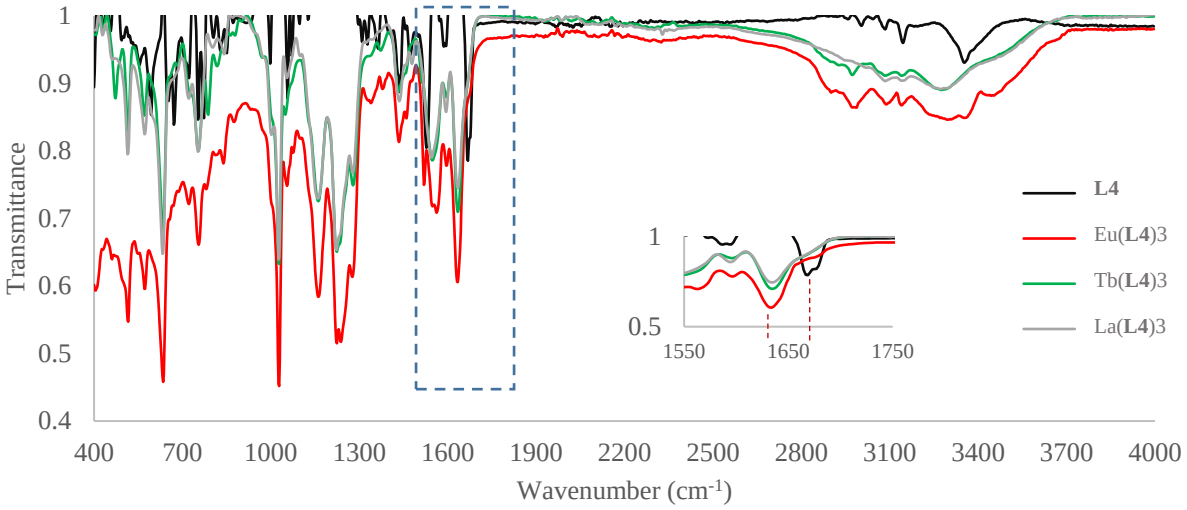

Stacked FT-IR spectra of **L4** and **L4** complexes (Eu, Tb and La) showing the peak shift around 1600 cm^{-1}.

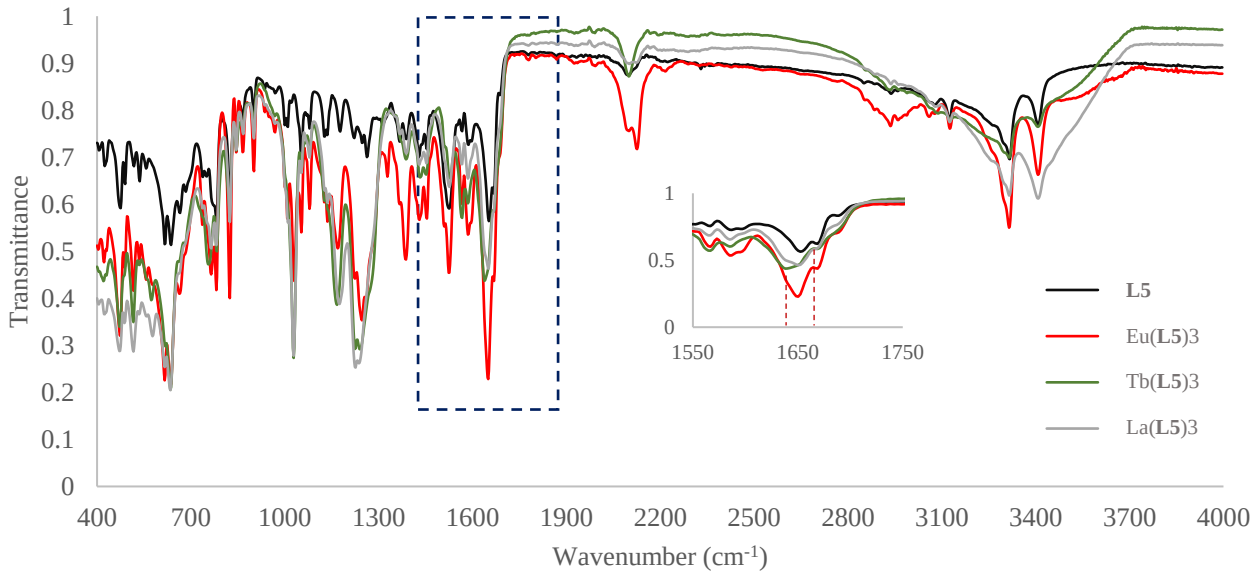

Stacked FT-IR spectra of **L5** and **L5** complexes (Eu, Tb and La) showing the peak shift around 1600 cm^{-1}.

Synthesized Ligands

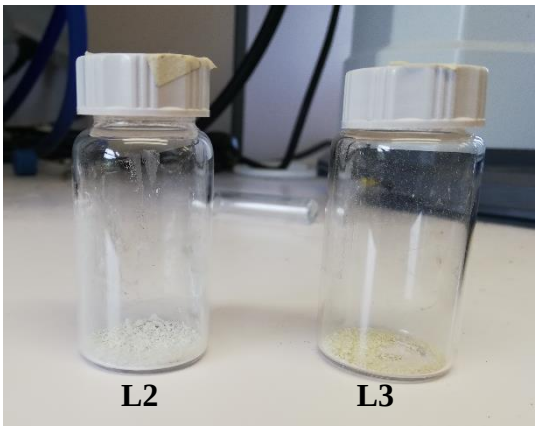

Figure a: L2 and **L3** ligands.

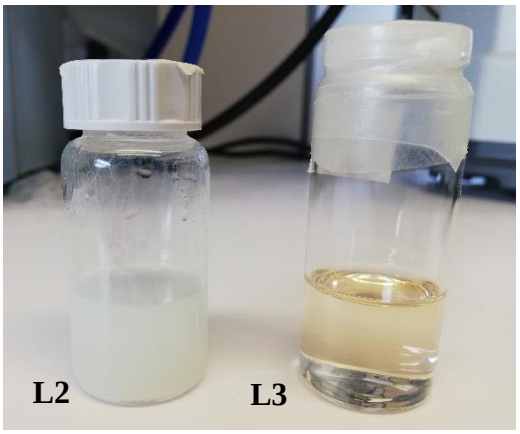

Figure b: L2 and **L3** ligands dissolved in ethanol at 60° C

Figure a shows the **L2** and **L3** ligands. **L2** was obtained as a white powder-like substance from the click reaction while **L3** was obtained as a pale-yellow compound after the reduction. **Figure b** shows the solubility of **L2** and **L3** in ethanol at 60° C. **L2** is immiscible in ethanol giving a cloudy solution. **L3** gives a yellow color solution at 60° C at a concentration of $1x10^{-3}$ M.

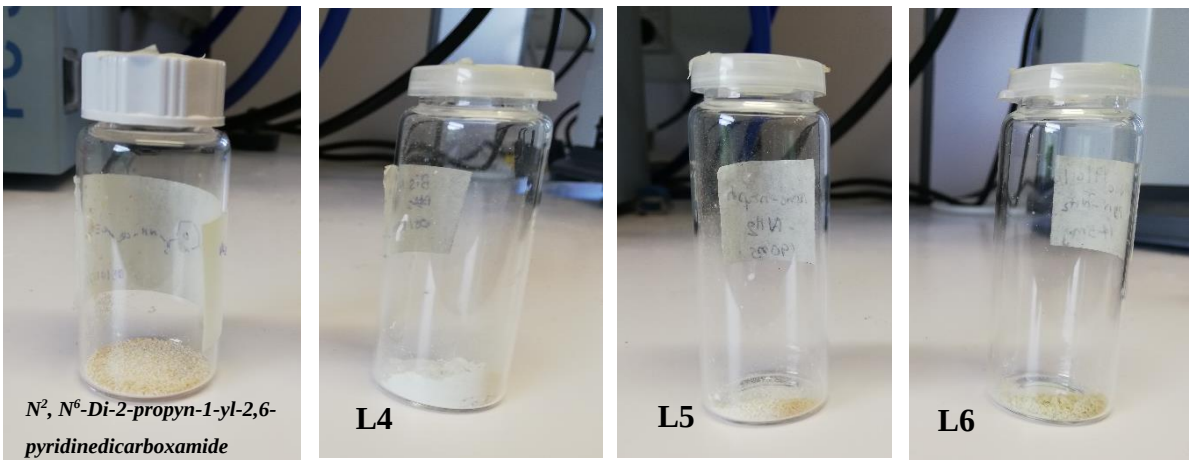

Figure c: N^2, N^6-Di-2-propyn-1-yl-2,6-pyridinedicarboxamide**, L4**, **L5,** and **L6**

UV/Vis data of ligands

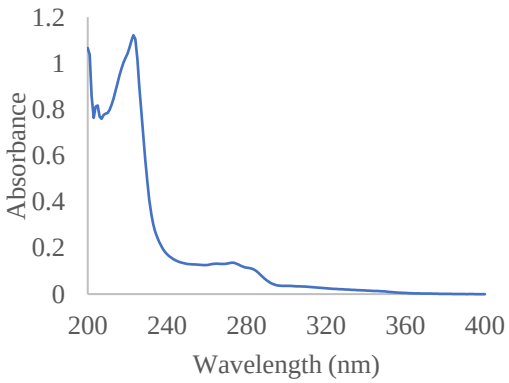

Absorption spectra of **L1** in acetonitrile (1x10^{-5} M, at 25° C)

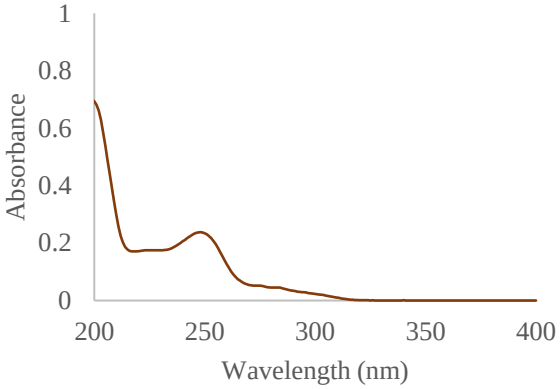

Absorption spectra of **L3** in acetonitrile (1x10^{-5} M, at 25° C)

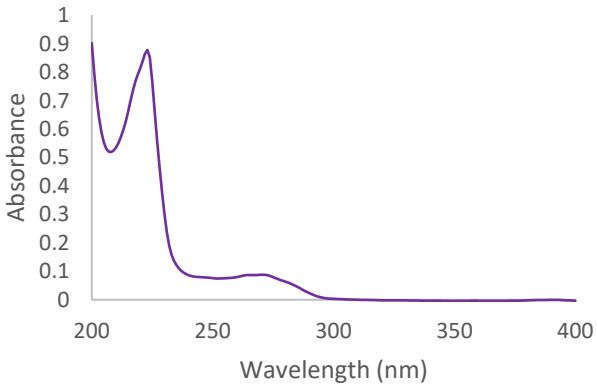

Absorption spectra of **L4** in acetonitrile (1x10^{-5} M, at 25° C)

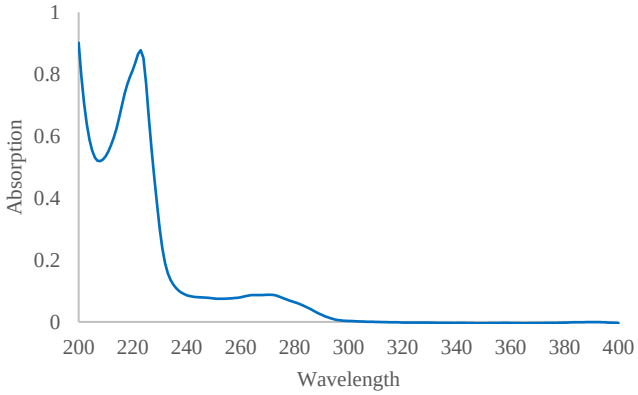

Absorption spectra of **L5** in acetonitrile (1x10^{-5} M, at 25° C)

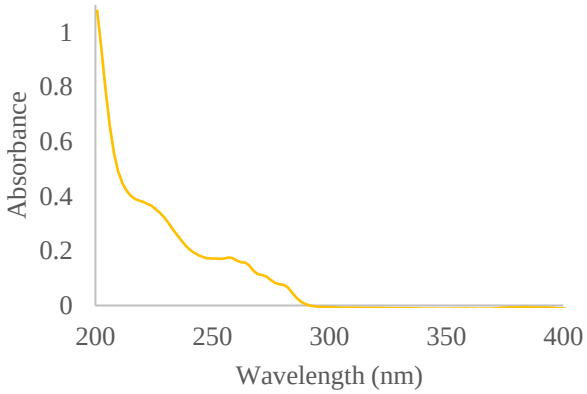

Absorption spectra of **L6** in acetonitrile (1 x 10^{-5} M at 25° C)

UV/Vis data of complexes

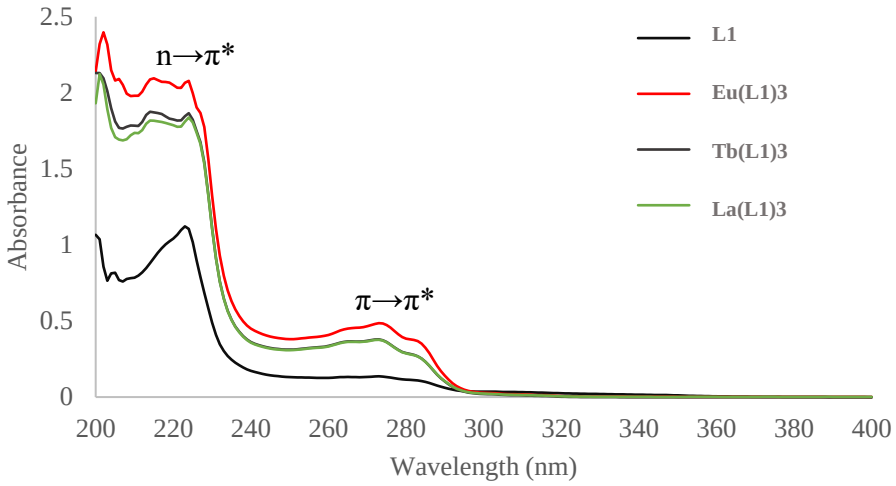

Absorbance spectra of **L1** and **L1** complexes showing n→π* and π→π* transitions

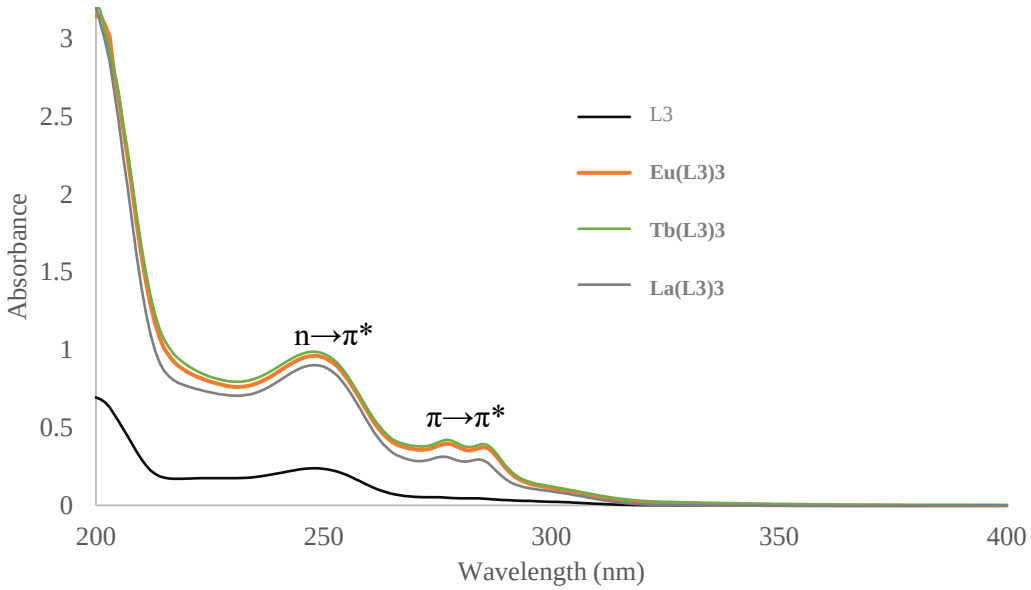

Absorbance spectra of **L3** and **L3** complexes showing n→π* and π→π* transitions

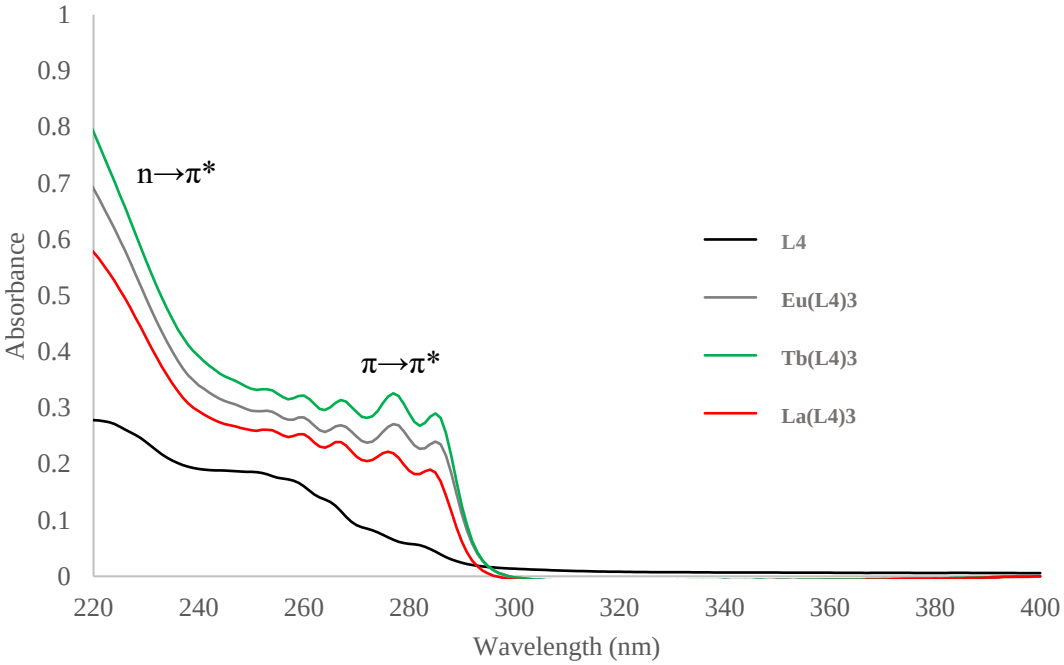

Absorbance spectra of **L4** and **L4** complexes showing n→π* and π→π* transitions

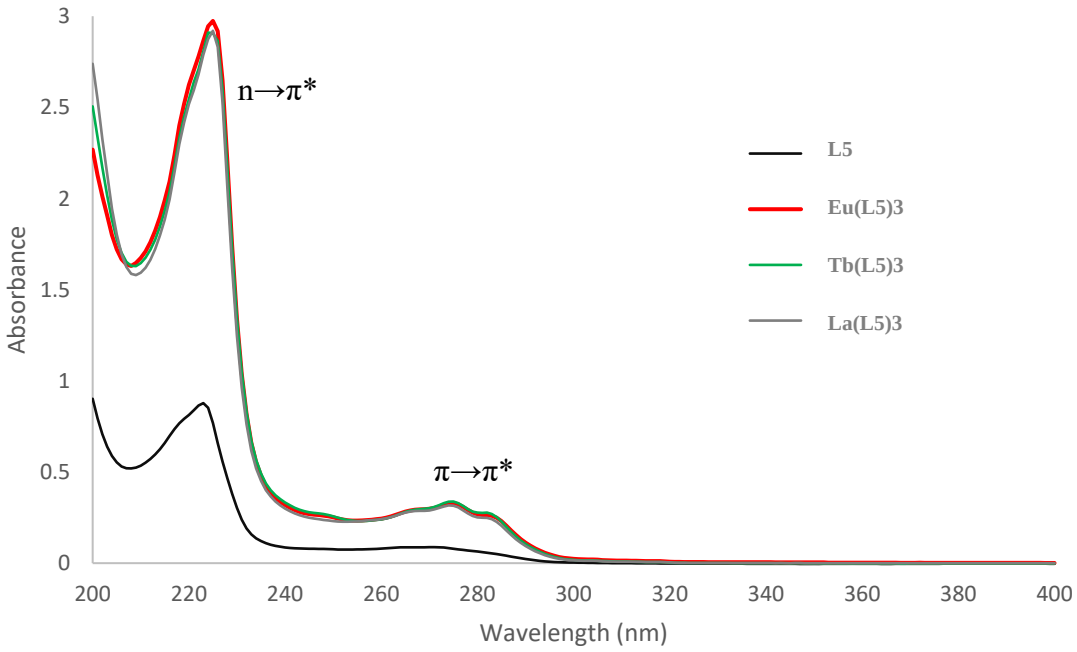

Absorbance spectra of **L5** and **L5** complexes showing n→π* and π→π* transitions

Photophysical properties of complexes

Eu(**L5**)$_3$

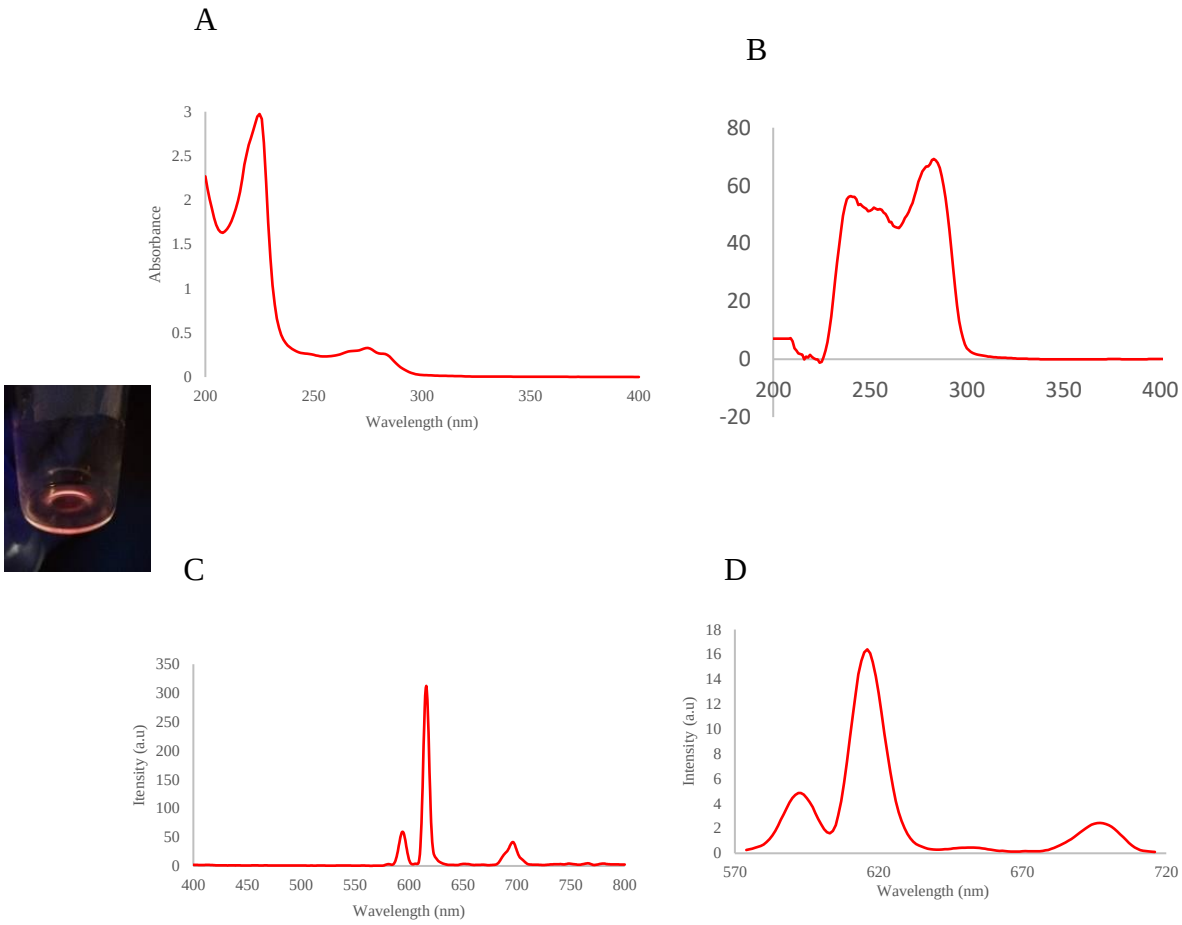

(A) The absorption spectrum, (B) the excitation spectrum, λ_{em} = 617 nm and (C) the fluorescence emission spectrum λ_{em} = 617 nm, (D) the phosphorescence emission spectrum, λ_{ex} = 286 nm of of Eu(**L5**)$_3$ in MeCN solution at RT (1 X 10^{-5} M)

Tb(**L5**)$_3$

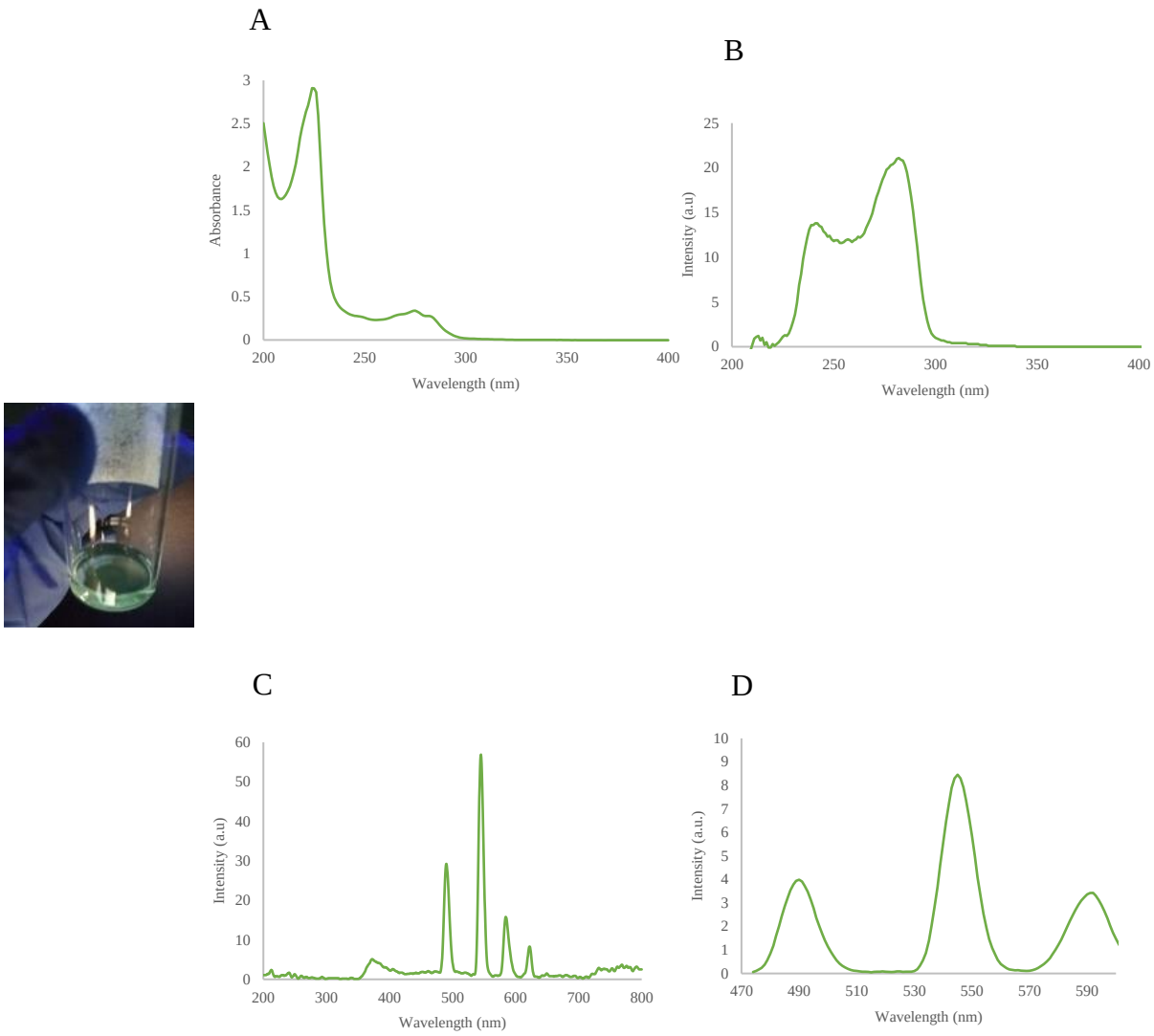

(A) The absorption spectrum, (B) the excitation spectrum, λ_{em} = 547 nm and (C) the fluorescence emission spectrum λ_{em} = 547 nm, (D) the phosphorescence emission spectrum, λ_{ex} = 286 nm of of Tb(**L5**)$_3$ in MeCN solution at RT (1 X 10^{-5} M)

Eu(**L1**)$_3$

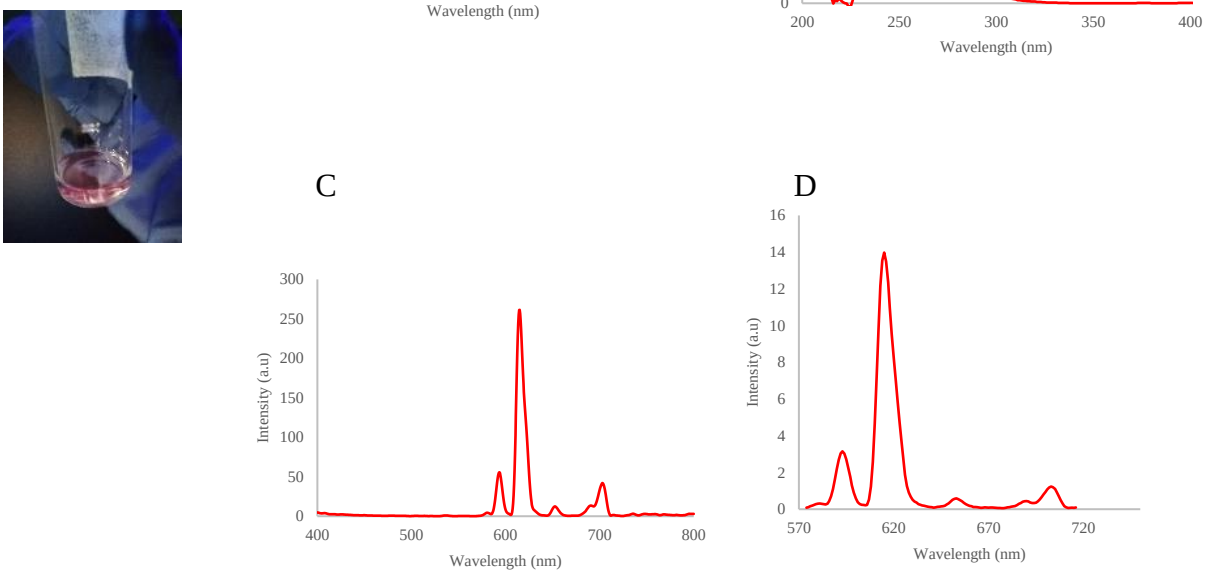

(A) The absorption spectrum, (B) the excitation spectrum, λ_{em} = 617 nm and (C) the fluorescence emission spectrum λ_{em} = 617 nm, (D) the phosphorescence emission spectrum, λ_{ex} = 286 nm of of Eu(**L1**)$_3$ in MeCN solution at RT (1 X 10^{-5} M)

Tb(**L1**)$_3$

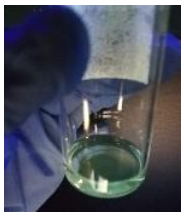

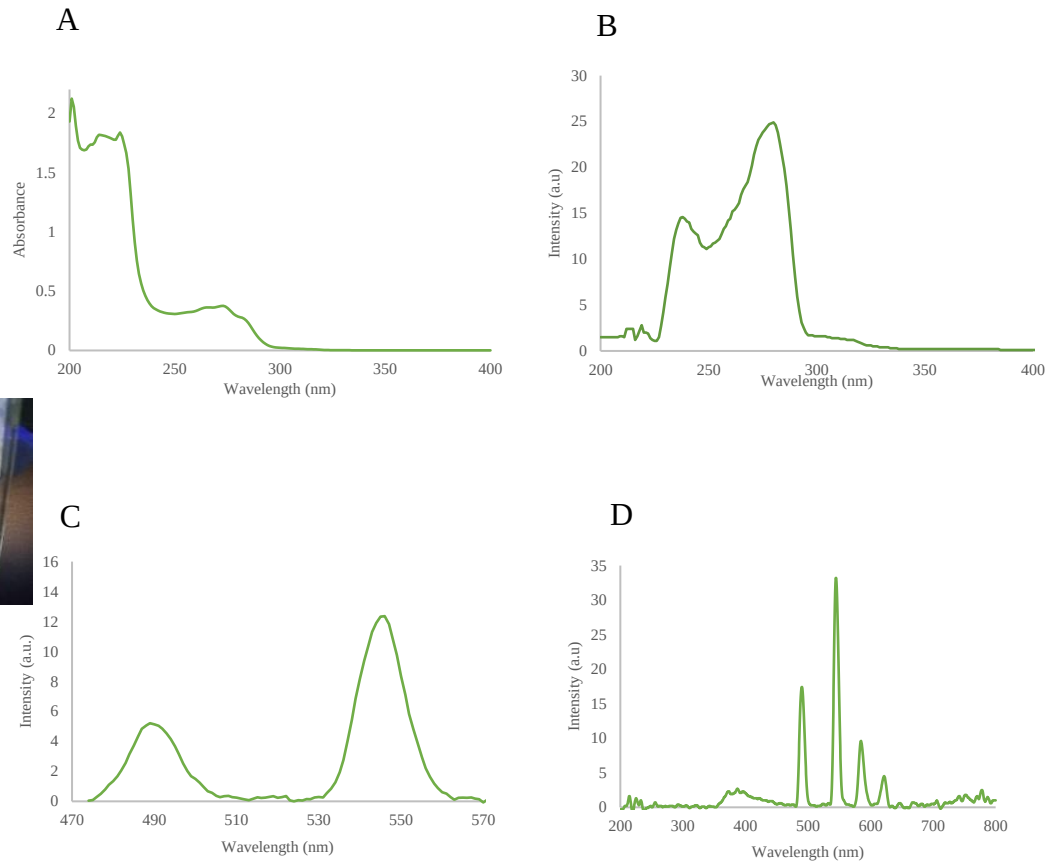

(A) The absorption spectrum, (B) the excitation spectrum, λ_{em} = 547 nm and (C) the fluorescence emission spectrum λ_{em} = 547 nm, (D) the phosphorescence emission spectrum, λ_{ex} = 286 nm of of Tb(**L1**)$_3$ in MeCN solution at RT (1 X 10^{-5} M)

Eu(**L4**)$_3$

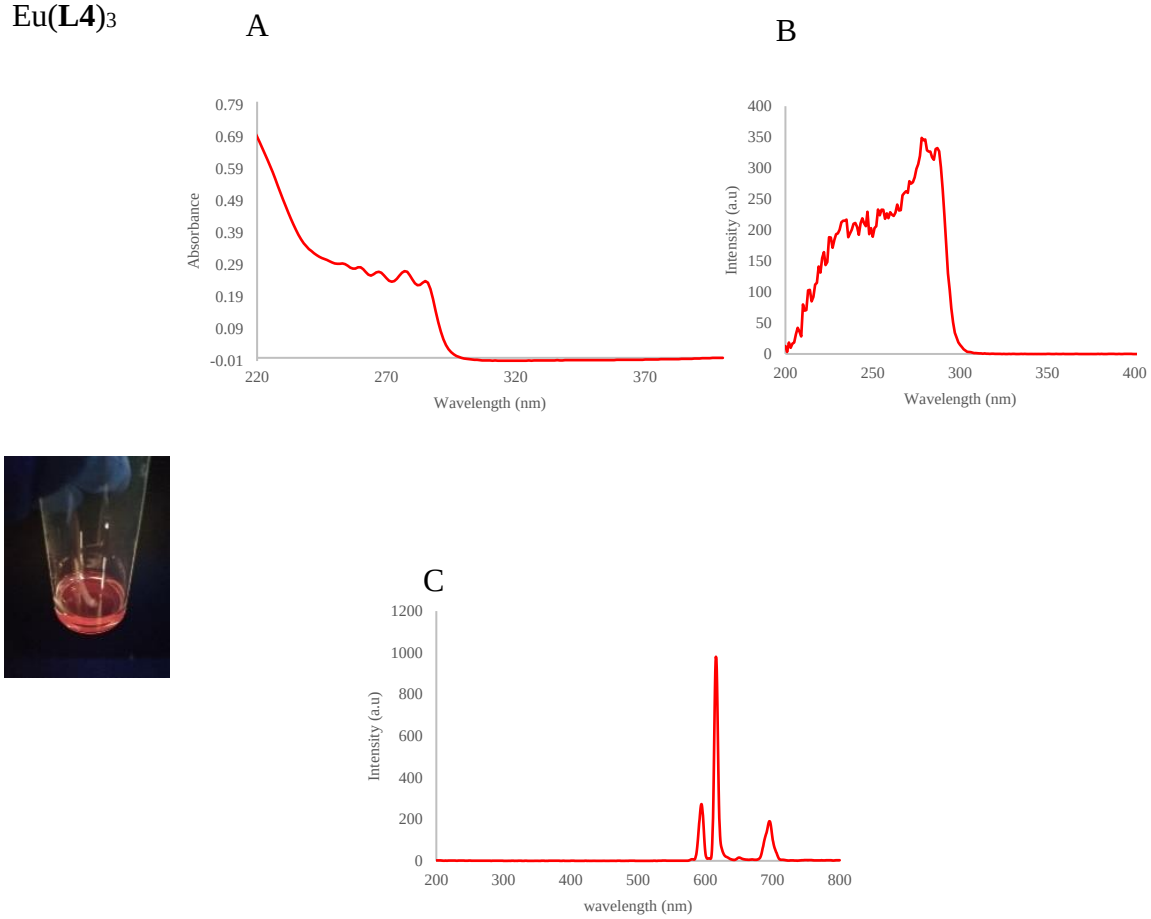

(A) The absorption spectrum, (B) the excitation spectrum, λ_{em} = 617 nm and (C) the fluorescence emission spectrum λ_{em} = 617 nm, of Eu(**L4**)$_3$ in MeCN solution at RT (1 X 10^{-5} M)

Tb(**L4**)$_3$

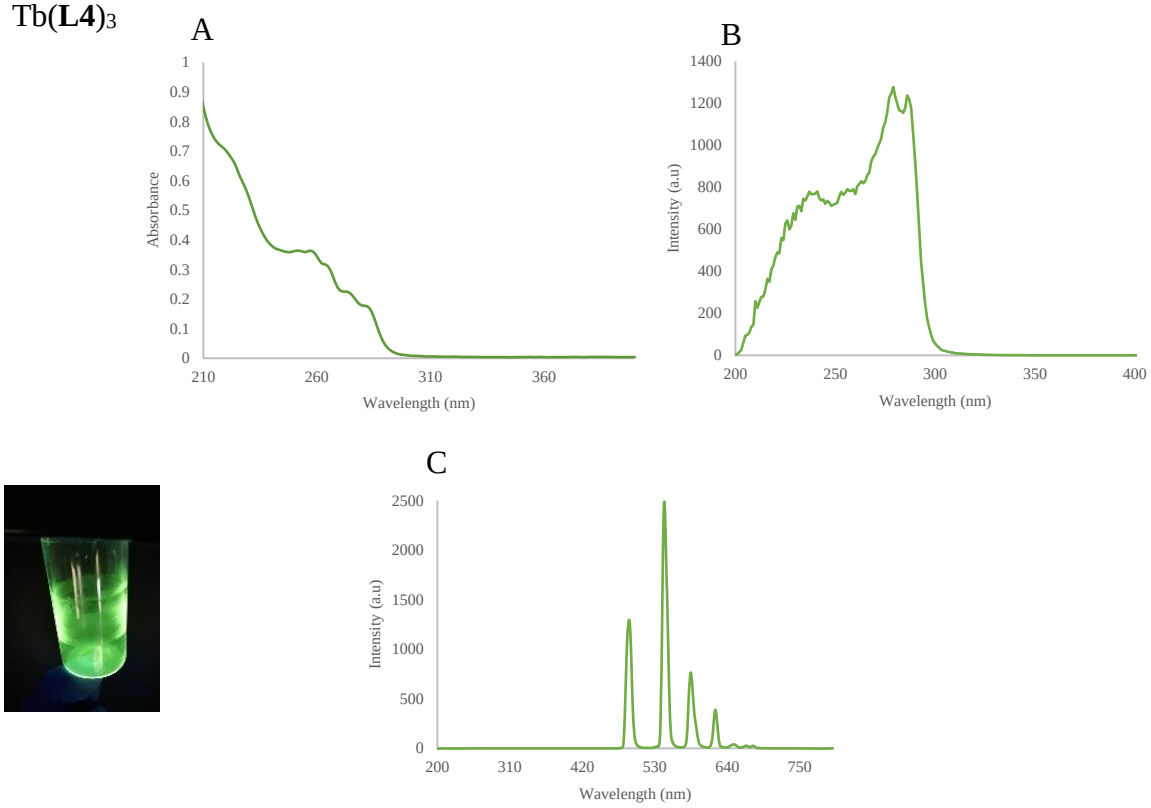

(A) The absorption spectrum, (B) the excitation spectrum, λ_{em} = 547 nm and (C) the fluorescence emission spectrum λ_{em} = 547 nm, of Tb(**L4**)$_3$ in MeCN solution at RT (1 X 10^{-5} M)

Eu(**L3**)$_3$

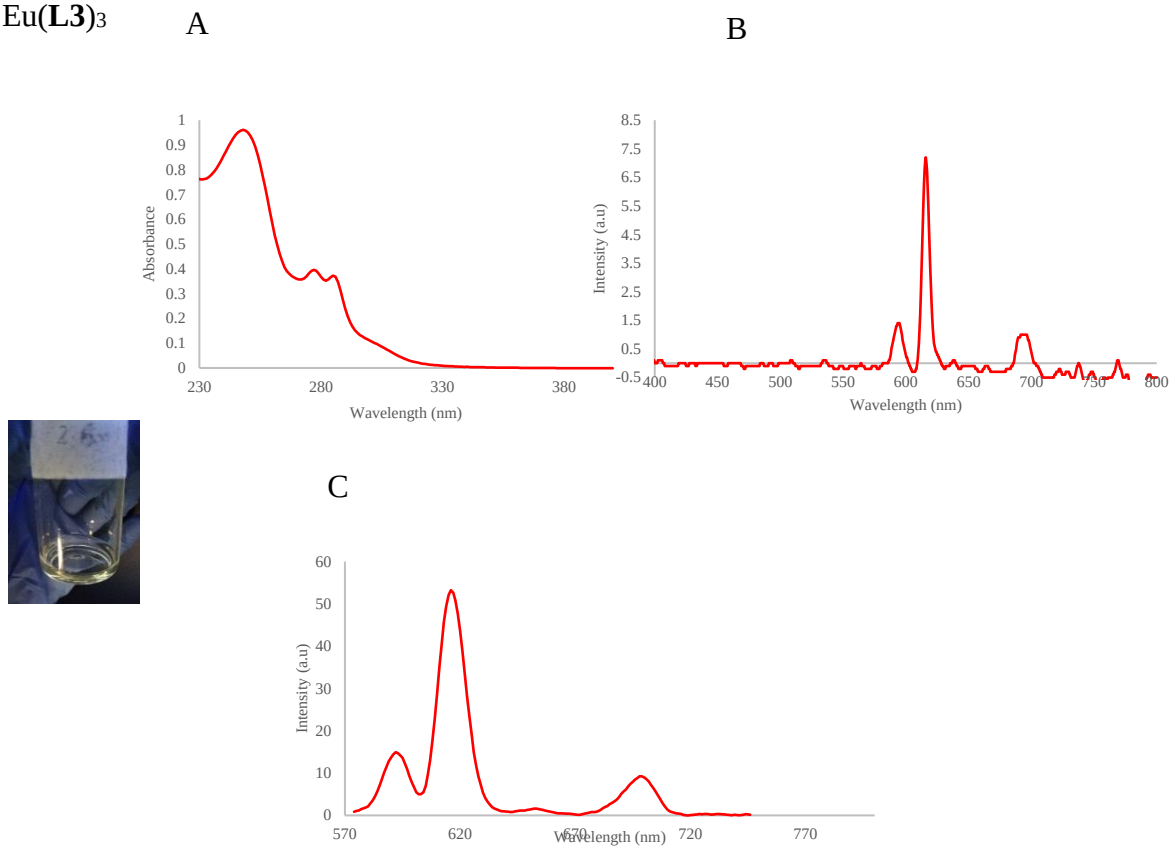

(A) The absorption spectrum, (B) the fluorescence emission spectrum λ_{em} = 617 nm, (C) the phosphorescence emission spectrum, λ_{ex} = 286 nm of of Eu(**L3**)$_3$ in MeCN solution at RT (1 X 10^{-5} M)

Tb(**L3**)$_3$

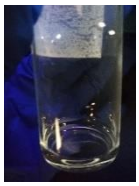

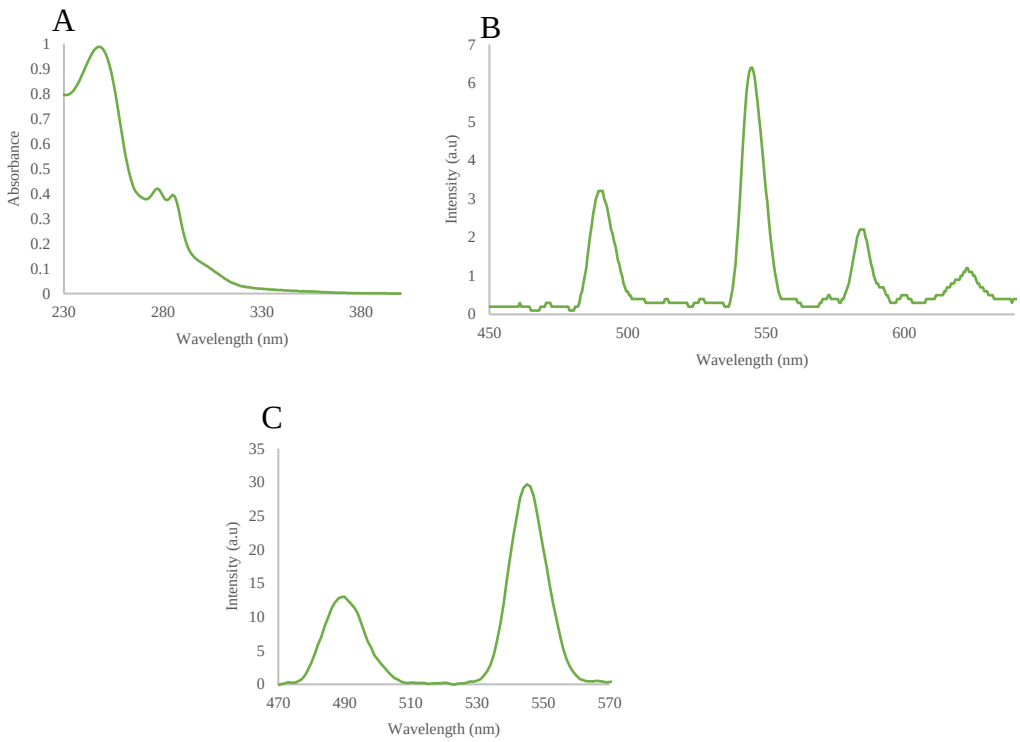

(A) The absorption spectrum, (B) the fluorescence emission spectrum λ_{em} = 547 nm, (C) the phosphorescence emission spectrum, λ_{ex} = 286 nm of of Tb(**L3**)$_3$ in MeCN solution at RT (1 X 10^{-5} M)

Eu(**L2**)$_3$

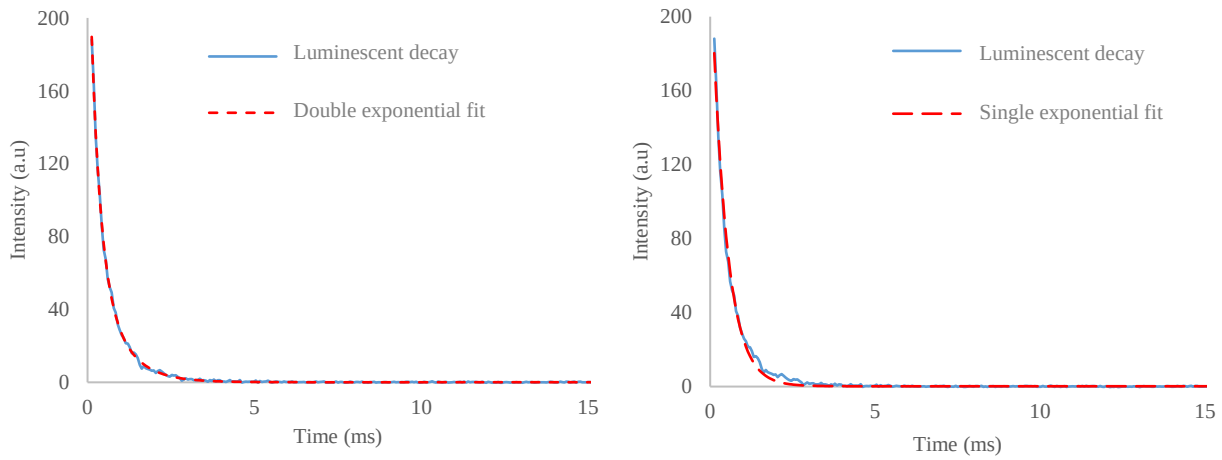

Figure shows the single and double exponential fit of Eu(**L2**)$_3$ complex. As shown in the diagram, Eu(**L2**)$_3$ was best fitted into a double exponential fit.

Tb(**L2**)$_3$

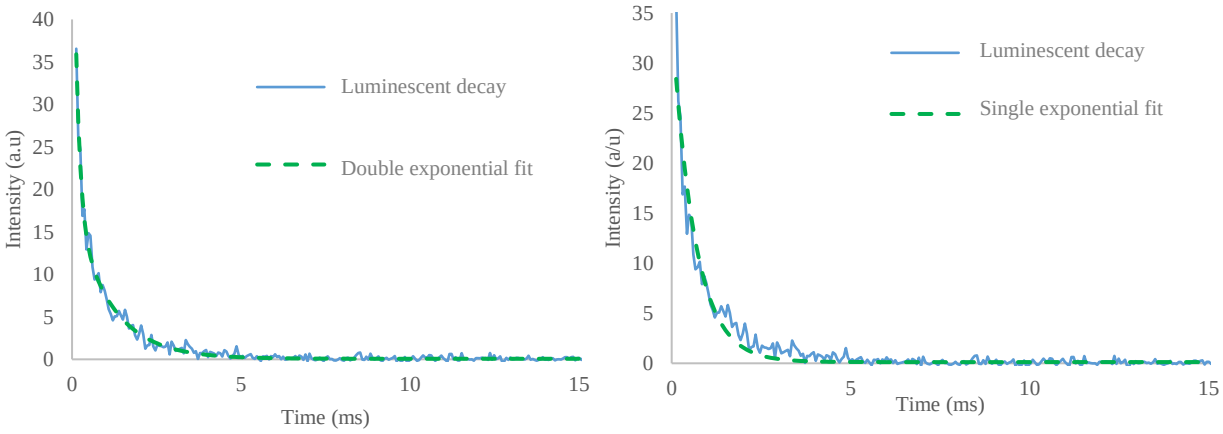

Figure shows the single and double exponential fit of Tb(**L2**)$_3$ complex. As shown in the diagram, Tb(**L2**)$_3$ was best fitted into a double exponential fit.

Eu(**L5**)$_3$

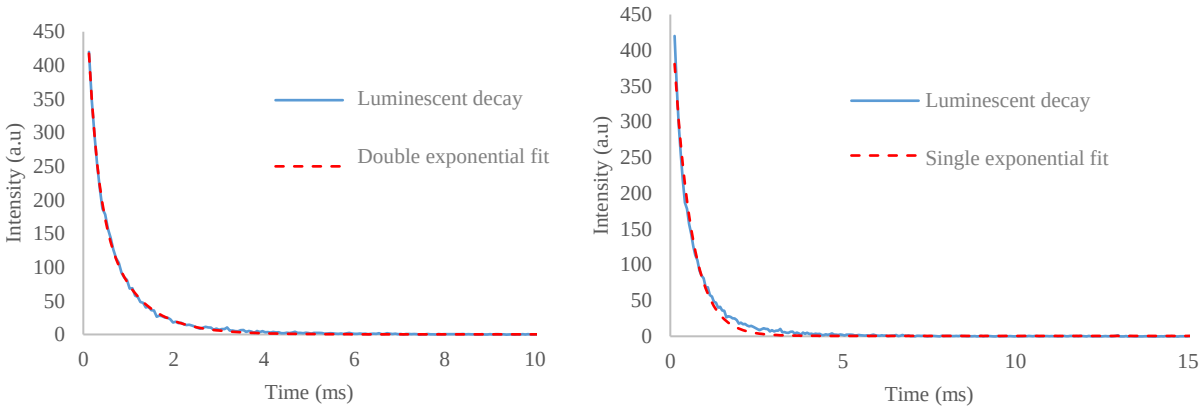

Figure shows the single and double exponential fit of Eu(**L5**)$_3$ complex. As shown in the diagram, Eu(**L5**)$_3$ was best fitted into a double exponential fit.

Tb(**L5**)$_3$

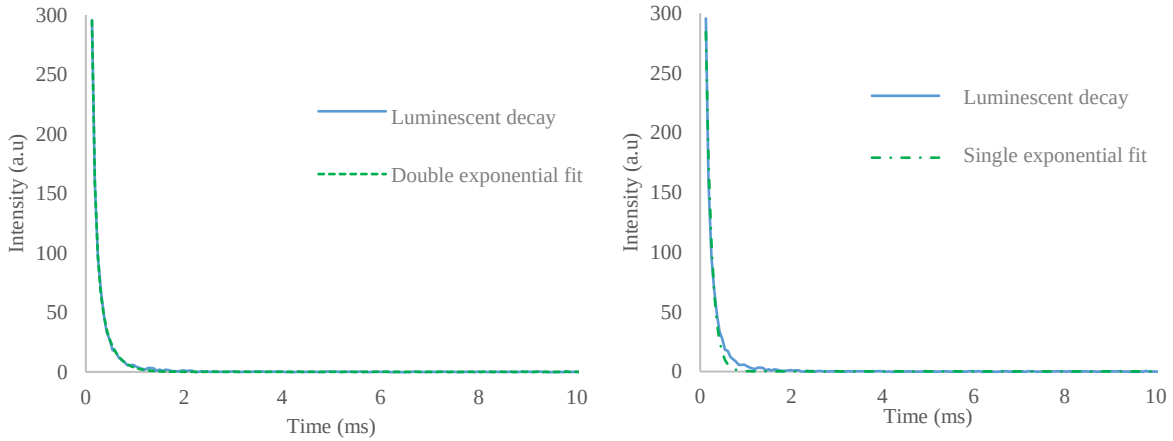

Figure shows the single and double exponential fit of Tb(**L5**)$_3$ complex. As shown in the diagram, Tb(**L5**)$_3$ was best fitted into a double exponential fit.

Mass spectroscopy data.

L6

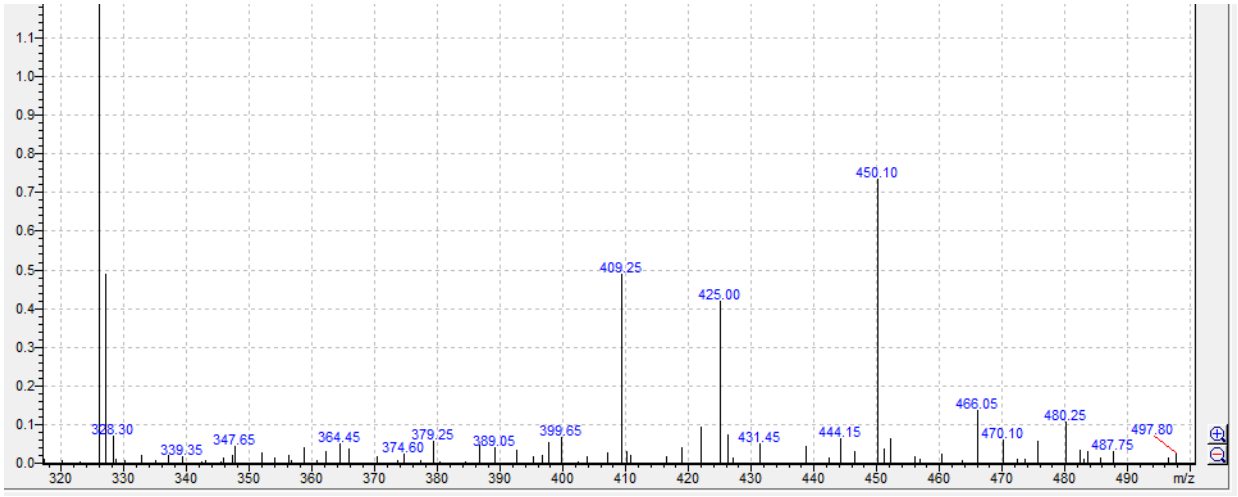

L5

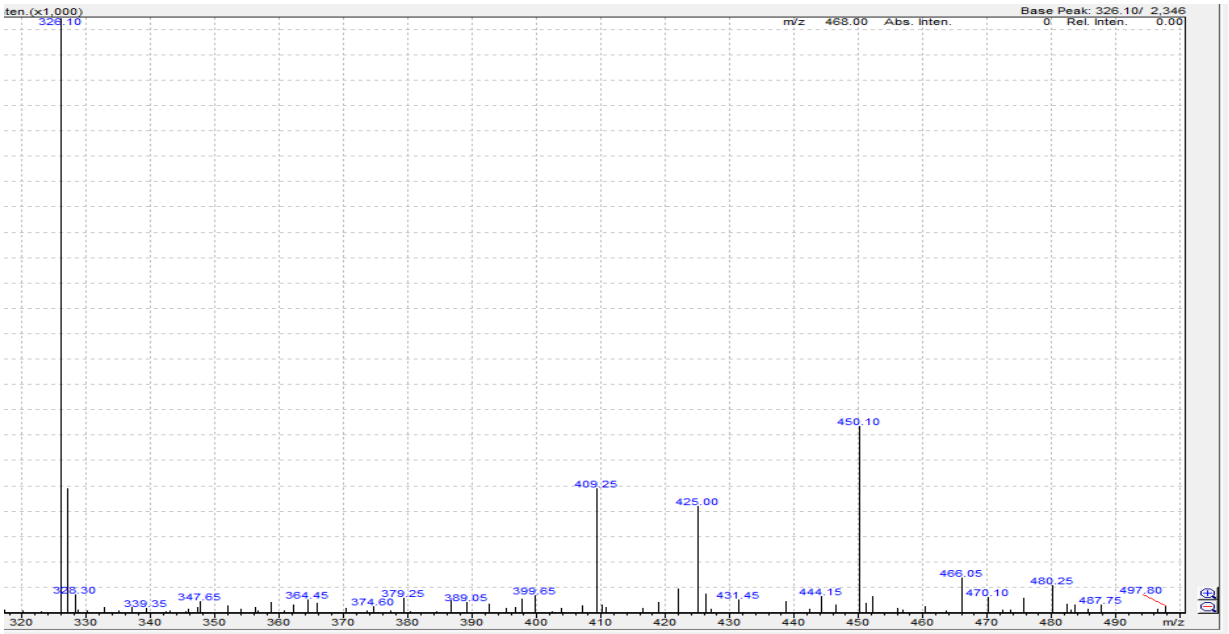

L4

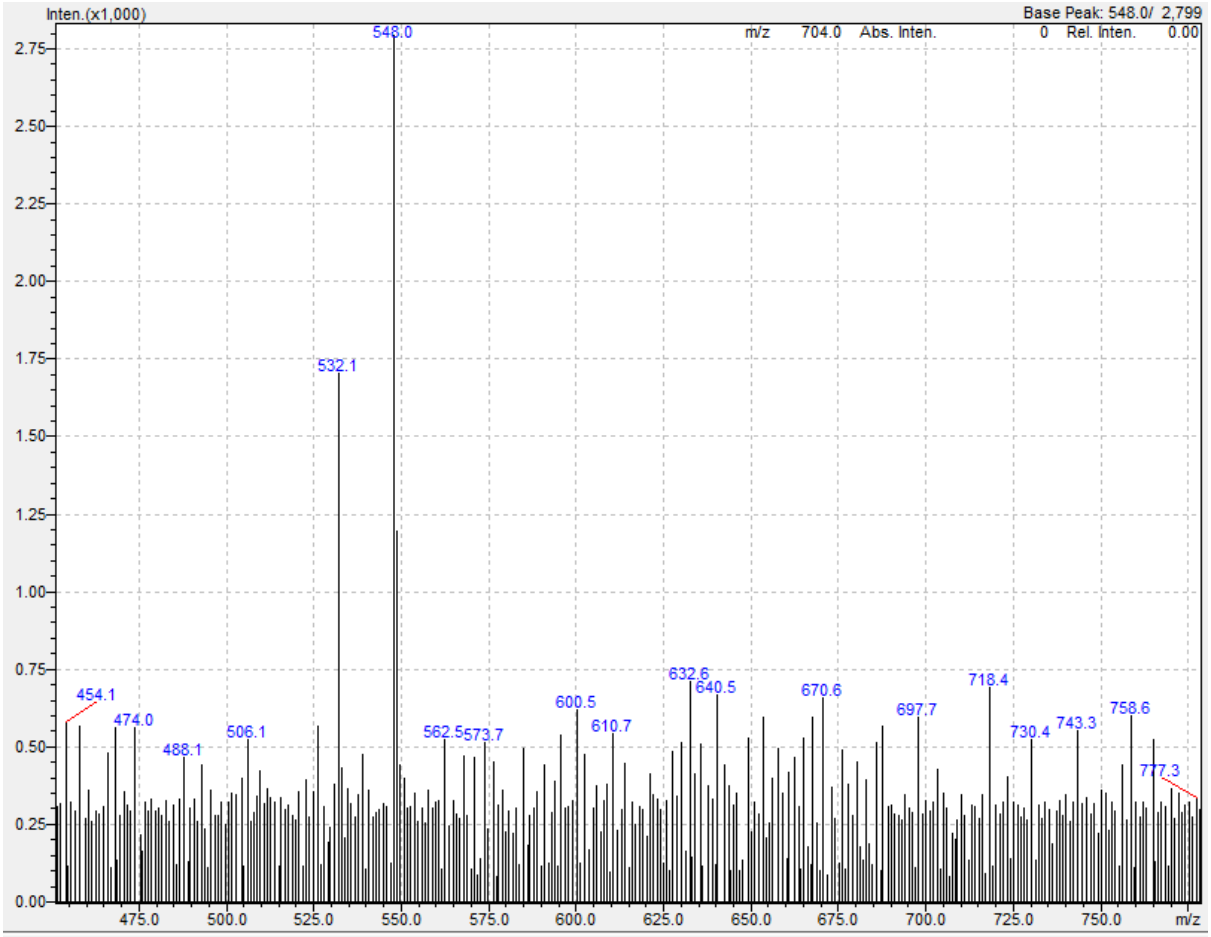
Inten.(x1,000)
Base Peak: 548.0/ 2,799
m/z 704.0 Abs. Inten. 0 Rel. Inten. 0.00
548.0
532.1
454.1
474.0
488.1
506.1
562.5
573.7
600.5
610.7
632.6
640.5
670.6
697.7
718.4
730.4
743.3
758.6
777.3
m/z

L1

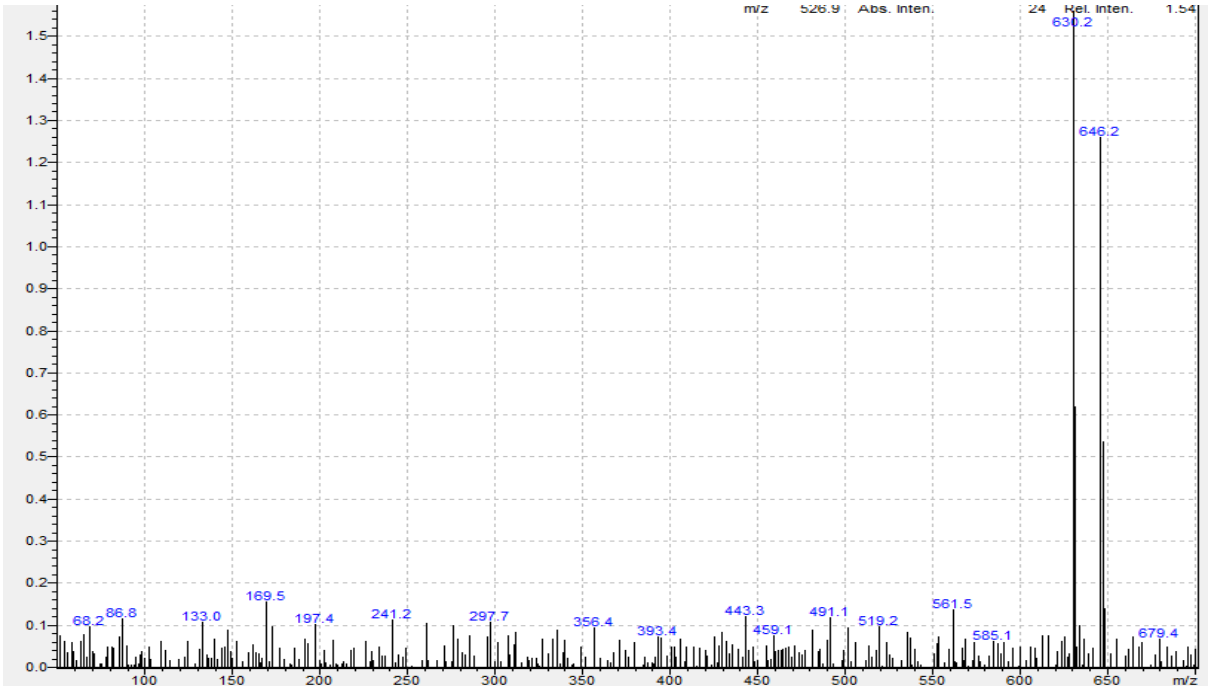
m/z 526.9 Abs. Inten. 24 Rel. Inten. 1.54
630.2
646.2
68.2
86.8
133.0
169.5
197.4
241.2
297.7
356.4
393.4
443.3
459.1
491.1
519.2
561.5
585.1
679.4
m/z

-The end-